# Alkali-Promoted Pt or Au Catalysts for the Low-Temperature Water-gas Shift Reaction

A dissertation

Submitted by

Yanping Zhai

In partial fulfillment of the requirements

for the degree of

Doctor of Philosophy

in

*Chemical Engineering*

**TUFTS UNIVERSITY**

November, 2011

**Advisor: Professor Maria Flytzani-Stephanopoulos**

# ABSTRACT

## "Alkali-Promoted Pt or Au Catalysts for the Low-Temperature Water-gas Shift Reaction"

In the process of producing hydrogen for PEM fuel cell applications from carbon-based fuels, an important stage is the catalytic water-gas shift (WGS) reaction, which is used to upgrade the hydrogen-rich fuel gas stream. The industrial Cu/ZnO catalyst lacks the required stability for this application which typically requires frequent shutdown-restart and may expose the catalyst to air and/or water. Based on numerous recent investigations, $CeO_2$- and modified-$CeO_2$-supported precious-metal catalysts, especially Pt and Au, have emerged as attractive alternatives possessing the required high activity for the low-temperature WGS, and no air or moisture sensitivity. The active sites comprise oxygen bound Pt or Au species, Pt-O-Ce or Au-O-Ce. Only a small number of these sites remain bound and active in realistic fuel gas streams; the number dictated by the oxygen potential of the gas and temperature. Another suitable support to bind Au-O sites is iron oxide. The apparent activation energy of the WGS reaction on gold is similar on both types of supports. From an economic viewpoint, it is interesting to design catalysts with just the right amount of a precious metal for a given set of operating conditions and avoid overdesigns that lead to destabilization, metal particle sintering, and therefore loss of the expensive precious metal. It is also interesting to examine whether non-reducible oxide supports can be used to stabilize Au-O and Pt-O species active for the WGS reaction. This information is also important from a mechanistic viewpoint, and if true, it would provide design flexibility and allow the use of abundant and cheap supports, such as silica and alumina. This hypothesis was tested in this thesis work.

Addition of alkali oxides on Pt-based WGS catalysts was effective in creating an active site comprising Pt-O and neighboring –OH groups that could be activated by CO at temperatures as low as 100 $^{o}$C, similar to the Pt-O sites on ceria. It does not matter what the support surface is when alkali promoters are used with Pt; silica or alumina is as effective a carrier of the active sites as ceria. This is the major finding of this thesis. Such

alkali-promotion was examined and identified on Au-based catalysts as well, but a detailed study of the latter was not conducted.

Characterization techniques such as XPS, aberration-corrected HAADF/STEM, XANES/EXAFS, CO chemisorption, and $H_2$/CO-TPR were used to probe and improve our mechanistic understanding of the alkali-promotion of the Pt-based catalysts. Guided by these findings, DFT calculations were performed by Prof. Mavrikakis and his group at the University of Wisconsin-Madison, and a few plausible structures for the active site were proposed for K-promoted Pt-O catalysts. The cluster K-$O_x$-Pt-$(OH)_y$ retains Pt in oxidized state, with a ratio of K:O=1:1; binds CO weakly; and adsorbs/dissociates $H_2O$ almost without energy demand (thermoneutral), similar to Cu (111), the best WGS catalyst.

In detailed studies with 1at%Pt-3at%Na on fumed silica, it was found that the active site stabilizes Pt as well as the alkali ions that comprise it. Thus, the alkali ions are not removed by repeated washings of the catalyst by de-ionized water at either ambient temperature or 70 $^{o}$C. Stability in realistic gas streams was found; Pt retained its oxidized state as shown by in-situ XANES, and no activity loss was found in isothermal experiments up to 275 $^{o}$C after 10-40 h-on-stream. Other alkali (Li, Cs) and alkaline-earth ions (Mg, Ca, Ba) added in small amounts were also effective, but Na provided the maximum promotion.

All the alkali-promoted Pt samples on the alumina or silica used here have similar apparent activation energy, 70 ± 5 kJ/mol, for the low-temperature WGS reaction, as reported also for Pt on $TiO_2$, $CeO_2$, or $ZrO_2$. Therefore, it is proposed that the key steps of the WGS reaction catalysis (CO adsorption and $H_2O$ activation) occur on Pt-$O_x$-$(OH)_y$ sites, irrespective of the type of support and the additive used.

Gold catalysts for the low-temperature WGS reaction were examined on various supports and their activity and stability was compared to that of the Au-$CeO_2$ system. The reaction-relevant Au structures on Au-$FeO_x$ were followed by in-situ XANES and EXAFS spectroscopy. Similar to ceria, the number of Au-O sites that remain bound on iron oxide depends on the oxygen potential of the fuel gas and operating temperature. Highly reducing fuel gas mixtures destabilize the [Au-O-Ce, -Fe] sites and cause gold cluster/particle formation and deactivation. Activity recovery is possible by re-oxidation in

air (350-400 $^{o}$C). Catalyst stability is improved if gas mixtures with higher oxygen potential are used. Oxygen-assisted WGS operation was found to stabilize the Au-O-Fe sites, and is recommended for practical applications.

OH-rich or alkali-modified surfaces can create more binding sites and disperse the Au species better during the synthesis and thermal treatment steps. As a result, the WGS reaction activity is proportionately increased. The alkali-free and alkali-promoted Au-$CeO_2$, Au-$Fe_2O_3$, Au-$La_2O_3$ catalysts have the same apparent activation energy, which indicates a common active site for all Au-based catalysts for the WGS reaction, regardless of the support or additive used. By analogy to the Pt catalysts, we propose a cluster of the type Au-$O_x(OH)_y$ stabilized by Ce, Fe, La, or alkali ions. This needs to be tested by DFT calculations.

Although enhanced WGS reactivity over Au-based catalysts was manifested with OH-rich or alkali-modified surfaces, the active Au species are more sensitive to destabilization than Pt. The electronegativity of the oxide/additive plays an essential role on the stability of the Au active sites, and is thus recommended to use this to guide the choice of additives and the optimization of the synthesis conditions of gold catalysts.

**Keywords:** Fuel cell, water-gas shift, platinum, gold, alkali-promotion, silica, alumina, ceria, iron oxide, lanthanum oxide

## Acknowledgement

I would like to thank my thesis advisor, Professor Maria Flytzani-Stephanopoulos, for her guidance, encouragement and support through all these years. I would also like to thank my thesis committee members: Professor Howard Saltsburg, Professor Terry Haas, Professor Chia-Kuang (Frank) Tsung, and Dr. Robert Weber, for their helpful insights and suggestions on my thesis.

I am also most appreciative for the knowledge and training I received by various key collaborators of our group, namely, Professor Manos Mavrikakis at the University of Wisconsin, Madison for his and his group's contributions to my thesis by their ab initio Molecular Dynamic modeling of the active sites of my catalysts, Professor Anatoly Frenkel at Yeshiva University for his guidance in the use of EXAFS software and on-site experiment training at the synchrotron facilities of Brookhaven National Laboratory, Dr. Qi Wang for her help with the Quick-XANES set up at Brookhaven National Laboratory, Dr. David Bell at Harvard University for his assistance with the aberration-corrected HAADF/STEM examination of my catalysts, and Professor Frederic Meunier at the University of Caen, France for conducting in situ DRIFTS investigations of my most active catalysts. Dr. Weiling Deng, currently at BASF, and Dr. Rui Si, currently at Brookhaven, both former members of our group, have taught a lot and I am grateful to them for their assistance throughout my doctoral study.

I would also like to thank all the former and current fellow students at the Nano Catalysis and Energy Laboratory of Tufts University, for their friendship, helpful discussions and sharing of equipment. Many thanks go out to our superb department staff, Erin Quigley, Beth Frasso, Julia Poirier, and Ann Tropeano for their kindness and eagerness to help each and every time their assistance was needed.

Finally, I want to thank all my family and friends, especially my Mom, my husband, Wei, and my cousin, Wenjun for their support and love throughout my study at Tufts. I am happy to finish this thesis with a precious new addition to my family, my beloved baby, Summer!

The financial support of my project by DOE/Basic Energy Sciences: Hydrogen Fuel Initiative Program (Grant No. DE-FG02-05ER15730) and the National Science Foundation

(NIRT Grant No. 0304515; and CBET Grant # 0828666) is gratefully acknowledged. I would also like to acknowledge the support by the Synchrotron Catalysis Consortium at Brookhaven National Laboratory, and the Micromeritics Corporation for generously supplying the AutoChem II 2920 to our group as part of their Instrument Grant Program.

# TABLE OF CONTENTS

# List of Tables

## List of Figures

# Chapter 1 Introduction

## 1.1 Hydrogen economy and PEM fuel cells

With the increasing demand for energy and more stringent emission control requirements there is an urgency in developing alternative fuels and more efficient energy utilization of fossil fuels. During the last twenty years, the United States, the European Union and other countries have invested billions of dollars in initiatives aimed at shifting a fossil fuel-based to a hydrogen economy. When oxidized, $H_2$ releases the highest amount of energy per unit mass of fuel without generating greenhouse gases or other pollutants at the point of usage. Fuel cells, generating electricity from the electrochemical reaction of hydrogen with oxygen, are slowly penetrating the market for both stationary and mobile applications. They are about twice as fuel efficient as the internal combustion engine and produce virtually no CO, HC, or NOx, and a lower overall level of $CO_2$ as a result of their better energy efficiency [1]. Due to its lower operating temperature, high efficiency and compact size, the proton exchange membrane (PEM) fuel cell is the most attractive one for residential heaters, transportation applications, and portable devices, such as laptop computers, cellular phones and personnel digital equipment.

Still, a major drawback of $H_2$ fuel is the fact that it is difficult to be stored compactly and safely. One of the most promising ways to overcome this is to produce $H_2$ on-site. It could be generated from hydrocarbons (i.e. natural gas, coal, oil or methanol) in a fuel processor by either stream reforming or autothermal reforming.

$$CH_{2n} + H_2O \rightarrow CO + (n+1)\, H_2 \quad \text{(steam reforming)}$$

$$2CH_{2n} + H_2O + \tfrac{1}{2}\, O_2 \rightarrow 2CO + (2n+1)\, H_2 \quad \text{(autothermal reforming)}$$

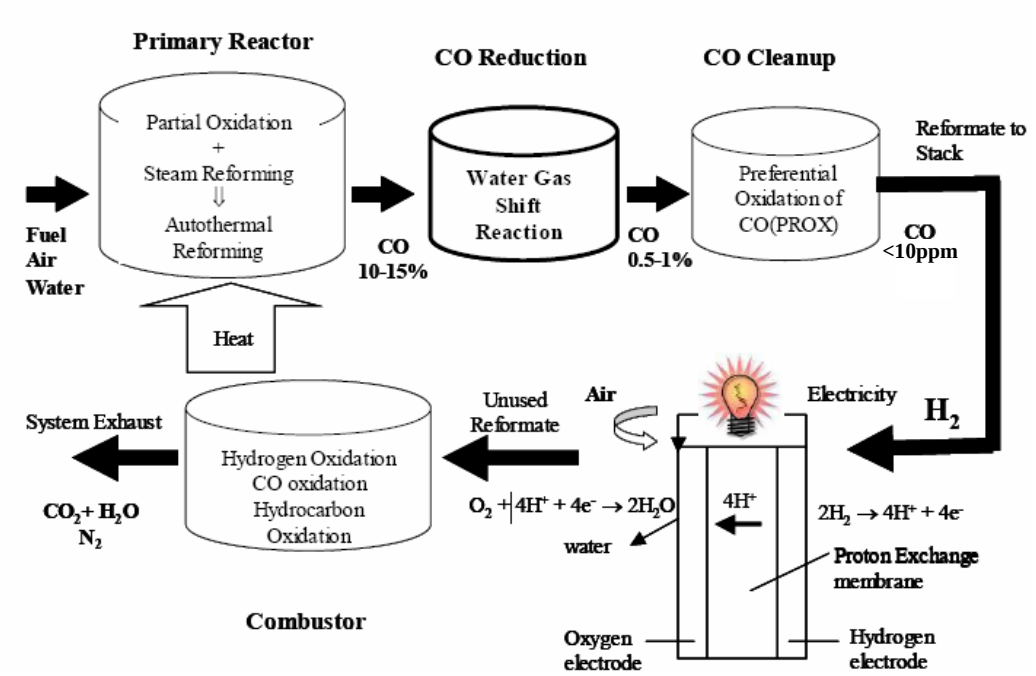


Figure 1.1 Fuel processing and fuel cell system for on-board hydrogen generation

The reforming step generates a gas mixture which contains 8-12%CO as well as $H_2$ and $CO_2$. However, fuel reforming requires the complete removal of CO down to <10 ppm upstream of the PEM fuel cell, because CO is not only a criterion pollutant, but also a poison for the platinum catalyst of the fuel cell anode [2]. The water-gas shift (WGS) reaction is used to decrease the CO level to less than 1%. Trace levels of CO could be handled by a preferential catalytic CO oxidation (PROX) cleanup system downstream.

$$CO\ (g) + H_2O\ (g) \rightarrow CO_2\ (g) + H_2\ (g) \quad \text{(WGS reaction)}$$

$$\Delta H = -41.2\ \text{kJ mol}^{-1}$$

$$\Delta G = -28.6\ \text{kJ mol}^{-1}$$

The WGS reaction is a mildly exothermic reaction. From a thermodynamic viewpoint, the equilibrium conversion is lower at high WGS reaction temperatures. Therefore, very active WGS catalysts operating in the low temperature range, usually from 200 to 250 $^{o}$C, are in demand for the PEM fuel cell application. For realistic shift reaction systems, the designed catalysts must meet requirements of being non-pyrophoric, an appropriate (wide) operating temperature window, high activity, good stability even during the cyclic shutdown-restart

operation, and also be economical [3]. The current commercial WGS technology to upgrade hydrogen for chemicals production involves multiple stages/catalysts, i.e. (i) a high-temperature WGS (350-500 $^{o}$C) ($Fe_2O_3/Cr_2O_3$) and (ii) a low-temperature WGS (200-250 $^{o}$C) ($Cu/ZnO/Al_2O_3$). This technology is excellent for large installations where the reactors run unperturbed for very long time, but it is not suitable for fuel cell applications. The $Cu/ZnO/Al_2O_3$ itself is very sensitive to temperature excursions, air exposure (pyrophoric), and requires a controlled and elaborate activation, such as in situ pre-reduction [4-6]. Precious metal-based catalysts (mainly platinum and gold), not suffering from the above drawbacks, have been under intensive investigation during the last decade for their potential use in fuel cell applications.

## 1.2 Literature review

### 1.2.1 Precious metal catalysts for the low-temperature WGS reaction

Although the precious metal catalysts are more expensive and may exhibit lower turnover rate than the most active copper-based catalysts, the recent interest in PEM fuel cell applications has generated a significant impetus to study supported precious metal catalysts, mainly due to being non-pyrophoric, stable in air and in cyclic operation [1]. Based on the experience from earlier studies of automotive exhaust catalysts, precious metals, such as Au [7, 8], Pd [9, 10] or Pt [5, 11-13] on different oxide supports, especially reducible oxides, such as ceria [5, 8, 11, 13, 14] have been the frontrunners in this area.

As one of the best catalysts for the water-gas shift reaction, $Pt\text{-}CeO_2$ has been extensively investigated. Zalc *et al.* [15] claimed that $Pt\text{-}CeO_2$ had a high rate of deactivation when used in realistic reformate gas streams due to the over-reduction of $CeO_2$. However, Wang *et al.* [16] showed that the deactivation at high temperature was caused by destabilization and agglomeration of the precious metal particles, which can be avoided by careful design of the catalysts. Under some conditions, Pt catalysts have good activity for the methanation reaction, which will consume valuable $H_2$ from the reformate gas. Yeung *et al.* [17, 18] reported a reverse microemulsion method to prepare a core-shell structured catalyst, Pt@Ceria. Such a structure eliminated the methanation reaction, but still allows the WGS reaction to occur, apparently by well dispersed Pt species in the shell of the structure. Liu

*et al.* [19] have found that the Pt-$CeO_2$ system suffers from deactivation through the ceria part, which forms a hydroxyl carbonate during the shutdown process in the full gas containing steam. This is a common problem that plagues all ceria-based catalysts. Deng *et al.* [20] have recently shown that this problem can be solved by adding a small amount (1 vol%) of $O_2$ in the reformate gas. The efforts to improve ceria-based catalysts are continuing since ceria disperses the metals atomically and this in turn imparts very high activity [21]. Alternatively, the modification of the ceria support is another way to solve the deactivation problem, *e.g.* the BASF group [22] have proposed addition of zirconia into ceria to stabilize the catalyst in shutdown-restart operation. Ruettinger *et al.* [23] have developed non-pyrophoric, copper-based WGS catalysts, containing also a small amount of platinum group metals, which have no methanation activity and are stable upon exposure to the fuel gas stream up to 220 $^{o}$C.

Gold, initially regarded as a catalytically inert precious metal, has been studied intensively for the past two decades ever since the discovery by Haruta that ultrafine gold particles (<10 nm) dispersed on metal oxides show surprisingly high catalytic activity for the CO oxidation reaction at ambient temperatures or lower (~ 200 K), which makes them unique [24]. Since then nanostructured gold catalysts have attracted interest as potential candidates for the CO removal process at ambient conditions. It has also been demonstrated that highly dispersed Au nanoparticles on oxide supports are as effective as Pt based catalysts for the selective removal of CO in the hydrogen streams used for fuel cells [8, 20, 25-33]. Our group at Tufts was the first to report on the particularly high activity of Au-$CeO_2$ for the low-temperature WGS reaction which makes them attractive prospects for a range of applications including feed gas cleanup for low-temperature fuel cells [30]. Of course, gold is preferred over platinum, as Au catalysts have lower light-off temperatures for both hydrocarbon and carbon monoxide oxidation by $H_2O$ and do not catalyze the undesired methanation reaction [34].

However, the commercial application of these catalysts has also been hindered by their tendency to deactivate rapidly under reaction conditions. The physical origin and mechanism of the deactivation of supported Au catalysts are still being debated in the literature; the formation of formate/ carbonate species [35-37], sintering of Au [38], loss of ceria supported surface area due to weakening of the gold-ceria interaction [39], and loss

of the contact between the Au and the support [40] have all being reported as the prevailing mechanisms.

### 1.2.2 Active sites for the WGS reaction

Although there is still no agreement on whether the WGS reaction follows the redox or formate mechanism in the case of Au- or Pt-metal modified ceria [41-49], and whether the active sites involve metallic Au or cationic Au (or Pt) [8, 18, 50-54], it is generally accepted that high dispersion of gold or platinum on the oxide support and the contact of Au (or Pt) with the oxide are necessary to produce very active catalysts for the WGS reaction [8, 22, 31, 51, 55-58]. Related to this is the contention that the reducibility of the oxide support plays an important role in the catalytic activity [26-29, 33, 57, 59-64].

Since 2001, a large number of papers have appeared in the literature on the properties of supported gold catalysts [24, 26, 27, 65, 66]. The importance of ceria surface oxygen for this reaction had already been pointed out in the literature by our group in 2001 [30]. Li *et al.* [33] have shown that doping the ceria with lanthanum increases the available surface oxygen from the support and improves the interaction with Cu or Ni. Later Luo *et al.* [67] and Fu *et al.* [30] reported a dramatic effect of gold on the reducibility of the surface oxygen of ceria and the available surface oxygen correlates well with the water-gas shift activity of the Au-$CeO_2$ system. Cyclic CO-TPR with intermittent re-oxidation has demonstrated an excellent stability of the redox properties of these surfaces [32].

Using FTIR Tabakova and co-workers [31] found that nanosized metallic gold particles in close contact with oxygen defects of $CeO_2$ are crucial for high catalytic activity. The high and stable activity of Au-$CeO_2$ catalysts could arise from the high and stable gold dispersion present during the catalytic operation [59]. Also Tibiletti *et al.* [68] combined DFT calculations together with XANES and EXAFS and reported that under the WGS reaction conditions the active form of gold comprises small metallic gold clusters in intimate contact with the oxide support. Such gold clusters would be expected to carry a small positive charge ($Au^{\delta+}$), and this may be very important for creating the active site for the WGS reaction.

In a key paper [8], published in 2003, Fu *et al.* used a NaCN leaching process to remove metallic gold nanoparticles and weakly bound gold species from ceria leaving ~10 % of oxidized gold species in close contact with ceria. The leached and parent materials exhibited identical WGS activities, which implies that only cationic gold or gold cluster species associated with ceria, as $Au_n$-O-Ce, are active for the WGS reaction, and that the more abundant gold nanoparticles, weakly bound to ceria are spectators. Similar results were reported for the Pt-ceria system [8]. This finding allowed us to produce a catalyst with one tenth of the normal loading of precious metal (Au, Pt), without altering the catalytic activity. This is a promising development for practical catalyst designs aimed at reducing the cost of catalytic fuel processing. Mechanistically, stabilization of gold cations on ceria oxygen vacancies has been put forth by DFT calculations to explain the activity of fully dispersed gold on ceria [69]. To explain the strong interaction of gold with support surfaces, Haruta and coworkers have advocated that the peripheral/interfacial gold atoms at the support/gold nanoparticles contact are the active sites for the CO oxidation reaction [70].

In regard to the charge of gold clusters in ceria, conflicting assignments have appeared in the literature, from negatively [71] to positively [8, 39, 69] charged clusters, and neutral [37, 43, 53, 68, 72] clusters as well. Some of the reported assignments are ambiguous, however, because of the presence of all types of structures of gold (atoms, clusters, and nanoparticles) in most of the examined catalysts. To clarify the roles of different Au species, Deng *et al.* [51] examined a leached Au-$CeO_x$ catalyst for the WGS reaction, by in situ XANES/EXAFS. Starting from a fully dispersed gold state, where no Au-Au, but only Au-O coordination was seen by EXAFS, they followed the gold structural evolution under reaction conditions. It was found that the oxidation state of gold depends on the reaction gas composition and the reaction temperature. The higher the reaction temperature or the more reducing reaction gas mixture, the less oxidized the Au species were. Interestingly, as the number of oxidized gold species dropped, and gold aggregation took place, this was accompanied by the loss of the catalytic activity. Hence, gold destabilization from the Au-O-Ce active site caused the deactivation [51]. It was further demonstrated that the destabilization was reversible, i.e., re-dispersion of gold onto the ceria surface was possible by oxidation at 400 $^{o}$C by gaseous $O_2$-He streams, accompanied by surface oxygen and

catalytic activity recovery [51]. These findings establish the Au-O-Ce species as the active sites for the low-temperature WGS reaction, and this result can guide the design of gold-ceria catalysts, and of the processing conditions, *e.g.* addition of small amounts of oxygen in the reformate gas, to suppress the deactivation and prolong the gold catalyst lifetime.

New questions can now be posed: is ceria unique? How about other reducible oxides, like iron oxide? Is the gold destabilization due to loss of Au-O-Fe sites? Is it reversible? How can one maximize the active sites through new catalyst synthesis procedures? How can one stabilize the active sites under operation?

$Fe_2O_3$-supported Au catalysts [7, 27, 52] have been reported to be very active for the WGS reaction. The importance of the iron oxide surface oxygen was first reported by the Andreeva group [27]; $FeO(OH)_x$ was identified as important. However the WGS reaction kinetics on the Au-$FeO_x$ were not evaluated. Deng *et al.* [52] investigated the WGS reaction kinetics, using both a commercial catalyst and its CN-leached derivative. The areal reaction rates, which are reaction rates normalized by the specific surface area of the catalyst, were about the same on both $CeO_2$ and $FeO_x$ supported Au catalysts. They were also the same for the parent and leached catalysts, providing strong support that the active sites are the atomically dispersed $Au_n$-O-Ce and $Au_n$-O-Fe surface species [52]. Therefore the Au-$Fe_2O_3$ type catalyst is a good system to further investigate mechanistically in order to arrive at proper design guidelines. Recently, it was reported that the deactivation of Au-$Fe_2O_3$ was mainly caused by the change of the support [73]. A significant reduction of the surface area of the iron oxide was found during the WGS reaction as a function of time on stream and this decrease of the surface area was used to explain the decrease of the catalytic activity.

To elucidate the nature of the interaction of finely dispersed gold with the support surfaces, complementary information can be sought by the investigation of model catalysts studied in a controlled, ultrahigh vacuum environment. Recently, Rim and co-workers in G. Flynn's lab at Columbia [74] prepared a sub-monolayer of gold adatoms on an Fe-terminated $Fe_3O_4$ (111) single crystal surface, to investigate the site-specific adsorption of Au adatoms using scanning tunneling microscopy and spectroscopy. Gold adatoms were

found to preferentially bind on the uncovered oxygen atoms, were positively charged, and the exclusive sites for CO adsorption at 260 K.

In more recent work, the same group [75] has investigated the adsorption of water molecules on $Fe_3O_4$ (111), and found that –OH adsorbs preferentially on the Fe atoms surrounding the uncoordinated oxygen. Thus, it is possible to activate these –OH groups by the CO adsorbed on the Au adatoms, hence demonstrating that an ensemble of [Au-$O_x(OH)_y$-Fe] bound onto $FeO_x$ surfaces may be where the active sites for the WGS reaction reside exclusively.

On the basis of the above discussion, atomic distributions of gold on oxides are important for the water-gas shift reaction, and should be possible to capture by various techniques. By using atomic-resolution electron microscopy at Oak Ridge National Lab, Allard *et al.* [76], examined NaCN-leached Au-$Fe_2O_3$ materials prepared at Tufts, and found them to contain a preponderance of gold ions. These were present in the "fresh" material after 400 $^oC$-air calcination, Figure 1.2, but also in the WGS-reaction used sample, and even in a 400 $^oC$-$H_2$ treated sample. The latter also had a number of sub-nm and nm-sized gold particles present, Figure 1.3. Allard *et al.* showed that the Au-$FeO_x$ interaction is very strong [76, 77]. By a series of in-situ heating tests in the microscope up to 700 $^oC$, sintering did not begin below 500 $^oC$ and even at 700 $^oC$, the Au NPs were below 2 nm size.

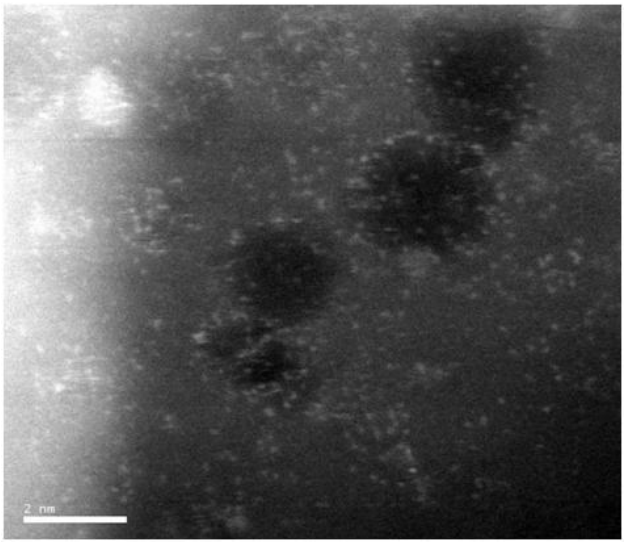


Figure 1.2 Aberration-corrected HREM images of fresh 0.7Au-$FeO_x$ [76]

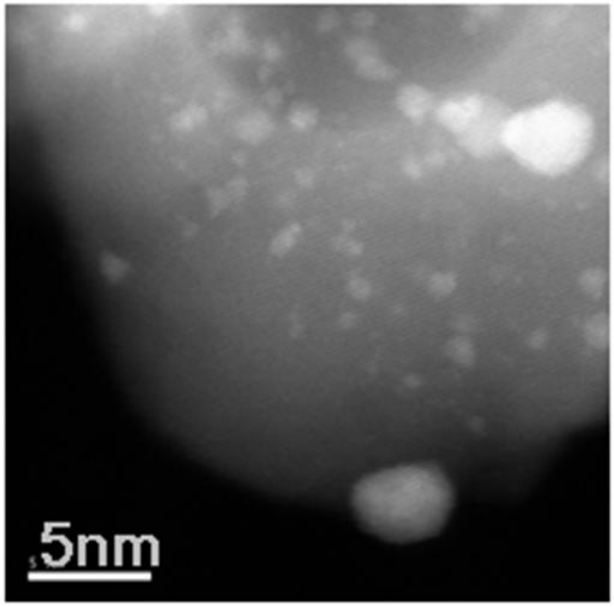


Figure 1.3 Aberration-corrected HREM image of $H_2$-reduced 0.7Au-$FeO_x$ [76]

Isolated Au cations on the $Fe_2O_3$ surfaces have been observed also by Herzing *et al.* [78] who used atomic resolution microscopy to analyze several iron oxide-supported Au catalyst samples, ranging from those with little or no activity to others with high activities for the CO oxidation reaction. High catalytic activity for the reaction was correlated with the presence of bilayer Au clusters that are ~0.5 nm in diameter and contain only ~10 gold atoms. More recently, Yates *et al.* [79] reported a dual catalytic site, Au-Ti, at the perimeter of 3-nanometer Au particles supported on $TiO_2$ during CO oxidation. The workers used transmission infrared spectroscopy and DFT calculations to conclude that CO molecules on $TiO_2$ sites are initially delivered to the active perimeter sites via diffusion on the $TiO_2$ surface, where they assist O-O bond dissociation and react with oxygen at these perimeter sites. After most of the CO/$TiO_2$ is depleted from $TiO_2$ in the perimeter zone, a small fraction of CO adsorbed on Au (at 120 K) with weaker binding energies and lower diffusion barriers is oxidized. The remaining tightly bonded CO/Au is kinetically isolated from the CO oxidation at 120 K. At higher temperatures, however, the CO on the Au sites becomes more mobile and begins to actively participate in catalytic $CO_2$ production.

Ribeiro *et al.* [80] used a physical model of Au particles on $TiO_2$ to show that corner atoms with fewer than seven neighboring gold atoms are the dominant active sites for the low-temperature WGS reaction. The number of corner sites does not vary as particle size increases above 1 nm, giving the surprising result that the rate per gold cluster is independent of size. Haruta *et al.* [81] found a hydroxide, $AuLa_2(OH)_9$, which was prepared by co-precipitation, showed markedly high catalytic activity for CO oxidation (100% conversion) at temperatures as low as 193 K after reduction at 373 K. The catalyst mainly consists of $Au^0$ clusters smaller than 1.5 nm, which are well-mixed with $La(OH)_3$ containing isolated $Au(OH)_3$ species. It was proposed that the requirement for the size of Au is very strict and the diameter should be far below 2 nm for the CO oxidation activity to be realized.

### 1.2.3 Activation of $H_2O$/OH

In general, it is agreed that both the metal and the support play essential roles in the WGS reaction. Among the two reactants for the WGS reaction, CO and $H_2O$, the latter is more difficult to activate [82] due to its thermodynamic stability. Metals such as Cu and Fe are reported to undergo oxidation by water, thereby activating it [83]. However, Pt or Au does not interact chemically with water because the $PtO_x$ or $AuO_x$ that would be formed is not thermodynamically stable at the WGS reaction temperatures. Thus, for precious-metal based WGS catalysts, a hydrophilic oxide support is essential to adsorb and activate water. Taking the most widely studied Pt-based catalyst as an example, water either re-oxidizes the support oxide after reduction by CO, activated on Pt, or forms hydroxyl groups and completes the catalytic cycle [83].

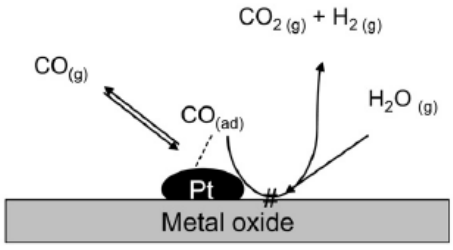


Figure 1.4 The role of the support in the WGS reaction sequence [83]

The exact nature of the relevant intermediates formed and the mechanistic routes for the WGS reaction are still a matter of debate. A regenerative redox mechanism [33, 47, 84-86] and associative (formate) mechanism [44, 87-93] are the two being proposed. For the redox mechanism, the possible elementary steps (1-8) in the WGS reaction are:

$$H_2O + * \leftrightarrow H_2O* \quad (1)$$

$$CO + \# \leftrightarrow CO\# \quad (2)$$

$$H_2O* + * \leftrightarrow OH* + H* \quad (3)$$

$$OH* + * \leftrightarrow O* + H* \quad (4)$$

$$CO\# + O* \leftrightarrow CO_2\# + * \quad (5)$$

$$CO\# + OH* \leftrightarrow CO_2\# + H* \quad (4\text{-}5)'$$

$$H* + H* \leftrightarrow H_2* + * \quad (6)$$

$$CO_2\# \leftrightarrow CO_2 + \# \quad (7)$$

$$H_2* \leftrightarrow H_2 + 2* \quad (8)$$

The mostly likely rate-limiting steps in this reaction are water activation and CO oxidation [94]. With a combination of DFT, micro-kinetic modeling and experiments, Mavrikakis and co-workers find that CO can not only be oxidized by the atomic oxygen, but OH groups also can function as the oxidizing agent, bypassing the total activation of $H_2O$ to atomic oxygen and hydrogen, as shown by step (4-5)'. Indeed, carboxyl is the key intermediate in CO oxidation by OH on Cu (111) [95] and other metallic sites, like Pt (111) [94], while formate acts as a spectator, which is also proved experimentally by Tibiletti *et al.* [96].

In the associative mechanism, instead of step (4) and (5), step (9) and (10) are used in the pathway. Surface formate species has been reported to be the active intermediate, the breaking of C-H bond of formate assigned as the rate limiting step [43, 97]. However despite experimental evidence of surface formate shown by IR it has not been proven that formate is the reaction intermediate. In fact, the formation of formate from CO and OH would involve several bond-breaking and bond-making steps which might involve significant activation energy barriers [94].

$$CO^* + OH^* \leftrightarrow HCOO^{**} \quad (9)$$

$$HCOO^{**} \leftrightarrow H^* + CO_2^* \quad (10)$$

Though there is no agreement for the WGS reaction mechanism yet, the presence of OH is decisively important for both of the reaction pathways discussed above.

A lot of effort has been devoted to understand the activation of the surface OH groups in the WGS reaction. Recently, Davis and co-workers claimed that the lower population of active OH sites on Pt-$MnO_2$ explained the lower CO conversion over Pt-$MnO_2$ relative to Pt-$CeO_2$ for the WGS reaction [98]. The main fraction of the OH groups formed on Pt-$MnO_X$ absorbed at higher wavenumbers than the active bridging OH groups on Pt-$CeO_X$. For Pt-$CeO_2$, the defect-associated bridging OH groups (~ 3650 $cm^{-1}$) are proposed as the major bands and these absorb at lower wavenumbers than the main OH groups on Pt-$MnO_X$ (3682 $cm^{-1}$).

Lefferts and co-workers [5, 99] identified two different types of hydroxyl groups present on monoclinic $ZrO_2$: mono- and multi-coordinated hydroxyls. Mono-coordinated hydroxyls are involved in formate formation, while multi-coordinated hydroxyls are needed for formate decomposition. And these sites can be regenerated by $H_2O$. Platinum is not involved in the formation of formate; but Pt is needed to enable formate decomposition, resulting in the production of $CO_2$ and $H_2$. However, these authors did not discuss the plausibility of their proposed scheme in terms of energetic.

Based on the association mechanism, Davis and co-workers [43] also explained the importance of surface OH groups on Au-$CeO_2$ to form formate intermediates. A bimetallic gold catalyst [100], Au/Pd-$CeO_2$ with good WGS reactivity was studied. It was claimed that the bimetallic promotion may be in facilitating the creation of a defective reduced surface by exerting its local electronic effect on ceria to form the surface geminal-OH groups in water which act as active sites for enhanced WGS activity. Again, this hypothesis has not been tested energetically.

As the activation of OH groups is regarded as a key step in the WGS reaction it may be possible to use supports that do not provide their own oxygen to the reaction, but on which an additive can assist the adsorption of OH in order to study the phenomenon. Besides the

reducible oxides, such as $CeO_2$ [8, 11, 13, 33, 41, 87, 93, 101] and $Fe_2O_3$ [52], largely irreducible oxides such as $ZrO_2$ can be selected as supports to distinguish the role of surface oxygen and hydroxyl groups for the reaction and also minimize or totally eliminate the interaction between the active metals and supports. A large promotion effect of the WGS reaction was recently reported for the alkali group metals [12, 102, 103] added on Pt-$TiO_2$ and Pt-$ZrO_2$ and calls for an explanation.

### 1.2.4 Effect of alkali additives

Alkali additives have been widely used as promoters in industrial catalysts, such as Rh, Pd, and Pt based catalysts, for various reactions, such as the synthesis of ammonia [104, 105], automotive emission control or CO hydrogenation [106-112]. The role of additives is understood either as a structural effect in terms of stabilizing the active metals in a highly dispersed state and suppressing the undesirable sintering, or as an electronic effect, whereby electron enrichment affects the relative adsorption strengths of the reactant species [112, 113].

Recently alkali additives were used to improve the performance of precious metal catalysts towards hydrocarbon oxidation and CO oxidation [114-118]. Pt-$Al_2O_3$ is one of the most widely studied systems. Although the mechanism of such promotion is not fully understood, most literature reports that alkali additives act as an electronic promoter [114-116]. Modeling studies [114-116] have shown that for the CO oxidation reaction the addition of alkali to noble metals can affect the properties of the latter in regard to adsorption of CO and $O_2$: a decrease of the binding energy of CO in chemisorbed state provided an increase of the oxygen coverage on the active site surface, in turn favoring the CO oxidation at lower temperatures. Minemura and co-workers [119] found that for the CO oxidation reaction over alkali metal doped Pt-$Al_2O_3$ the catalytic activity increased with the basicity strength of the added alkali ions, but no satisfactory explanation was given for the effect.

With the increasing interest in the PEM fuel cells, the alkali ions have also been applied to boost the performance of supported catalysts for the reactions involved in fuel processing to produce or upgrade hydrogen streams for this application, such as methanol steam

reforming [120-122], PROX [119, 123-132], and of course, the WGS reaction [102, 103, 133-143]. Some of the early investigations of the latter were of mechanistic nature, and not aimed at the application to PEM fuel cells [133-139].

Addition of alkali ions to precious metal catalysts (Au, Rh, and Pt) [119, 123-130] effectively enhances their activity for the PROX reaction which may be used to further purify the hydrogen stream from CO for fuel cell application (see Figure 1.1). This positive effect of the alkali additive is support-independent and the degree of such promotion strongly depends on the basicity and amount of the additives. However with too strong basicity or over-doping, a negative effect is observed [131, 132]. The promoted performance and the mechanism of such effects were carefully checked over $\gamma$-$Al_2O_3$ supported Pt samples by means of TEM, EXAFS, XANES, and in situ FTIR spectroscopy. The proposed mechanism was that alkali metal weakens the bond of CO with the Pt surface and disrupts the CO monolayer, thus increasing the number of CO-free surface sites for the activation of $O_2$ co-reactants. Rb and Cs cations, which are more electropositive than Na cations, increase the CO oxidation turnover rates more strongly [126]. The effect of alkali addition on the CO adsorption over noble metals has been widely discussed in the literature [144, 145]. Consensus is still lacking, however. For example, Kondarides and co-workers [146] found that the alkali-modified Pt site adsorbed CO stronger, while Kunimori and co-workers [131] reported a weakened adsorption of CO on alkali-modified Pt.

The addition of MgO and $MnO_x$ in Au-$Al_2O_3$ has been reported to improve the CO oxidation activity and selectivity towards $CO_2$ in the PROX reaction [147]. The beneficial effect of MgO was attributed to the stabilization of the small Au particles, which are intrinsically more active in CO and $H_2$ oxidation. $MnO_x$ was thought to be able to supply the active O needed for CO oxidation. Au catalysts containing both MgO and $MnO_x$ were extremely active for the reaction. An earlier work reported by Behm *et al.* [148] claimed that Na impurity from the synthesis, > 0.5 %, would significantly decrease the activity of Au catalysts for the CO oxidation reaction, which is opposite to the reports mentioned above.

In 1981, Amenomiya and co-workers [133] reported that addition of potassium enhanced the high temperature WGS reaction activity of $\gamma$-$Al_2O_3$, and more reducible surface oxygen was found on the modified alumina. The catalytic activity increased with the concentration of $K^+$ ions. They also found that the presence of alkali metals on $Al_2O_3$ increased the formate concentration on the catalyst surface, and the reaction rate was proportional to the surface concentration of the formate ions.

The promotion of the low-temperature WGS reaction by cesium surface doping of Cu-ZnO was reported thereafter [134, 135]. Klier *et al*. [134, 136] suggested that the alkali should be present at concentrations less than a monolayer such that the hydrogen transfer reactions could take place without being impeded. Campbell *et al.* [137] observed a much greater promotion with the Cs addition on the Cu (111) single-crystal surface at a pressure near 40 Torr. The activity of the Cu (111) surface increases with increasing Cs coverage until it reaches a maximum, where the rate is fifteen times that for Cs-free Cu (111). The promotion by Cs is attributed to a mechanism where the surface Cs-O complex participates directly in the dissociation of adsorbed $H_2O$, which is their proposed rate-determining step for the WGS reaction [137]. Later on the same group [138] extended the investigation on the Cs-promoted Cu(110) model catalyst for the same reaction, and claimed that cesium caused an acceleration in water dissociation on the surface and in the conversion of surface oxygen to $CO_2$ by CO. The former reaction is rate-limiting with no Cs present, whereas the latter partially controls the rate on the optimally promoted surface.

An alkali-promotion effect was also reported for the reverse WGS reaction over Cu-$SiO_2$ [149]. After addition of even a small amount of potassium, Cu-$K_2O$-$SiO_2$ clearly had a better catalytic activity than Cu/$SiO_2$. The coverage of formate species increases on Cu-$K_2O$-$SiO_2$ catalyst. $CO_2$-TPD and $H_2$-TPR profiles on Cu-$K_2O$-$SiO_2$ showed that new active sites could be created at the interface between Cu and K. $K_2O$ was thought to provide catalytic activity for the decomposition of formate, besides acting as a promoter for $CO_2$ adsorption.

In 1997, Domka *et al.* [140] showed that addition of most alkali metals (Na, and especially K, Rb, or Cs) to Ru-$\alpha$ or $\delta$–$Fe_2O_3$ led to remarkable improvements in the WGS reaction

rates, the role of the alkali metal was described as stabilizing the structure of the support, in turn, keeping the Ru dispersed.

In 2004, Hagemeyer *et al.* at Honda Motor Co. using combinatorial screening methods, found that alkali ions greatly enhanced the activities of supported Pt and Ru catalysts for both the low and medium temperature WGS reaction [103].

More recently, further investigations of alkali ion modified Pt-$ZrO_2$, $CeO_2$, or $TiO_2$ were performed to address the mechanism of the alkali effect for the WGS reaction [102, 103, 142, 143, 150-152]. With the help of in situ SSITKA-DRIFTS techniques, Davis and co-workers [142, 153] claimed that the alkali ions weakened the C-H bond of the formate, which was proposed to be the rate-limiting step of the low temperature WGS reaction. However, these conclusions are all drawn with the hypothesis of a formate mechanism for the WGS reaction, and under particular reaction conditions. Such analysis has been challenged by others [45, 48, 154]. Also, no detailed analysis of the surface properties of the alkali-modified samples has been done to date, especially during and after the WGS reaction.

Panagiotopoulou *et al.* [150] reported that the low-temperature WGS reaction activity of NM-$TiO_2$ catalysts (NM (noble metal) = Pt, Ru, Pd) can be modified appreciably by addition of small amounts of alkali (X = Li, Na, K, Cs) on the $TiO_2$ support prior to the loading of the noble metals. Added alkali metals interact strongly with the $TiO_2$ surface and result in the creation of $\square_s$–$Ti^{3+}$ defects which, in turn, affect the chemisorptive properties of NM atoms located at the metal-support interface. The formed NM–□s–$Ti^{3+}$ sites were proposed to be the catalytically active sites for the WGS reaction, since they are capable of adsorption and activation of both CO and $H_2O$. Increasing alkali loading results in an increase of the number of these sites. The effects of alkali promotion on the chemisorptive and catalytic properties of NM-$TiO_2$ catalysts were described as a "permanent" strong metal-support interaction effect. With a detailed kinetic and mechanistic study of the (WGS) reaction on a Pt-$TiO_2$ catalyst, the same research group found that the reaction rate increased with an increase in the concentration of CO or $H_2O$ in the feed stream, while it decreased significantly with the addition of $H_2$ in the feed stream. And the alkali loading led to a monotonic decrease (increase) of adsorption

strength of active sites toward hydrogen (carbon monoxide). Therefore, a volcano-type relation exists between the turnover frequency of CO and the chemisorptive strength of NM–□s–$Ti^{3+}$ sites toward hydrogen (or CO). Optimal results are obtained for Na-promoted Pt-$TiO_2$ catalysts with Na:Pt = 1:1, the specific activity (TOF) of which is about three times higher, compared to that of the unpromoted catalyst.

Mallinson and co-workers [151, 152] found that with Na additives, Pt in Pt-$TiO_2$ was more oxidized by Pt electron donation to O in $NaO_x$ through Pt–O–Na. The strong metal–promoter interactions provide highly active sites for the WGS reaction at the periphery of the Pt–$NaO_x$ interface and also inhibit Pt particles from sintering. Na:Pt = 34 was proposed to be the optimum ratio to achieve maximal promotion.

On the other hand, Hwang *et al.* [155] have reported that Na doping on Pt-$CeO_2$ induced negative charge on the Pt species on the basis of XPS and FTIR data. The higher density of the active surface OH population with Na doping was correlated with the enhanced catalytic activity for the WGS reaction.

No promotion effect of the alkali metals for the WGS reaction over supported Au samples has been reported in the literature to date, other than to mention that Au addition in Pt has a negative effect [103]. And recently, Dai and co-workers [156] claimed that the addition of Ca in Au-$TiO_2$ did not promote the activity for the WGS reaction. However, it was beneficial structurally, since it inhibited the sintering of Au after exposure to severe thermal treatments and thus maintained the gold reactivity for the WGS reaction.

In his Master's thesis work [157], Pierre has established that addition of Na (1.5%) into a low-content (<3 wt.%) Pt-$SiO_2$ material rendered the latter a very active low-temperature WGS catalyst, which was as active as Pt-$CeO_2$. This is a new development in the WGS reaction literature, since no previous report exists on the promotion of precious metal supported on an inert support like silica for the WGS reaction. Such exciting results have motivated us to investigate further, whether and how, Na and other alkali metal oxides can influence the catalytic performance of Au or Pt catalysts supported on the inert oxides for the WGS reaction.

## 1.3 Thesis Objectives

As discussed above, PEM fuel cells require highly active and stable WGS reaction catalysts to reduce CO to trace levels in the $H_2$-rich reformate gas. Based on a lot of recent work, supported precious-metal catalysts, especially Pt and Au have emerged as potential candidates for this CO removal process in the PEM fuel cell applications. Attempts are now focused towards the development of low-content robust precious-metal based catalysts which are non-pyrophoric with high activity and good stability to reduce the CO content to less than 5 ppm at low-temperatures in the hydrogen stream [1, 8]. This goal will be met if one understands, to a good extent, what constitutes an active site to elucidate the mechanism of the WGS reaction over the supported precious-metal catalysts.

Previous work done in our lab has demonstrated out that Pt or Au nanoparticles are spectator species for the WGS reaction [8]. Instead Au-O and Pt-O species anchored on ceria or iron oxide have been found active [8, 21, 51, 52]. Both strong metal-support interaction [8] and coordinatively unsaturated sites on small Pt or Au nano-particles have been proposed as crucial to create and stabilize such Pt-O or Au-O species [158, 159]. A lot of effort has been devoted on dispersing and stabilizing the precious metals on the supports by optimizing the synthesis approaches [18, 160-164], and by modifying the supports with various treatments [29, 165, 166] or additives [156, 163].

Since the costs of both precious metals and rare-earth elements are on the rise, rather low precious metal loadings as well as alternative supports are highly desirable. The search for earth-abundant, cheaper supports, which can provide active and stable sites or promote the rate limiting step (*e.g.* activation of OH groups) for the reaction, and do not deactivate during cyclic shutdown-restart operation, is a main research focus in many labs, including ours.

Due to their hydrophilic properties, alkali-ions have been widely studied as promoters for Pt supported on reducible oxides [103, 152]. In his Master's thesis work [157], Pierre found that the Na impurity in an encapsulated Pt material (core-shell structure, $Pt@SiO_2$) with Pt species dispersed in the silica shell rendered the latter a very active low-temperature WGS catalyst, which was as active as $Pt\text{-}CeO_2$. This is a new development in the WGS reaction literature, since no other reported the WGS activity of precious metal

supported on an inert support like silica. From a practical viewpoint, silica is one of the most abundant and low-cost oxides available. These preliminary findings motivated us to further investigate these systems to answer the following questions:

Do all the alkali ions have the same promotion effect for the WGS reaction?

Is the effect structural or electronic? Because of the particular hydrophilic properties of alkali ions do the alkali-modified catalysts promote the reaction by facilitating the regeneration of OH groups?

Can we find a particular trend to predict the effect and to optimize the performance of the catalysts by tailoring the alkali ion:Pt ratio? Is the effect manifested on Au-based WGS catalysts?

By answering the above and related questions, we expect to promote the activity of nanoscale Pt catalysts for the low-temperature WGS reaction, even as we lower the amount of Pt used; while making it more robust to changes in the gas feed composition or preparation method; and expand the choice of supports to earth-abundant materials. Mechanistic studies were carried out to shed light on the promotion effect. DFT calculations were done at University of Wisconsin-Madison to complement the experimental work.

The main objectives of this thesis were:

1. To examine the effect of alkali addition on the properties and reactivity of Pt-based catalysts for the low-temperature WGS reaction.
2. To identify the active sites in the alkali-promoted Pt catalysts for the WGS reaction.
3. To follow the gold structure evolution in Au-$Fe_2O_3$ during the WGS reaction and tailor the activity of the Au-based catalyst by using OH-rich oxide as the supports or using alkali-ions as promoters.

## 1.4 References

[1] R. Farrauto, S. Hwang, L. Shore, W. Ruettinger, J. Lampert, T. Giroux, Y. Liu, O. Ilinich, Annual Review of Materials Research 33 (2003) 1-27.

[2] F.C. Meunier, D. Tibiletti, A. Goguet, D. Reid, R. Burch, Appl. Catal., A 289 (2005) 104-112.

[3] Q. Fu, Thesis (Ph.D.)--Tufts University (2004).

[4] W. Ruettinger, O. Ilinich, R.J. Farrauto, J. Power Sources 118 (2003) 61-65.

[5] K.G. Azzam, I.V. Babich, K. Seshan, L. Lefferts, J. Catal. 251 (2007) 163-171.

[6] D.S. Newsome, Catalysis Reviews-Science and Engineering 21 (1980) 275-318.

[7] T. Tabakova, V. Idakiev, D. Andreeva, I. Mitov, Appl. Catal., A 202 (2000) 91-97.

[8] Q. Fu, H. Saltsburg, M. Flytzani-Stephanopoulos, Science 301 (2003) 935-938.

[9] X. Wang, R.J. Gorte, Appl. Catal., A 247 (2003) 157-162.

[10] Y. Sato, K. Terada, S. Hasegawa, T. Miyao, S. Naito, Appl. Catal., A 296 (2005) 80-89.

[11] G. Jacobs, L. Williams, U. Graham, D. Sparks, B.H. Davis, J. Phys. Chem. B 107 (2003) 10398-10404.

[12] H. Iida, A. Igarashi, Appl. Catal., A 303 (2006) 48-55.

[13] T. Bunluesin, R.J. Gorte, G.W. Graham, Appl. Catal., B 15 (1998) 107-114.

[14] Y. Bi, W. Zhang, H. Xu, W. Li, Catal. Lett. 119 (2007) 126-133.

[15] J.M. Zalc, V. Sokolovskii, D.G. Loffler, J. Catal. 206 (2002) 169-171.

[16] X. Wang, R.J. Gorte, J.P. Wagner, J. Catal. 212 (2002) 225-230.

[17] C.M.Y. Yeung, K.M.K. Yu, Q.J. Fu, D. Thompsett, M.I. Petch, S.C. Tsang, J. Am. Chem. Soc. 127 (2005) 18010-18011.

[18] C.M.Y. Yeung, F. Meunier, R. Burch, D. Thompsett, S.C. Tsang, J. Phys. Chem. B 110 (2006) 8540-8543.

[19] X. Liu, W. Ruettinger, X. Xu, R. Farrauto, Appl. Catal., B 56 (2005) 69-75.

[20] W. Deng, M. Flytzani-Stephanopoulos, Angew. Chem. Int. Ed. 45 (2006) 2285-2289.

[21] D. Pierre, W. Deng, M. Flytzani-Stephanopoulos, Top. Catal. 46 (2007) 363-373.

[22] W. Ruettinger, X. Liu, R.J. Farrauto, Appl. Catal., B 65 (2006) 135-141.

[23] W.F.L. Ruettinger, Xinsheng; Farrauto, Robert J, Enhanced stability water-gas shift reaction catalysts in: U.S.P. Application (Ed.), USA, 2002.

[24] M. Haruta, N. Yamada, T. Kobayashi, S. Iijima, J. Catal. 115 (1989) 301-309.

[25] S. Hiroaki, U. Atsushi, K. Tetsuhiko, H. Masatake, Chem. Commun. 3 (1997) 271-272.

[26] D. Andreeva, I. Ivanov, L. Ilieva, M.V. Abrashev, Appl. Catal., A 302 (2006) 127-132.

[27] D. Andreeva, V. Idakiev, T. Tabakova, A. Andreev, J. Catal. 158 (1996) 354-355.

[28] A. Venugopal, M.S. Scurrell, Appl. Catal., A 258 (2004) 241-249.

[29] J. Hua, K. Wei, Q. Zheng, X. Lin, Appl. Catal., A 259 (2004) 121-130.

[30] Q. Fu, A. Weber, M. Flytzani-Stephanopoulos, Catal. Lett. 77 (2001) 87-95.

[31] T. Tabakova, F. Boccuzzi, M. Manzoli, D. Andreeva, Appl. Catal., A 252 (2003) 385-397.

[32] W. Deng, J.D. Jesus, H. Saltsburg, M. Flytzani-Stephanopoulos, Appl. Catal., A 291 (2005) 126-135.

[33] Y. Li, Q. Fu, M. Flytzani-Stephanopoulos, Appl. Catal., B 27 (2000) 179-191.

[34] J.R. Mellor, A.N. Palazov, B.S. Grigorova, J.F. Greyling, K. Reddy, M.P. Letsoalo, J.H. Marsh, Catal. Today 72 (2002) 145-156.

[35] M.M. Schubert, V. Plzak, J. Garche, R.J. Behm, Catal. Lett. 76 (2001) 143-150.

[36] Y. Denkwitz, A. Karpenko, V. Plzak, R. Leppelt, B. Schumacher, R.J. Behm, J. Catal. 246 (2007) 74-90.

[37] C.H. Kim, L.T. Thompson, J. Catal. 230 (2005) 66-74.

[38] A. Luengnaruemitchai, S. Osuwan, E. Gulari, Catal. Commun. 4 (2003) 215-221.

[39] Q. Fu, W. Deng, H. Saltsburg, M. Flytzani-Stephanopoulos, Appl. Catal., B 56 (2005) 57-68.

[40] A. Goguet, R. Burch, Y. Chen, C. Hardacre, P. Hu, R.W. Joyner, F.C. Meunier, B.S. Mun, D. Thompsett, D. Tibiletti, J. Phys. Chem. C 111 (2007) 16927-16933.

[41] G. Jacobs, L. Williams, U. Graham, G.A. Thomas, D.E. Sparks, B.H. Davis, Appl. Catal., A 252 (2003) 107-118.

[42] G. Jacobs, P.M. Patterson, U.M. Graham, D.E. Sparks, B.H. Davis, Appl. Catal., A 269 (2004) 63-73.

[43] G. Jacobs, S. Ricote, P.M. Patterson, U.M. Graham, A. Dozier, S. Khalid, E. Rhodus, B.H. Davis, Appl. Catal., A 292 (2005) 229-243.

[44] G. Jacobs, S. Ricote, U.M. Graham, P.M. Patterson, B.H. Davis, Catal. Today 106 (2005) 259-264.

[45] D. Tibiletti, A. Goguet, D. Reid, F.C. Meunier, R. Burch, Catal. Today 113 (2006) 94-101.

[46] R. Burch, Phys. Chem. Chem. Phys., 8 (2006) 5483 - 5500.

[47] R.J. Gorte, S. Zhao, Catal. Today 104 (2005) 18-24.

[48] F.C. Meunier, D. Reid, A. Goguet, S. Shekhtman, C. Hardacre, R. Burch, W. Deng, M. Flytzani-Stephanopoulos, J. Catal. 247 (2007) 277-287.

[49] X. Zhao, S. Ma, J. Hrbek, J.A. Rodriguez, Surf. Sci. 601 (2007) 2445-2452.

[50] X. Wang, J. Rodriguez, J. Hanson, D. Gamarra, A. Martínez-Arias, M. Fernández-García, Top. Catal. 49 (2008) 81-88.

[51] W. Deng, A.I. Frenkel, R. Si, M. Flytzani-Stephanopoulos, J. Phys. Chem. C 112 (2008) 12834-12840.

[52] W. Deng, C. Carpenter, N. Yi, M. Flytzani-Stephanopoulos, Top. Catal. 44 (2007) 199-208.

[53] A. Karpenko, R. Leppelt, V. Plzak, R.J. Behm, J. Catal. 252 (2007) 231-242.

[54] C.H. Kim, L.T. Thompson, J. Catal. 244 (2006) 248-250.

[55] P. Panagiotopoulou, D.I. Kondarides, Proceedings of the First Conference of the European Union Coordination Action, Louvain-la-Neuve, Belgium, 2005, 49-52.

[56] H. Iida, A. Igarashi, Appl. Catal., A 298 (2006) 152-160.

[57] D. Andreeva, Gold Bulletin 3 (2002) 82-88.

[58] D. Andreeva, T. Tabakova, V. Idakiev, P. Christov, R. Giovanoli, Appl. Catal., A 169 (1998) 9-14.

[59] D. Andreeva, V. Idakiev, T. Tabakova, L. Ilieva, P. Falaras, A. Bourlinos, A. Travlos, Catal. Today 72 (2002) 51-57.

[60] A.A. El-Moemen, A. Karpenko, Y. Denkwitz, R.J. Behm, J. Power Sources 190 (2009) 64-75.

[61] P. Panagiotopoulou, A. Christodoulakis, D.I. Kondarides, S. Boghosian, J. Catal. 240 (2006) 114-125.

[62] H. Yahiro, K. Murawaki, K. Saiki, T. Yamamoto, H. Yamaura, Catal. Today 126 (2007) 436-440.

[63] E. Fox, A. Lee, K. Wilson, C. Song, Top. Catal. 49 (2008) 89-96.

[64] A. Khan, P.G. Smirniotis, J. Mol. Catal. A: Chem. 280 (2008) 43-51.

[65] W. Liu, M. Flytzanistephanopoulos, J. Catal. 153 (1995) 304-316.

[66] M. Haruta, S. Tsubota, T. Kobayashi, H. Kageyama, M.J. Genet, B. Delmon, J. Catal. 144 (1993) 175-192.

[67] T. Luo, J.M. Vohs, R.J. Gorte, J. Catal. 210 (2002) 397-404.

[68] D. Tibiletti, A.A. Fonseca, R. Burch, Y. Chen, J.M. Fisher, A. Goguet, C. Hardacre, P. Hu, D. Thompsett, J. Phys. Chem. B 109 (2005) 22553-22559.

[69] Z.-P. Liu, S.J. Jenkins, D.A. King, Phys. Rev. Lett. 94 (2005) 196102-196104.

[70] H. Sakurai, T. Akita, S. Tsubota, M. Kiuchi, M. Haruta, Catalysis by Gold 291 (2005) 179-187.

[71] T. Tabakova, F. Boccuzzi, M. Manzoli, J.W. Sobczak, V. Idakiev, D. Andreeva, Appl. Catal., A 298 (2006) 127-143.

[72] X. Wang, J.A. Rodriguez, J.C. Hanson, M. Perez, J. Evans, The Journal of Chemical Physics 123 (2005) 221101-221105.

[73] B. Silberova, M. Makkee, J. Moulijn, Top. Catal. 44 (2007) 209-221.

[74] K.T. Rim, D. Eom, L. Liu, E. Stolyarova, J.M. Raitano, S.-W. Chan, M. Flytzani-Stephanopoulos, G.W. Flynn, The Journal of Physical Chemistry C 113 (2009) 10198-10205.

[75] K.T. Rim, M. Flytzani-Stephanopoulos, G.W. Flynn, ACS Nano submitted (2011).

[76] L.F. Allard, A. Borisevich, W. Deng, R. Si, M. Flytzani-Stephanopoulos, S.H. Overbury, J Electron Microsc (Tokyo) 58 (2009) 199-212.

[77] L.F. Allard, M. Flytzani-Stephanopoulos, S.H. Overbury, Microsc. Microanal. 16 (2010) 375-385.

[78] A.A. Herzing, C.J. Kiely, A.F. Carley, P. Landon, G.J. Hutchings, Science 321 (2008) 1331-1335.

[79] I.X. Green, W. Tang, M. Neurock, J.T. Yates, Science 333 (2011) 736-739.

[80] W.D. Williams, M. Shekhar, W.-S. Lee, V. Kispersky, W.N. Delgass, F.H. Ribeiro, S.M. Kim, E.A. Stach, J.T. Miller, L.F. Allard, J. Am. Chem. Soc. 132 (2010) 14018-14020.

[81] T. Takei, I. Okuda, K.K. Bando, T. Akita, M. Haruta, Chem. Phys. Lett. 493 (2010) 207-211.

[82] M.A. Henderson, Surf. Sci. Rep. 46 (2002) 1-308.

[83] K.G. Azzam, I.V. Babich, K. Seshan, L. Lefferts, J. Catal. 251 (2007) 153-162.

[84] C.V. Ovesen, B.S. Clausen, B.S. Hammershoi, G. Steffensen, T. Askgaard, I. Chorkendorff, J.K. Norskov, P.B. Rasmussen, P. Stoltze, P. Taylor, J. Catal. 158 (1996) 170-180.

[85] G.C. Chinchen, P.J. Denny, J.R. Jennings, M.S. Spencer, K.C. Waugh, Applied Catalysis 36 (1988) 1-65.

[86] C.M. Kalamaras, S. Americanou, A.M. Efstathiou, J. Catal. 279 (2011) 287-300.

[87] G. Jacobs, U.M. Graham, E. Chenu, P.M. Patterson, A. Dozier, B.H. Davis, J. Catal. 229 (2005) 499-512.

[88] A. Goguet, S.O. Shekhtman, R. Burch, C. Hardacre, F.C. Meunier, G.S. Yablonsky, J. Catal. 237 (2006) 102-110.

[89] G. Jacobs, E. Chenu, P.M. Patterson, L. Williams, D. Sparks, G. Thomas, B.H. Davis, Appl. Catal., A 258 (2004) 203-214.

[90] T. van Herwijnen, W.A. de Jong, J. Catal. 63 (1980) 83-93.

[91] D.C. Grenoble, M.M. Estadt, D.F. Ollis, J. Catal. 67 (1981) 90-102.

[92] T. Salmi, R. Hakkarainen, Applied Catalysis 49 (1989) 285-306.

[93] T. Shido, Y. Iwasawa, J. Catal. 141 (1993) 71-81.

[94] L.C. Grabow, A.A. Gokhale, S.T. Evans, J.A. Dumesic, M. Mavrikakis, J. Phys. Chem. C 112 (2008) 4608-4617.

[95] A.A. Gokhale, J.A. Dumesic, M. Mavrikakis, J. Am. Chem. Soc. 130 (2008) 1402-1414.

[96] D. Tibiletti, F.C. Meunier, A. Goguet, D. Reid, R. Burch, M. Boaro, M. Vicario, A. Trovarelli, J. Catal. 244 (2006) 183-191.

[97] S. Ricote, G. Jacobs, M. Milling, Y. Ji, P.M. Patterson, B.H. Davis, Appl. Catal., A 303 (2006) 35-47.

[98] M.C. Ribeiro, G. Jacobs, U.M. Graham, K.G. Azzam, L. Linganiso, B.H. Davis, Catal. Commun. 11 (2010) 1193-1199.

[99] P.O. Graf, D.J.M. de Vlieger, B.L. Mojet, L. Lefferts, J. Catal. 262 (2009) 181-187.

[100] M.a.-A. Hurtado-Juan, C.M.Y. Yeung, S.C. Tsang, Catal. Commun. 9 (2008) 1551-1557.

[101] S. Hilaire, X. Wang, T. Luo, R.J. Gorte, J. Wagner, Appl. Catal., A 215 (2001) 271-278.

[102] J.M. Pigos, C.J. Brooks, G. Jacobs, B.H. Davis, Appl. Catal., A 319 (2007) 47-57.

[103] A.C. Hagemeyer, Raymond E.; Yaccato, Karin; Lesik, Andreas; Brooks, Christopher James;, Alkali-containing catalyst formulations for low and medium temperature hydrogen generation, United States, 2004.

[104] K.-i. Aika, H. Hori, A. Ozaki, J. Catal. 27 (1972) 424-431.

[105] Z. Kowalczyk, J. Sentek, S. Jodzis, E. Mizera, J. Góralski, T. Paryjczak, R. Diduszko, Catal. Lett. 45 (1997) 65-72.

[106] I.V. Yentekakis, R.M. Lambert, M.S. Tikhov, M. Konsolakis, V. Kiousis, J. Catal. 176 (1998) 82-92.

[107] M.P. Kiskinowa, Studies in Surface Science and Catalysis 70 (1992).

[108] F.J. Maldonado, T. Becue, J.M. Silva, M.F. Ribeiro, P. Massiani, M. Kermarec, J. Catal. 195 (2000) 342-351.

[109] N.I. H. Shinjoh, H. Sobukawa, M. Sugiura, N. Kruse, A. Frennet, J.-M. Bastin, , Stud. Surf. Sci. Catal. 116 (1992).

[110] W. Ngantsoue-Hoc, Y. Zhang, R.J. O'Brien, M. Luo, B.H. Davis, Appl. Catal., A 236 (2002) 77-89.

[111] M. Konsolakis, N. Macleod, J. Isaac, I.V. Yentekakis, R.M. Lambert, J. Catal. 193 (2000) 330-337.

[112] M. Konsolakis, I.V. Yentekakis, Appl. Catal., B 29 (2001) 103-113.

[113] T. Kobayashi, T. Yamada, K. Kayano, Appl. Catal., B 30 (2001) 287-292.

[114] N. Pavlenko, P.P. Kostrobij, Y. Suchorski, R. Imbihl, Surf. Sci. 489 (2001) 29-36.

[115] I.N. Yakovkin, G.A. Katrich, A.T. Loburets, Y.S. Vedula, A.G. Naumovets, Prog. Surf. Sci. 59 (1998) 355-365.

[116] L.F. Liotta, G. Deganello, P. Delichere, C. Leclercq, G.A. Martin, J. Catal. 164 (1996) 334-340.

[117] C.H. Lee, Y.W. Chen, Ind. Eng. Chem. Res. 36 (1997) 1498-1506.

[118] Y. Minemura, S.-i. Ito, T. Miyao, S. Naito, K. Tomishige, K. Kunimori, Chem. Commun. 11 (2005) 1429-1431

[119] Y. Minemura, M. Kuriyama, S.-i. Ito, K. Tomishige, K. Kunimori, Catal. Commun. 7 (2006) 623-626.

[120] H. Evin, G. Jacobs, J. Ruiz-Martinez, U. Graham, A. Dozier, G. Thomas, B. Davis, Catal. Lett. 122 (2008) 9-19.

[121] P.O. Graf, B.L. Mojet, L. Lefferts, Appl. Catal., A 362 (2009) 88-94.

[122] P.O. Graf, B.L. Mojet, L. Lefferts, Appl. Catal., A 346 (2008) 90-95.

[123] H. Tanaka, S.-i. Ito, S. Kameoka, K. Tomishige, K. Kunimori, Appl. Catal., A 250 (2003) 255-263.

[124] S.-i. Ito, H. Tanaka, Y. Minemura, S. Kameoka, K. Tomishige, K. Kunimori, Appl. Catal., A 273 (2004) 295-302.

[125] M. Kuriyama, H. Tanaka, S.-i. Ito, T. Kubota, T. Miyao, S. Naito, K. Tomishige, K. Kunimori, J. Catal. 252 (2007) 39-48.

[126] C. Pedrero, T. Waku, E. Iglesia, J. Catal. 233 (2005) 242-255.

[127] B. Mirkelamoglu, G. Karakas, Appl. Catal., A 299 (2006) 84-94.

[128] N. Iwasa, S. Arai, M. Arai, Appl. Catal., B 79 (2008) 132-141.

[129] F. Wang, G. Lu, Catal. Lett. 115 (2007) 46-51.

[130] L.-H. Chang, Y.-W. Chen, N. Sasirekha, Ind. Eng. Chem. Res. (2008).

[131] H. Tanaka, M. Kuriyama, Y. Ishida, S.-i. Ito, T. Kubota, T. Miyao, S. Naito, K. Tomishige, K. Kunimori, Appl. Catal., A 343 (2008) 125-133.

[132] H. Tanaka, M. Kuriyama, Y. Ishida, S.-i. Ito, K. Tomishige, K. Kunimori, Appl. Catal., A 343 (2008) 117-124.

[133] Y. Amenomiya, G. Pleizier, J. Catal. 76 (1982) 345-353.

[134] K. Klier, C.W. Young, J.G. Nunan, Ind. Eng. Chem. Fund. 25 (1986) 36-42.

[135] C.T. Campbell, B.E. Koel, Surf. Sci. 186 (1987) 393-411.

[136] K. Klier, Catal. Today 15 (1992) 361-382.

[137] C.T. Campbell, B.E. Koel, K.A. Daube, J. Vac. Sci. Technol., A 5 (1987) 810-813.

[138] J.M. Campbell, J. Nakamura, C.T. Campbell, J. Catal. 136 (1992) 24-42.

[139] J. Nakamura, J.M. Campbell, C.T. Campbell, J. Chem. Soc., Faraday Trans. 86 (1990) 2725 - 2734.

[140] A. Basinska, F. Domka, Catal. Lett. 43 (1997) 59-61.

[141] A. Basinska, W.K. Jozwiak, J. Goralski, F. Domka, Appl. Catal., A 190 (2000) 107-115.

[142] H. Evin, G. Jacobs, J. Ruiz-Martinez, G. Thomas, B. Davis, Catal. Lett. 120 (2008) 166-178.

[143] E. Chenu, G. Jacobs, A.C. Crawford, R.A. Keogh, P.M. Patterson, D.E. Sparks, B.H. Davis, Appl. Catal., B 59 (2005) 45-56.

[144] S. Derrouiche, P. Gravejat, B. Bassou, D. Bianchi, Appl. Surf. Sci. 253 (2007) 5894-5898.

[145] P.A.J.M. Angevaare, H.A.C.M. Hendrickx, V. Ponec, J. Catal. 110 (1988) 11-17.

[146] P. Panagiotopoulou, D.I. Kondarides, J. Catal. 260 (2008) 141-149.

[147] R.J.H. Grisel, B.E. Nieuwenhuys, J. Catal. 199 (2001) 48-59.

[148] B. Schumacher, V. Plzak, M. Kinne, R.J. Behm, Catal. Lett. 89 (2003) 109-114.

[149] C.-S. Chen, W.-H. Cheng, S.-S. Lin, Appl. Catal., A 238 (2003) 55-67.

[150] P. Panagiotopoulou, D.I. Kondarides, J. Catal. 267 (2009) 57-66.

[151] X. Zhu, T. Hoang, L. Lobban, R. Mallinson, Catal. Lett. 129 (2009) 135-141.

[152] X. Zhu, M. Shen, L.L. Lobban, R.G. Mallinson, J. Catal. 278 (2011) 123-132.

[153] J.M. Pigos, C.J. Brooks, G. Jacobs, B.H. Davis, Appl. Catal., A 328 (2007) 14-26.

[154] F.C. Meunier, A. Goguet, C. Hardacre, R. Burch, D. Thompsett, J. Catal. 252 (2007) 18-22.

[155] K.-r. Hwang, S.-k. Ihm, J.-s. Park, Fuel Process. Technol. 91 (2010) 729-736.

[156] Z. Ma, H. Yin, S. Dai, Catal. Lett. 136 (2009) 83-91.

[157] D. Pierre, M.S., Tufts University, 2006.

[158] I.N. Remediakis, N. Lopez, J.K. Nørskov, Angew. Chem. 117 (2005) 1858-1860.

[159] T. Tabakova, F. Boccuzzi, M. Manzoli, J.W. Sobczak, V. Idakiev, D. Andreeva, Appl. Catal., B 49 (2004) 73-81.

[160] R. Zanella, L. Delannoy, C. Louis, Appl. Catal., A 291 (2005) 62-72.

[161] R. Zanella, C. Louis, Catal. Today 107-108 (2005) 768-777.

[162] A.K. Medina-Mendoza, M.A. Cortes-Jacome, J.A. Toledo-Antonio, C. Angeles-Chavez, E. Lopez-Salinas, I. Cuauhtemoc-Lopez, M.C. Barrera, J. Escobar, J. Navarrete, I. Hernandez, Appl. Catal., B 106 (2011) 14-25.

[163] D. Andreeva, I. Ivanov, L. Ilieva, M.V. Abrashev, R. Zanella, J.W. Sobczak, W. Lisowski, M. Kantcheva, G. Avdeev, K. Petrov, Appl. Catal., A 357 (2009) 159-169.

[164] J. Radnik, L. Wilde, M. Schneider, M.M. Pohl, D. Herein, J. Phys. Chem. B 110 (2006) 23688-23693.

[165] J.H. Kwak, J. Hu, D. Mei, C.-W. Yi, D.H. Kim, *e. al.*, Science 325 (2009) 1670-1673.

[166] F. Menegazzo, F. Pinna, M. Signoretto, V. Trevisan, F. Boccuzzi, A. Chiorino, M. Manzoli, ChemSusChem 1 (2008) 320-326.

# Chapter 2 Experimental Procedures

## 2.1 Catalyst Preparation

### 2.1.1 Incipient wetness impregnation (IMP)

Impregnation is a common technique used to prepare precious metal-based catalysts. However, catalyst properties such as dispersion and morphology are influenced by the properties of the impregnating solution (i.e. volume, pH, and temperature). Due to the nature of the synthesis it is difficult to obtain both high loading and high dispersion in one step, and typically the impregnation with excess solutions requires several steps. An alternative approach is the incipient wetness impregnation (IMP), whereby in one step a measured amount of aqueous solution (the volume of the solution is equal to the pore volume of the oxide support) carrying the required metal ion concentration is added drop wise (or by spray drying industrially) to fill the pore volume of the solid. One disadvantage of such technique, however, is that control of the metal particle size and location on the support is more difficult, which leads to the non uniformity of structures. The solution-based preparation techniques, such as co-precipitation can maximize the metal-support interaction to reach a more uniform Pt-$CeO_2$ structure [1, 2]. While because of the weak interaction between platinum and $SiO_2$, the solution-based preparation techniques would lead to an ultra low Pt-loading.

IMP was used here to prepare Pt-$SiO_2$ and Pt-$Al_2O_3$ materials. Typically, the commercial support, $\gamma$-$Al_2O_3$ (Condea alumina, $S_{BET}$=210 $m^2$/g, pore volume: 0.55 ml/g) or $SiO_2$ (Sigma-Aldrich, fumed, $S_{BET}$=243 $m^2$/g, pore volume: 3 ml/g), was impregnated with an aqueous solution of the metal precursor, tetraammineplatinum (II) nitrate ($Pt(NH_3)_4(NO_3)_2$, Sigma-Aldrich, 99.995% trace metals basis). The volume of the solution was equal to the pore volume of the support. The wet powder was dried under vacuum at 60 $^oC$ overnight.

Na (K) ions were added to the dried samples also by IMP using sodium or potassium nitrate as the precursor (Sigma-Aldrich). To check the effect of the loading sequence of Pt and Na (K), Na (K) ions were added before or after loading Pt or co-impregnated with Pt.

These samples are denoted as αPt-βNa/K-$SiO_2$, where α and β are the atomic percentage of Pt and Na (K) respectively, they were calculated as:

$$\alpha\% = \frac{Pt\ mol}{Pt\ mol + Na\ mol + Si\ mol} \times 100\%$$

$$\beta\% = \frac{Na\ mol}{Pt\ mol + Na\ mol + Si\ mol} \times 100\%$$

### 2.1.2 Deposition-precipitation (DP)

To investigate the influence of preparation methods and the impregnation sequence on the catalyst performance, a Pt-$SiO_2$ sample was prepared by deposition–precipitation (DP). The procedure was carried out by the following steps:

1) Suspending the fumed $SiO_2$ in powder form in 500 ml de-ionized water (D.I. water) at room temperature.
2) Adjusting the pH of the suspension at 9 by adding 1 M ammonium carbonate with vigorous stirring at room temperature.
3) Dissolving the desired amount of Pt precursor, $Pt(NH_3)_4((NO_3)_2$, in D.I. water at room temperature, and adding the solution drop wise into the slurry of $SiO_2$. The pH=9 was maintained with the aid of 1M $(NH_4)_2CO_3$.
4) Upon completion, aging the mixture at room temperature for 1 h.
5) Filtering and washing the precipitate with sufficient amount of D.I. water at 60 $^oC$ three times.
6) Drying the solid sample at 60 $^oC$ under vacuum overnight, referred as Pt-$SiO_2$.

Different amounts of Na (K) ions were used to modify the dried Pt-$SiO_2$ sample with an aqueous solution of $NaNO_3$ ($KNO_3$) by the IMP method as described above, followed by drying under vacuum at 60 $^oC$ overnight. These samples were denoted as αNa (K)-Pt-$SiO_2$. Na- or K-modified $SiO_2$ and $Al_2O_3$ supports were prepared by the IMP method as well and denoted as αNa (K)-$SiO_2$ ($Al_2O_3$), where α was the atomic percentage of Na (K) and the calculation of α was the same as described by the above equation.

Prior to testing, all samples were calcined in air at 400 $^{o}$C for 4 h. A heating rate of 2 $^{o}$C/min from room temperature to 400 $^{o}$C was used.

## 2.2 Water washing treatment

Selected, calcined Na-modified samples were suspended in D.I. water to remove Na ions. If there was no Na association with the dispersed Pt species, the washing would remove all Na (or other alkali additive) from the surface of the support (silica or alumina). The sample in powder form was suspended in sufficient amount of D.I. water to create a dilute suspension.

1) To study the influence of washing time on the Na removal, the suspension was stirred at room temperature for 1, 5, 20, or 60 min, respectively.
2) To investigate the influence of temperature on the Na removal, some samples were washed with D.I. water at 70 $^{o}$C for 60 min.

This was followed by filtering the suspension and drying the solid at 60 $^{o}$C under vacuum overnight, further calcining it in static air at 400 $^{o}$C for 4 h before testing. A heating rate of 2 $^{o}$C/min from room temperature to 400 $^{o}$C was used.

## 2.3 Catalytic activity tests

### 2.3.1 Steady-state WGS reaction activity

Steady-state WGS reaction light-off tests and measurements of kinetics were conducted at atmospheric pressure in a packed-bed flow micro reactor. The reactant gases, all certified calibration gas mixtures with helium (Airgas), were controlled by mass flow rate controllers and mixed prior to the reactor inlet. Water was injected into the flowing gas stream by a calibrated syringe pump and vaporized in the heated gas line before entering the reactor. A water condenser in ice bath was installed after the reactor exit. The inlet and outlet gas streams were analyzed using an HP-5890 gas chromatograph (GC) equipped with a thermal conductivity detector (TCD). Typically 0.1g catalyst was used for each test. The wet feed gas composition for the WGS tests was either the product-free gas, 2%CO-

10%$H_2O$-He (70 ml/min) or the full reformate gas, 11%CO-26%$H_2O$-26%$H_2$-7%$CO_2$-He (207 ml/min), the latter used for the kinetics measurements, with the reactor operated in a differential mode keeping the CO conversion below 15%.

The percent CO conversion ($X_{CO}$) was determined by:

$$X_{CO}(\%) = \frac{CO^{in} - CO^{out}}{CO^{in}} \times 100\%$$

The production rate of $CO_2$ was used to calculate the reaction rate:

$$Rate = \frac{N_t^{out} \times CO_2^{out} - N_t^{in} \times CO_2^{in}}{W_{cat}} (^{mol}/_{g.s})$$

Where $N_t^{in}$ or $N_t^{out}$ was the total molar flow rate in mol/s of the dry feed or product gas stream. $CO^{in}$, $CO^{out}$, $CO_2^{in}$, or $CO_2^{out}$ was the molar fraction of CO or $CO_2$ in the dry feed or product gas stream, and the $W_{cat}$ was the amount of catalyst loading in grams. Since $N_t^{out}$ can not be monitored continuously, it is expressed based on carbon mass balance as,

$$N_t^{out} = N_t^{in} \times \frac{CO_2^{in} + CO^{in}}{CO_2^{out} + CO^{out}}$$

Where $N_t^{in}$ was constant and measured before reaction, the concentrations of CO and $CO_2$ were measured by GC. The rate is based on CO consumption being equal to the rate of $CO_2$ production. There was no methane formed under the conditions of the tests performed here.

### 2.3.2 Temperature-programmed surface reaction (TPSR)

The temperature-programmed surface WGS reaction (TPSR) was used to probe the surface reactivity of the catalyst dynamically. The onset temperature of reaction is followed by the first appearance of $H_2$ product. Testing was performed in a Micromeritics AutoChem II 2920 apparatus. The sample was degassed in He at room temperature for 30 min, and then exposed to 5%CO-3%$H_2O$-He, 30 ml/min. Water was introduced by passing diluted CO gas through a vapor generator, which was set at room temperature. The sample was heated

from room temperature to 350 $^{o}$C at 10 $^{o}$C/min in 5%CO-3%$H_2O$-He. The composition of the outlet gas was monitored by an on-line residual gas analyzer (SRS, RGA 200).

### 2.3.3 Catalyst stability tests

Long-term isothermal stability tests of catalysts for the WGS reaction were conducted at atmospheric pressure in a heated quartz tube microreactor containing the catalyst powder as a packed-bed. The feed and product gas streams were analyzed by a HP-5890 GC equipped with a TCD. The WGS reaction gas composition was a simulated (autothermal reforming) reformate gas composition comprising 11%CO–26%$H_2O$-26%$H_2$–7%$CO_2$-He (207 ml/min); with He used instead of $N_2$.

## 2.4 Catalyst characterization

### 2.4.1 Surface area measurements

The BET surface area of each sample was measured by single-point $N_2$ adsorption/desorption cycles in a Micromeritics AutoChem II 2920 apparatus. Each sample was degassed in He at 250 $^{o}$C for 30 min before the adsorption. A 30%$N_2$-He gas mixture was used in the BET measurement.

### 2.4.2 Catalyst composition

Bulk composition and element concentrations of the catalysts were analyzed by inductively coupled plasma atomic emission spectrometry (ICP-OES). The silica- or alumina-supported samples were tested in EAGLABS (NY), where the ICP-OES is equipped with a HF-resistant torch. The silica or alumina-supported catalyst powder was dissolved in the diluted HF solution (A.C.S. reagent). The solution was further diluted before ICP tests. The Au-based catalysts were dissolved in the diluted HCl-$H_2O_2$ mixture and analyzed by ICP-OES (Perkin Elmer Plasma 40) in the Department of Chemistry, Tufts University.

### 2.4.3 CO Chemisorption

CO chemisorption tests were carried out at 25 $^{o}$C to characterize the surface Pt dispersion in the Micromeritics AutoChem II 2920 instrument equipped with a TCD. Pretreatment was in 10%$H_2$-Ar at 350 $^{o}$C for 2 h, followed by cooling down to room temperature in He. A linear CO adsorption on Pt (CO:Pt=1:1) was assumed for the Pt dispersion calculation [3].

### 2.4.4 Electron microscopy

The development of the electron microscopy and related micro-analytical techniques has allowed comprehensive structural and chemical analysis of catalysts at a submicron or even atomic scale. It can also provide information on the elemental composition of the particles (EDS), for example by detecting the X-rays which are produced by the interaction of electrons with the matter or by analyzing the way the electrons are diffracted [4]. X-ray fluorescence can be used for elemental analysis, but this technique was not employed in this thesis work.

High resolution transmission electron microscopy (HRTEM) was used to study the structure and morphology of the supported precious metal catalysts. HRTEM is useful to measure the size of supported metal crystallites and changes in their size, shape, and position with catalyst use. In this work, HRTEM data were collected on a JEOL 2010 instrument (MIT CSME facility) with an ultimate point-to-point resolution of 1.9 Å and lattice resolution of 1.4 Å. The sample powder was suspended in isopropyl alcohol using an ultrasonic bath and deposited on a carbon coated 200 mesh Cu grid.

To investigate Pt particle sizes and morphologies at the atomic level, high angle annular dark field (HAADF) imaging was done with aberration-corrected scanning transmission electron microscopy (STEM) on a Zess Linra 200-80 MC operating at 200 kV with the detector acceptance angle for the imaging of 24 mRad. The microscopy is located at the Center for Nanoscale Systems, Harvard University. The samples were suspended in high purity ethanol and loaded on lacey carbon coated 300 mesh Cu grids (TED PELLA INC.).

### 2.4.5 X-ray diffraction (XRD)

XRD analysis was used in this work to identify the crystalline phase and crystal particle size based on the diffraction peak position and pattern. XRD patterns were recorded on a Rigaku RU300 X-ray generator (MIT CSME facility) with a 185 mm diffractometer, using copper Kα1 radiation ($\lambda$ = 1.5406 Å). The voltage and current were set to 50 kV and 300 mA, respectively.

### 2.4.6 X-ray photoelectron spectroscopy (XPS)

A Kratos AXIS Ultra Imaging XPS (MIT CSME facility) was used to determine the atomic metal ratios of the elements on the surface region and the oxidation state of precious metals in selected catalysts. Samples in powder form were pressed on a double-sided adhesive copper tape for analysis. All measurements were carried out at room temperature without any pre-treatment. An Al $K_\alpha$ X-ray source was used in this work. The X-ray generator power was typically set at 15 kV and 10 mA.

A broad scan survey spectrum is from 1100 to 0 eV binding energy (BE). The resolution ΔE is 3.2 eV for the analyzer with the pass energy of 160 eV for the survey, while the higher resolution ΔE 0.1 eV (with the pass energy 40 eV) was used for the oxidation state analysis. The surface composition of each element is obtained by the peak area integration using the high resolution scan data. An approximate and general expression for the calculation of the atomic fraction of, $C_x$, of any constituent, x, in a sample is given by:

$$C_x = \frac{I_x/S_x}{\sum_i \mathrm{I_i}/\mathrm{S_i}}$$

where I is the peak area of a specific peak for certain element and S is the atomic sensitivity factor that is usually provided in the instrument manual.

The identification of the oxidation states for the studied element depends primarily on the accurate determination of line energies. Since the C1s peak from adventitious hydrocarbons present on the samples was found in all the measurements, it was used as internal standard for the charge correction. Therefore, all the binding energies were aligned to the C1s peaks at 285.0 eV.

### 2.4.7 X-ray absorption spectroscopy (XAS)

The electronic and structural properties of the precious metal-based catalyst system were examined with X-Ray absorption experiment, including X-ray absorption near edge spectroscopy (XANES) and extended X-ray absorption fine structure (EXAFS). In this X-ray absorption experiment, a monochromatic X-ray beam is directed at the sample. The photon energy of the X-rays is gradually increased such that it traverses one of the absorption edges of the element (*e.g.* Pt) within. Below the absorption edge, the photons cannot excite the electrons of the relevant atomic level and thus absorption is low. However, when the photon energy is just sufficient to excite the electrons, then a large increase in absorption occurs which is known as the absorption edge. Some spectra show a sharp feature at the top of the sharply rising part of the spectrum. This feature is called the white line, which can reflect the electron deficiency of the element [5]. The resulting photoelectrons have a low kinetic energy and can be backscattered by the atoms surrounding the center atom. The probability of backscattering is dependent on the energy of the photoelectrons. The backscattering of the photoelectron affects whether the X-ray photon is absorbed in the first place. Hence, the probability of X-ray absorption will depend on the photon energy (as the photoelectron energy will depend on the photon energy). The net result is a series of oscillations on the high photon energy side of the absorption edge. These oscillations can be used to determine the atomic number, distance and coordination number of the atoms surrounding the element whose absorption edge is being examined [5]. The XAS experiments were run with the synchrotron radiation at National synchrotron Light Source, Brookhaven National Lab (NSLS, BNL).

For experiments using the near edge region (up to 40 eV above the edge), the name XANES usually applies. XANES can provide information about vacant orbits, electronic configuration and site symmetry of the absorbing atom. The absolute position of the edge contains information about the oxidation state of the absorbing atom. The intensity of the white line directly reflects the electron deficiency of the absorbing atom [6].

In this work, XANES was employed to examine the oxidation state of Pt in various samples when exposed to different gas atmosphere. The in-situ XANES spectra were

collected in the transmission mode over selected samples under isothermal WGS reaction condition (1%CO–3%$H_2O$-He, at 275 $^oC$) or $H_2$-reduction at the X18A and X19A beam line of NSLS at BNL. The samples were loaded in a multi-sampler, which allows loading six samples simultaneously. The scheme of the setup is shown in Figure 2.1. The samples were pelletized in the holes of the multi-sampler. This enables comparison of the samples under exactly the same conditions. The X-ray absorption edge energy was calibrated with Pt foil at 11.564 keV. The reported XANES data are the averages of three scans (lasting approximately 15 min/scan), and no changes were detected between the first and last scan.

Quick-XANES was also used to check the dynamic changes of Pt oxidation state during the temperature-programmed surface reaction of WGS or $H_2$ reduction at the X18A beam line of NSLS at BNL.

XANES was also conducted over selected gold-iron oxide samples under the WGS reaction and re-oxidation conditions. The spectra were collected with the beam line X18B of NSLS at BNL. For the ex-situ XANES experiment, each catalyst was pressed on a Kapton tape as a thin film. For the in-situ experiment, the sample was loaded into a polyimide tube reactor with quartz wool blocking both ends of catalysts bed to prevent the movement of the catalyst powder, only allowing the gas flowing through the tube. The spectra were taken in the fluorescence mode with a Ge 13-element detector. The detector was placed at a position at $90^o$ with respect to the incident beam. The sample was placed at $45^o$ both to the incident beam and the Ge detector. The reported data were the averages of 15 scans (lasting approximately 30 min/scan), and no detectable changes were detected between the first and the last scan [7].

The analysis and modeling were done by using Athena and Artemis programs [8-10].

### 2.4.8 Temperature-programmed reduction (TPR)

TPR is the technique in which a surface reduction is monitored while the temperature increases linearly with time.

$H_2$-TPR technique can be used to obtain qualitative and quantitative information on the oxidation state of the reducible species and intrinsic information correlating with the

catalyst reducibility. In this work $H_2$-TPR was run in the Micromeritics AutoChem II 2920 instrument equipped with a TCD. The samples were pre-oxidized in a 10%$O_2$-He gas mixture (50 $cm^3$/min) at 350 $^oC$ for 30 min, cooled to room temperature in He, purged at room temperature for 30 min, then heated in 20%$H_2$-$N_2$ (50 $cm^3$/min) from room temperature to the target temperatures at 5 $^oC$/min. A cold trap at 0 $^oC$ was placed in the gas line upstream of the TCD to remove the water vapor.

CO-TPR was used to sample the different surface oxygen species by products from the reduction, for example,

$$CO + O^* \rightarrow CO_2$$

$$CO + OH \rightarrow CO_2 + \frac{1}{2}H_2$$

CO-TPR was also performed in the Micromeritics AutoChem II 2920 instrument coupled with a RGA (SRS, RGA 200). The samples were pre-oxidized in a 10%$O_2$-He gas mixture (50 $cm^3$/min) at 350 $^oC$ for 30 min, cooled to room temperature in He, purged at room temperature in He for 30 min, then heated in 5%CO-He (30 $cm^3$/min) from room temperature to the target temperatures at 5 $^oC$/min.

If doing cyclic CO-TPR without any treatment in between, after the first reduction run, the sample was cooled down to room temperature in He, and then the next CO-TPR cycle was conducted similar to the first run.

If doing cyclic CO-TPR with a water-treatment, after the first reduction run, the sample was cooled down to room temperature in He, then exposed to 3%$H_2O$-He (30 $cm^3$/min) and kept for 30 min. Here the He gas stream was passed through a bubbler filled with water at room temperature and saturated with $H_2O$ vapor (~3%) before flowing to the reactor. After further He purge, the next CO-TPR cycle was conducted similar to the first run.

### 2.4.9 Diffuse reflectance Fourier transform spectroscopy (DRIFTS)

The DRIFTS measurements were designed to identify the possible reaction intermediates over alkali-modified Pt-$SiO_2$ catalysts for the WGS reaction. They were conducted by Prof.

Frederick Meunier at CNRS, University of Caen, France. A diffuse reflectance reaction cell from Spectra-Tech fitted with KBr windows was used (picture and scheme given in Figure 2.2). Between 5 and 10 mg of sample were deposited in the crucible, on top of a quartz wool layer. 2%CO-6%$H_2O$ (-26%$H_2$ if any) -$N_2$-Ar was passed over the sample. Water was introduced via a saturator kept at 55 °C (vapor pressure = 160 mBar) swept by a flow of Ar and then diluted by other gases. Total flowrate was 30 sccm.

Surface spectra (DRIFTS) and gas-phase spectra (FTIR gas-cell located after the DRIFTS cell) were collected sequentially, while the RGA signal was continuously recorded for a qualitative monitoring.

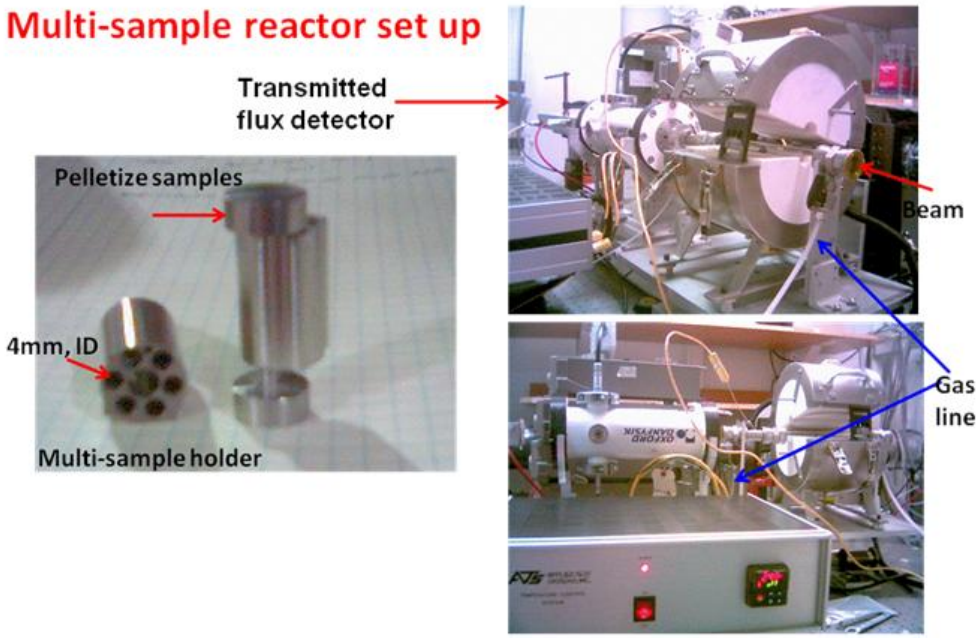


Figure 2.1 Scheme of the multi-sample reactor setup for the XAS analysis at X19A/18A, NSLS, Brookhaven National Lab.

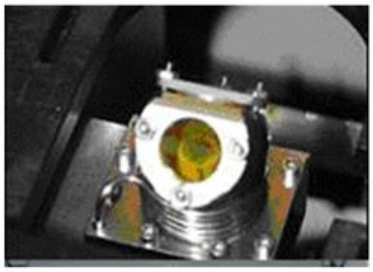

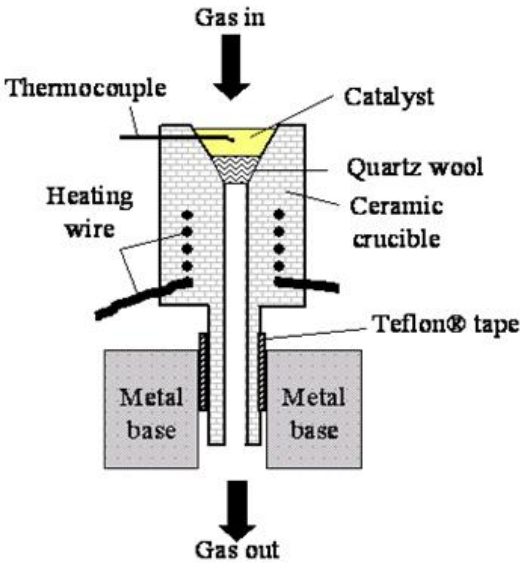


Figure 2.2 Scheme and configuration of the DRIFTS measurement setup at Prof. F. Meunier's laboratory, Caen University, Caen, France.

## 2.5 References

[1] D. Pierre, M.S., Tufts University, 2006.

[2] D. Pierre, W. Deng, M. Flytzani-Stephanopoulos, Top. Catal. 46 (2007) 363-373.

[3] S. Derrouiche, P. Gravejat, B. Bassou, D. Bianchi, Appl. Surf. Sci. 253 (2007) 5894-5898.

[4] F. Delannay, Characterization of Heterogeneous Catalysts, Dekker, New York, 1984.

[5] M. Newville, Fundamentals of XAFS, Consortium for Advanced Radiation Sources, University of Chicago, Chicago, IL, 2004.

[6] W. Deng, PhD, Tufts University, 2007.

[7] W. Deng, A.I. Frenkel, R. Si, M. Flytzani-Stephanopoulos, J. Phys. Chem. C 112 (2008) 12834-12840.

[8] M. Newville, Journal of Synchrotron Radiation 8 (2001) 322-324.

[9] M. Newville, IFEFFIT, http://cars9.uchicago.edu/ifeffit/, 2009.

[10] B. Ravel, M. Newville, Journal of Synchrotron Radiation 12 (2005) 537-541.

# Chapter 3 Alkali-promoted Pt catalysts for the low temperature WGS reaction

## 3.1 Introduction

In order to tailor and optimize the performance of the catalysts, the importance of precious metal and oxide support interaction has been recognized and investigated extensively in the literature for hydrogenation reactions, the WGS reaction, CO and hydrocarbon oxidations [1-7]. While conventional preparation techniques like deposition precipitation or co-precipitation can not give the level of control required to systematically investigate the metal-support interaction and to maximize the metal-support interface, novel techniques are continually considered and applied. A novel synthesis approach was recently used, demonstrating and maximizing the interaction between Pt and ceria, as reported by Yeung *et al.* [8]. Encapsulation of platinum particles inside a nanoscale shell of ceria was achieved by a reverse microemulsion technique. The resulting material showed excellent activity for the WGS reaction, while the undesired methanation reaction was suppressed by not exposing the metallic Pt sites.

Regarding the price and the availability of rare-earth oxides, it would be desirable to find alternatives to ceria and other rare-earth oxides as supports for the precious metals. It is possible that by using suitable additives on non-reducible oxide supports, such as alumina, the activity of Pt-supported on alumina may be boosted to the levels reported for the Pt-ceria system, *e.g.* for the WGS reaction. As stated in Chapter 1, this is a major hypothesis of this thesis work. In early 1980s, Amenomiya and co-workers reported that addition of potassium rendered γ–alumina a high-temperature WGS reaction catalyst by introducing reducible oxygen species on the γ-alumina surface [9]. Alkali promotion was extended recently to Pt-based catalysts for the low-temperature WGS reaction with reducible or partially reducible oxides as the support, *e.g.* titania [10, 11], zirconia [12], and ceria [13]. Davis and workers [14, 15] claimed that the alkali ions weakened the C-H bond for the formate, which was proposed to be the rate-limiting step of the low temperature WGS reaction. Panagiotopoulou *et al.* [11] and Zhu *et al.* [10, 16] reported that alkali additives

favored the dispersion of Pt and creating more defects on titania, leading to more active site for the WGS reaction. However, these interpretations are complicated by the nonzero activity of the alkali-free state of the catalyst.

In his Master's thesis work at Tufts, D. Pierre [17] followed the same approach as Yeung *et al.* [8] to prepare encapsulated Pt particles within a shell of various oxides to evaluate their catalytic performance for the WGS reaction. During the synthesis of Pt@$SiO_2$ which was going to be a blank, zero-activity material, Pierre found measurable activity. In fact, the activity he measured was comparable to Pt-$CeO_2$ catalysts [18]. By examining all the possible causes for this unexpected activity, Pierre found the presence of Na, as the reason. NaOH was used in the synthesis of Pt particles. Thus, alkali ions, *e.g.* $Na^+$, activated the Pt species for the reaction. The steady-state WGS reaction performance of the Pt-Na@$SiO_2$ is shown in Figure 3.1, while Pt-$SiO_2$ is barely active [17]. Pt clusters were found dispersed in the silica shell, hence accessible by the gases. They could also be promoted by the addition of a small amount (2 wt%) of ceria, as demonstrated by Pierre [17].

This exciting finding, motivated the early work of the present thesis, namely, if alkali promotion could be used to activate Pt on an inert support, such as silica, what was the underlying reason? And could this approach be used to activate Pt on other supports, such as alumina, zeolites, *etc.*? Indeed, could we envision that addition of alkali metals be used to render Pt-$\gamma$-$Al_2O_3$ as active as Pt-$CeO_2$ for the WGS reaction? The main reason for using ceria as a support of Pt in the three-way automotive exhaust, is the roughly 2 orders of magnitude higher activity of Pt-$CeO_2$ over Pt-$Al_2O_3$ as shown by many literature reports, most notably by the early finding of Gorte and his group in the late 1990s [19]. Finally, assuming the activity improvement could be realized, it is important to determine how stable are these catalysts under realistic WGS conditions; and find ways to improve their stability, if found lacking.

These are the major issues addressed in this chapter of the thesis. Mechanistic questions are addressed in Chapter 4.

## 3.2 Materials and Methods

0.6 at.% Pt-$Al_2O_3$ catalyst prepared by IMP, is denoted as 0.6Pt-$Al_2O_3$. 1.0 at.% Pt-$SiO_2$ sample prepared by DP, is referred as 0.8Pt-$SiO_2$. The preparation procedures were detailed in Chapter 2.

A certain amount of Na (K) was used to modify uncalcined 0.6Pt-$Al_2O_3$ and 0.8Pt-$SiO_2$ with an aqueous solution of $NaNO_3$ ($KNO_3$) by IMP. The samples are denoted as αNa (K)-0.6Pt-$Al_2O_3$, αNa (K)-0.8Pt-$SiO_2$, where α is the atomic percent of Na (K). Na modified $SiO_2$ and $Al_2O_3$ supports were prepared by IMP method as well and denoted as αNa-$SiO_2$ ($Al_2O_3$), where α is the atomic percent of Na (K).

Pt-Na-$SiO_2$ samples with different bulk Na:Pt ratios were prepared by a two-step IMP method. Na was impregnated before Pt loading.

All samples were calcined in air at 400 $^oC$ for 4 h at a heating rate of 2 $^oC$/min prior to testing.

5.3Pt-$CeO_2$ was used as reference catalyst in this chapter, which was prepared by one-pot synthesis using the urea gelation/co-precipitation (UGC) method. Details about this preparation technique and material properties can be found in [18]. The surface area of 5.3Pt-$CeO_2$ was 140 $m^2$/g. No visible Pt particles were found by TEM and no Pt peak was identified by XRD. XPS shows 3.5 at% Pt on the surface. Turnover frequencies were calculated based on the initial amount of surface Pt species found by XPS [18].

Catalysts were characterized by BET surface area, ICP, TEM/HRTEM, XRD, XPS, CO chemisorption, $H_2$/CO-TPR measurements and XANES. Catalyst activities were evaluated for the WGS reaction under various conditions that included product-free and full reformate gas mixtures. Long term stability was checked with the full reformate gas mixtures under isothermal conditions.

## 3.3 Results and discussion

### 3.3.1 Characterization

Table 3.1 lists the physical properties of the Pt-$SiO_2$ and Pt-$Al_2O_3$ samples after calcination. The commercial $SiO_2$ and $Al_2O_3$ supports have surface areas as high as 243 and 210 $m^2/g$, respectively. Surface modification of the supports with platinum and subsequent addition of alkali (Na or K) ions decreased the surface areas to 131 – 187 $m^2/g$ by the sequential impregnation of Pt and alkali oxides. This drop in surface are, especially for the fumed silica, is a result of pore collapsing with the applied impregnation and heat treatment. However, from Table 3.1, we can still observe the beneficial effect of Na or K addition on suppressing the Pt particle growth on both the 0.8Pt-$SiO_2$ and 0.6Pt-$Al_2O_3$ samples. The mean platinum particle size was decreased from 5.0 nm (alkali-free) to 2.0 nm (alkali-modified) after 400 $^oC$ air calcination on both oxide supports. Interestingly, the different Pt loading procedures *e.g.* DP or IMP, and the sequence of Pt and alkali ion addition, *e.g.* Co-IMP, Pt-IMP followed by Na-IMP, or *vice versa*, did not have any detectable effect on the physical properties of the resulting Pt-based samples, in as far as the mean Pt particle size and specific surface areas are concerned.

Over the last decade, one of the most advanced electron microscopy techniques, namely, aberration-corrected (ac)-HAADF/STEM has become available and has allowed investigation of supported precious metal species at atomic resolution. Au atoms and clusters on iron oxide [20-22] as well as Pt atoms and clusters on $\gamma$–$Al_2O_3$ [23], in both cases after a prolonged high-temperature annealing, have been imaged with aberration-corrected HAADF/STEM. In this work, the technique was also used to investigate any structural alkali-effect on Pt dispersion at the atomic level. Shown in Figure 3.2 (B), atomically dispersed Pt species (atoms, ions, and few-atom clusters) were observed on the Na-promoted $Al_2O_3$ with higher Pt loading and harsher calcination conditions than what was used in the recently reported fully dispersed Pt over bare $\gamma$-$Al_2O_3$ [23]. Sub-nanometer Pt on Na-promoted $SiO_2$ can be clearly seen in Figure 3.2 (A). However we were not able to capture the Pt at atomic resolution on silica because of the high mobility of Pt atoms on the inert support under the electron beam. Pt particle size distributions on Pt-$SiO_2$ w/o Na-promotion, inserted in Figure 3.3 (A) and (B), based on the ac-HAADF/STEM images

show that the sub-nanometer Pt clusters and atoms were abundant (>65%) in the Na-promoted (washed) sample, but scarce (<5%) in the Na-free sample. Combining the analysis from both HRTEM and ac-HAADF/STEM it was determined that the residual (after washing) alkali ions bind onto the atomically dispersed Pt species on the Pt-$SiO_2$ (Pt-$Al_2O_3$) surfaces, and they suppress the sintering of Pt particles upon high-temperature heating (to 400 $^oC$, air).

Similar findings had been reported by Konsolakis *et al.* [24], who showed that at low or moderate loadings of Na, a higher dispersion of Pt on $\gamma$-$Al_2O_3$ was achieved than in the Na-free samples. More recently, better dispersion of Pt with Na addition was also reported for Pt-$TiO_2$ by two different research groups [10, 25], and the improved Pt dispersion was attributed to the creation of more defect (binding) sites on $TiO_2$ created by the alkali additives. Hatanaka *et al.* explained that a more basic support yielded better Pt stabilization through the formation of rigid Pt-O-M (where M is the support cation) bonds, thus inhibiting Pt sintering due to the different electron density of the support [26]. Therefore, here, alkali ions could play the role of the basic support, which would render any support surface a mere carrier of the Pt-O-Na, K ensemble. Thus, at low temperatures, all these support oxides would be equivalent. This hypothesis will be examined in Chapter 4 on the basis of the collected experimental evidence and DFT calculations performed by the Mavrikakis group at Wisconsin.

CO chemisorption was used to measure the Pt dispersion on the samples examined by microscopy. However, no big difference was found between the alkali-free and alkali-promoted samples, when the alkali loading was low, Na:Pt < 3. When the alkali loading was high, a decreased Pt dispersion was even found. This result is opposite to what has been observed by microscopy. Konsolakis *et al.* [24] also reported that when Na loading was high, similar Pt dispersion was measured on both Na-modified and Na-free Pt-$Al_2O_3$. One possibility with the high coverage of alkali is encapsulation of some part of the platinum, which is then inaccessible to CO. When examining the adsorption of CO on the alkali-modified Pt sites, Tanaka *et al.* [27] reported that the strength of CO adsorption on Pt in alkali-modified Pt-$Al_2O_3$ was weakened and the mode of CO-Pt adsorption was partially changed from linear adsorption to bridged adsorption, which means the assumption of CO:Pt = 1 for the calculation of Pt dispersion is no longer valid. Due to this

difficulty, it was not possible to precisely measure the Pt dispersion with the CO chemisorption technique.

### 3.3.2 Reducibility

#### 3.3.2.1 $H_2$-TPR

As the reducibility of surface oxygen in the catalyst is typically correlated with its potential reactivity for the WGS reaction, $H_2$-TPR measurements were carried out to probe the surface oxygen of the alkali-modified Pt materials. TPR profiles of the Pt samples are depicted in Figures 3.4 and 3.5. Detailed information about the reduction peaks and $H_2$ consumption amounts is included in Table 3.2. As inert oxides, neither $Al_2O_3$ nor $SiO_2$ has reducible surface oxygen. With Na-impregnation on $SiO_2$ or $Al_2O_3$, a large amount of surface oxygen was present, but the reduction only took place above 400 $^oC$. As shown in Figure 3.4, when Pt was added (at 0.6 at%) into the Na-modified $Al_2O_3$, the reduction onset was lowered to *ca.* 100 $^oC$. $H_2$ consumption, *i.e.* the amount of surface oxygen, increases with the content of alkali additives (Table 3.2). Similar results were obtained over the Na (K) modified Pt-$SiO_2$ system, in Figure 3.5 and Table 3.2. Since the Na (K)-free Pt-$Al_2O_3$ and Pt-$SiO_2$ samples have no reducible surface oxygen, the low-temperature $H_2$ consumption in the alkali-modified samples should be mainly due to the oxygen associated with both the alkali ions and the Pt species.

K-modified samples behave a little differently from the Na-modified ones, as the same amount of K ions leads to a higher amount of surface oxygen on either support, but the center of the reduction peak shifts to higher temperatures on both supports. As early as 1997, Chen and co-workers [28] reported similar findings, namely the K-modified sample has more surface oxygen, but its reduction is more difficult (higher temperature) than Na-modified samples. This was attributed to the different basicity of the alkali ions, but no details were given. A brief discussion is present in Chapter 4.

Here we found that the Na (K):Pt ratio determines the amount of reducible surface oxygen at temperatures lower than 400 $^oC$. As can be seen in Table 3.2, 3Na-$SiO_2$ has a large amount of reducible oxygen at temperatures higher than 300 $^oC$. With Pt loading, a fraction

of the surface oxygen becomes reducible at low temperatures (<200 $^{o}$C). Figure 3.6 and Table 3.2 show that for the 3Na-$SiO_2$ samples with different platinum loading contents, the hydrogen consumption at low temperature first largely increases (from 1 to 2%Pt), and then drops (from 2 to 3% Pt), and the same trend is seen for the shift of the reduction peak, the largest shift associated with the 2% Pt-loaded sample. The extra amount of Pt may simply lead to the formation of Pt particles, as shown by the TEM images of 3Pt-3Na-$SiO_2$ (Figure 3.7). Severe aggregation of Pt particles takes place in the Pt-rich sample. According to the $H_2$-TPR results, an optimum Na:Pt ratio exists around 1.5 to maximize the reducible surface oxygen at low temperatures. We tentatively assign this to the maximum interaction between the Pt and Na-O sites. However this ratio is calculated based on the bulk concentrations of Pt and Na (by ICP). Since $H_2$-TPR is a technique for near-surface oxygen characterization, to more accurately estimate the Na:Pt ratio and the surface oxygen relevant for the reaction (*i.e.* in –OH form), surface concentrations (from XPS) and CO-TPR data will be combined and considered below, especially for the washed samples.

As alkali oxides are not easy to be reduced to or be stabilized as alkali metals at low temperatures, also it is noticed that the measured surface oxygen amount is much more than the calculated values from the $NaO_x$ ($KO_x$) stoichiometry ($x$ = 0.5, *e.g.* 250 μmol/g for sample 3Na-$SiO_2$) and non-linear with the amount of Na or K doping. One possible explanation is that alkali ions are hydrophilic and more surface OH groups are now adsorbed on the support *via* alkali ions, which also will lead to higher $H_2$ consumption. Previously, Krupay *et al.* [29] reported that excess surface oxygen amount and more OH groups by alkali doping were present on pure γ-$Al_2O_3$, and this rendered the alumina a high-temperature shift catalyst [9]. A higher concentration of OH groups was also reported on the alkali-modified Pt-$TiO_2$ compared to the unpromoted samples [16]. We may speculate that the presence of Pt enhances the reducibility of the surface oxygen by $H_2$ or CO spillover from the platinum sites to the surface oxygen species, such as OH groups associated with the alkali ions.

### 3.3.2.2 CO-TPR

Complementing the above $H_2$-TPR tests, CO-TPR was used to sample the surface oxygen species and identify the light-off temperature of the WGS reaction (between adsorbed CO and OH groups on the surface). As shown in Figure 3.8, the Na addition on the $SiO_2$ surface introduces reducible surface oxygen (as seeing by the $CO_2$ production) on the inert support as well as surface OH groups (as seeing the $H_2$ production along with further $CO_2$ production).

Addition of Pt lowers the reduction temperature of the surface oxygen species (from 250 $^oC$ to 50 $^oC$) and the activation temperature of surface OH groups (from 600 $^oC$ to 100 $^oC$). The same trend as what was found by $H_2$-TPR is observed here, namely, the total surface oxygen amount increases with the Na content, but the amount activated at low temperatures depends on the amount of Pt that can interact with it. The excess oxygen bound to the alkali on the silica surface is still reduced at higher temperatures, as shown by the 1Pt-15Na-$SiO_2$ in Figure 3.8. Alkali-free Pt-$SiO_2$ has no reducible surface oxygen species or active OH groups; hence the reducible sites at low temperatures appear to be an ensemble of Pt-$O_x(OH)_y$-Na sites, similar to what our group has proposed for the Pt-$CeO_2$ system [1]. More work is necessary to further test this hypothesis, including XAS analysis, atomic-resolution microscopy, and computational chemistry work, as will be discussed in Chapter 4.

### 3.3.3 Structural Investigations of the Alkali Promotion Effect

XRD analysis, in Figure 3.9, shows that the Na-free 0.8Pt-$SiO_2$ sample contains Pt metal nanoparticles with an average particle size of 6.6 nm, in agreement to the TEM results (Table 3.1). However, after impregnation with 5%Na, these Pt particles disappeared, either due to the small grain size and/or the formation of an atomically dispersed Pt-$O_x$ structure. Such phenomena were also observed for other Na (K) modified 0.8Pt-$SiO_2$ samples. 15%Na was used to modify the $SiO_2$ support, but even after 800 $^oC$ air calcination no sodium silicate structure was observed, therefore we believed that the alkali-modified samples are free of the formation of bulk alkali silicates. Of course a very small amount of surface silicates, XRD-invisible, may be formed. However, XPS test over the washed

15%Na-$SiO_2$ did not pick up any Na on the surface, which confirms the absence of surface alkali silicate.

XPS analysis was applied to study the surface concentrations of Pt and Na, and the oxidation states of Pt in the samples. For $Pt_{4f}$ core, the XPS peaks were assigned with binding energy at 71.0 and 74.2 eV for $Pt^o$, binding energy at 71.9 and 75.1 eV for $Pt^{2+}$, and binding energy at 74.3 and 77.5 eV for $Pt^{4+}$. In Figure 3.10, it is clear that with the addition of Na ions, the peaks for Pt were shifted to higher binding energies. This peak shift can be due to very fine (sub-nm) Pt species and/or the formation of ionic platinum ($Pt^{2+}$, $Pt^{4+}$) species on the $SiO_2$ surface [30]. As found by TEM, alkali-ions do suppress the sintering of Pt particles but they also significantly increase the amount of Pt ions/clusters on the catalyst surface. Thus, the peak shifts here could come from both the smaller Pt particle size and the more electron deficient Pt species. The spectra of 3Pt-3Na-$SiO_2$ shows a significant amount of metallic Pt, compared with that of 2Pt-3Na-$SiO_2$ and 1Pt-3Na-$SiO_2$, indicating that 3%Na is not enough to associate all of the 3%Pt, hence the excess Pt forms Pt particles on the surface. These data are in agreement with the previous $H_2$-TPR and TEM findings. Further deconvolution of the peaks for $Pt_{4f}$ was done with selected samples. As listed in Table 3.3, the addition of Na ions significantly enhances the fraction of oxidized Pt species. The higher Na:Pt ratio, the bigger fraction of oxidized Pt species. To remove the ambiguity from the final state effects, the same samples were examined by XANES.

The higher oxidation state of Pt species in alkali-modified samples was confirmed by XANES. Figure 3.11 (A) shows the results of XANES at the Pt $L_{III}$-edge. The white line intensity of Pt $L_{III}$-edge provides strong evidence of the electronic state of Pt, the larger the white line the greater the electron deficiency in the d-orbital [31]. The relative electron deficiency of the Pt species can be determined based on the white line intensity. Apparently, Pt was more oxidized, *i.e.* electron deficient in the samples with alkali-promoters according to its much higher white line intensity.

Therefore, combining the information from XPS, XRD, HAADF/STEM and XANES, we have found that the addition of alkali ions ($Na^+$, $K^+$) not only inhibits the sintering of Pt particles, but also enhances the fraction of nonmetallic Pt species on Pt-$SiO_2$, which are

likely the active sites for the WGS reaction on ceria [1, 18, 32] and other supports [10], thus boosting dramatically the catalytic activity, as will be shown below.

### 3.3.4 WGS reaction activity

The steady-state WGS reaction activities of the abovementioned catalysts were firstly measured in product-free gas. Figure 3.12 shows the steady-state WGS reaction performance of the Pt samples. The WGS reaction activities of Na-free and Na-doped $Al_2O_3$ ($SiO_2$) samples were also tested under the same conditions. Tests were conducted first in temperature rising mode, followed by temperature decreasing. Na addition increases the catalytic activity of bare $\gamma$-$Al_2O_3$ only at temperatures higher than 350 $^oC$, as had been reported many years ago by Amenomiya and co-workers [9], while no activity was observed over either the Na-free or the Na-doped $SiO_2$.

A significant promotion effect of Na (K) on the Pt-$Al_2O_3$ and Pt-$SiO_2$ samples is clear from the lower onset of the WGS reaction. Especially, the 0.8Pt-$SiO_2$ sample is activated at an elevated temperature of 300 °C, if no alkali is present on its surface. This was expected since the Pt-$SiO_2$ is inert for the WGS reaction at low temperatures [33]. At high temperatures, Pt alone has active sites for the WGS reaction [33]. Here we show that with Na (K) promotion Pt-$SiO_2$ catalysts are as active as $CeO_2$-supported Pt catalysts [1, 18] at low temperatures, an example shown in Figure 3.13. No activation (hysteresis) or deactivation of the catalysts was observed during ramping up and down the temperature. Temperature-programmed oxidation of the used samples found no evidence of carbon deposition.

K-modified samples, compared with the Na-modified ones, have a higher amount of surface oxygen as found already by $H_2$-TPR, in Table 3.2, but they show lower catalytic activity for the WGS reaction regardless of the support, Figure 3.12. However, it should be noted that the optimal ratio of K:Pt may differ from that of Na:Pt, as a result of potentially different Pt-O-K and Pt-O-Na interaction/stability. The Pt particle size and surface area of the Na- or K-promoted samples examined here are about the same, Table 3.1. The data indicates that only the low-temperature (< 200 $^oC$) reducible surface oxygen is relevant to the removal of CO by $H_2O$, as will be discussed in more detail in the next chapter.

The CO conversion increases with the amount of Na (K) added. Above a certain Na (K):Pt ratio, however, no further improvement of the CO conversion to $CO_2$ is observed, Figure 3.12. There is a maximum in the Na (K):Pt ratio, i. e. 3%Na (K) for 0.8Pt-$SiO_2$ and 6%Na (K) for the 0.6Pt-$Al_2O_3$ samples. We further tuned the Na:Pt ratio on Pt-$SiO_2$ to optimize its WGS reaction activity. For a fixed Na amount, 3 at%, the best Pt content was about 2 at% from the $T_{50}$ values (Figure 3.14), consistent with the $H_2$-TPR findings.

The WGS reaction light-off performance of Na-promoted Pt samples is compared with that of Pt-$CeO_2$ catalyst in Figure 3.13. Interestingly, the light-off of the WGS catalysts is not lowered by the presence of the promoter, and is typically ~ 100 $^oC$. With similar surface Pt loadings, the Na-promoted samples have identical performance for the WGS reaction as Pt-$CeO_2$ [18], suggesting that Na or K addition provides a similar interaction with Pt as the Pt-O-Ce sites. It will be intriguing to further investigate the potential similarities of the reaction pathway on all supports. Firstly, we conducted a kinetics analysis as presented below.

### 3.3.5 Kinetic Measurements

WGS reaction kinetics measurements were performed to further probe the alkali promotion effect and the support-independent activity of the catalysts. In these tests the full reformate gas mixture containing the reaction products, $H_2$ and $CO_2$, was used. Arrhenius-type plots of the steady-state WGS reaction rates are shown in Figure 3.15 for the $SiO_2$-supported catalysts and in Figure 3.16 for the $Al_2O_3$-supported catalysts.

The WGS reaction rates are significantly increased by the addition of alkali ions on both Pt-$SiO_2$ and Pt-$Al_2O_3$ samples. No methanation reaction was observed over any of the samples even with high $H_2$ concentration (26%) in the reactant gas mixture at temperatures as high as 350 $^oC$. Typically Pt-$Al_2O_3$ shows methanation activity at 350 $^oC$ [34]. Therefore the Na modification has changed the Pt species and their methanation reaction selectivity. Significant differences appear for the reaction rates over Pt catalysts with different doping ions (Na and K) and concentrations. For example, the 3Na-0.8Pt-$SiO_2$ shows the highest reaction rate of 12.4 μmol $CO_2/g_{cat}/s$ at 225 $^oC$, suggesting 3% is the optimal loading amount of sodium ions for 0.8%Pt on $SiO_2$. Similarly, 3K-0.8Pt-$SiO_2$ gives the best

catalytic performance. The apparent optimum Na (K):Pt is higher than 3 here; but as we will see below, there is excess (washable) Na (K) in these samples. And the surface also contains inactive Pt particles, so both the Na and Pt are overestimated in these "optimum alkali:Pt" ratio estimates. Since the alkali-free Pt particles on the support are spectators for the reaction, more work is needed to minimize the "inert" Pt species on the supports. Further lowering the Pt loading makes sense from the practical viewpoint as the cost of catalyst will be lower. Thus, it is important to prepare just atomically dispersed Pt on these surfaces, stabilized in place by the correct (optimal) amount of alkali. Potentially, different methods of preparation other than impregnation will be successful.

Remarkably, the WGS reaction activity of these alkali modified platinum catalysts is comparable to, or even higher than, the very active Pt-$CeO_2$ with a higher Pt loading, as shown in Figure 3.17. These results further confirm that the addition of alkali (Na, K) induced a Pt-O-Na (K) interaction on the inert supports ($SiO_2$, $Al_2O_3$) as good as the Pt-O-Ce interaction, so far as the activation of Pt species is concerned. Similar to ceria, the alkali additives provide OH groups important for the water-gas shift reaction pathway.

Kondarides and co-workers [11] explained the promotion effect of Na ions on Pt-$TiO_2$ as one whereby the added alkali ions creates defects on titania, which favors the dissociative adsorption of $H_2O$. Hence, the alkali promotion can be understood as a means of stabilizing and providing the oxygen-containing (OH) species to the Pt atoms. These OH groups are not present on the alkali-free silica surfaces, and relatively a small amount is present on the alkali-free alumina surfaces, while a large amount is present on ceria. An alternative to the explanation provided by Kondarides and co-workers [11] is that of Na- or K-stabilization of Pt-$O_x(OH)_y$-Na (K) ensembles on the titania surface. It would be interesting to further test this hypothesis.

From the Arrhenius-type plot, values for the apparent activation energy ($E_{app}$) were calculated. These are in the range of 70 ± 5 kJ/mol for both the Na (K)-free and Na (K)-promoted Pt samples. Interestingly, the same apparent activation energy of the WGS reaction was measured on an alkali-free Pt-$CeO_2$ sample. A thorough check of the reported $E_{app}$ values shows that the apparent activation energies of the WGS reaction on all Pt-based WGS catalysts, for example, Pt-$CeO_2$ [1, 35], Pt-$TiO_2$ [36], Pt-$Al_2O_3$ [35], Pt-$ZrO_2$ [37],

and even the alkali-promoted Pt-$TiO_2$ [11] are similar, all of them falling into the same range 70 ± 5 kJ/mol, irrespective of the support or the promoters used. Thus, a similar structure of the active sites and the same reaction pathway over all the Pt-based WGS reaction catalysts becomes plausible.

### 3.3.7 Stability of the alkali-promoted Pt catalysts

As discussed above, Pt is in more oxidized state when alkali-promoters are used, according to the XPS and XANES analysis (Figure 3.10 and Figure 3.11 (A)). This is true for the fresh, as prepared samples after air calcination at 400 $^oC$. How stable are these structures in the WGS reaction gas mixture? In Figure 3.10, the XPS of the used samples are also plotted (after use in the WGS reaction light-off tests for 14 hours) for comparison. The shift of the peaks to lower binding energies indicates reduction of the oxidized Pt species in all samples, but compared with the Pt oxidation state in the Na-free sample, the Pt species in the Na-promoted samples are still more oxidized.

To further probe the stability during reaction, in situ XANES was collected over the Na-promoted Pt-$SiO_2$ after exposure to 1%CO-3%$H_2O$-He mixture at 275 $^oC$ for 1 h. These are plotted in Figure 3.11 (B). The high white line intensity at Pt $L_{III}$ edge in the used sample confirms that Pt was still more oxidized in the used samples. Also, we found that after a $H_2$-treatment (20%$H_2$-He, at 250 $^oC$ for 1 h), Pt in the Na-promoted samples is still more electron deficient than in the Na-free samples, and the former were as active as the samples without $H_2$-treatment. Accordingly, we believe there is a strong interaction between Pt and Na-O species which preserves the oxidized state of Pt even in the highly reducing reformate gas mixture. Of course, life tests should be performed to evaluate the long term stability of these catalysts.

A long-term stability test was conducted over the 1Pt-3Na-$SiO_2$ washed sample for the WGS reaction in the full reformate gas stream, 11%CO-26%$H_2O$-26% $H_2$-7%$CO_2$-He, at 275 $^oC$ for about 50 h, as shown in Figure 3.18. A small decrease of CO conversion was observed during the first hour. However, it was stabilized rapidly and maintained throughout the end of the test. Ac-HAADF/STEM image, Figure 3.19, shows that the Pt dispersion did not change appreciably in the spent material. Pt clusters still dominate on

the $SiO_2$ surface with the modification of Na ions. Combining these findings with the XPS and XANES data, we propose that Na-free oxidized Pt species, or the oxidized Pt species without enough Na associated with, will get reduced in the reductive WGS reaction atmosphere and aggregated into particles as seen in Figure 3.19, while the part of the Pt species that is dispersed and stabilized by the Na ions will remain stable, positively charged, and active in long term WGS reaction testing as shown in Figure 3.18.

The stability of the alkali-promoted catalysts was also evaluated with the 0.6Pt-6Na-$Al_2O_3$, Figure 3.20. No appreciable change of Pt dispersion was observed on the spent material by electron microscopy. Na-free Pt-$Al_2O_3$ is active for the WGS reaction at this temperature (275 $^oC$), but these unprotected Pt clusters may grow and get deactivated at the reaction conditions. This can happen very fast, potentially explaining the large initial loss of catalyst activity. After this, the active Pt-O-Na sites remain active over the time of the stability test, Figure 3.20.

Overall, the stability of the alkali-promoted Pt-$SiO_2$ and Pt-$SiO_2$ prepared in this work is very good under realistic WGS conditions, and the materials may be further optimized for practical applications.

## 3.4 Summary

In this Chapter we showed strong evidence that alkali ions (Na, K) added in small amounts activate Pt for the low-temperature WGS reaction even when the Pt is supported on inert oxide supports, such as $SiO_2$ and $Al_2O_3$. Interestingly, these materials are as active as $CeO_2$-supported Pt catalyst which is arguably one of the most active catalysts for the WGS reaction.

Various characterizations have been conducted to understand the promotion effect. As demonstrated by TEM images, the presence of alkali ions suppresses the Pt metal particle growth during the thermal treatment step, a beneficial structural effect which has been reported before. Using the most advanced ac-HAADF/STEM for the first time in this work, sub-nm Pt clusters and atoms were found to dominate the alkali-promoted Pt samples.

$H_2$-TPR probed a significant amount of reducible surface oxygen at low temperatures in the alkali-promoted Pt samples, absent from the alkali-free materials. Both XPS and XANES showed that Pt species were positively charged in the alkali-promoted surface. Hence, the addition of alkali ions not only suppresses the growth of Pt particles, but also increases the fraction of oxidized Pt species, which is important for the WGS reaction.

Alkali ions also introduce surface OH groups, which are activated by the CO at temperatures as low as ~100 $^{o}$C, hence, the WGS reaction can now occur at low temperature.

The apparent activation energy over all Pt-based catalysts is in the same range, 70 ± 5 kJ/mol, independent of the oxide support and additive. A common site, Pt-$O_x(OH)_y$-M is proposed to be the active site for the WGS reaction in all Pt-based catalysts. We probe this further in Chapter 4.

The WGS reaction stability of the alkali-promoted Pt catalysts is very good. The characterization of the used samples reveals that alkali-ions can stabilize the dispersed Pt species (HAADF/STEM), while XANES and XPS show that a part of Pt remains electron deficient even after several hours under the WGS reaction at realistic conditions.

Considering the cost and deactivation problem of Pt-$CeO_2$, we believe that the alkali-modified Pt catalysts on inert oxide supports are more promising for the fuel cell applications. Of course, further development is in order, especially to reduce the amount of Pt to much less than 1 wt% while retaining the same high activity. Potentially, a different synthesis method whereby all Pt will be atomically dispersed and stabilized on any of these supports with the aid of a suitable additive should be developed next.

**Table 3.1 Physical properties of Pt-based catalysts**

| Sample* | Bulk Composition (at.%) [a] | | | Surface concentration (at.%) [b] | | | Surface Area ($m^2/g$) | Pt Particle Size[c] (nm) |
|---|---|---|---|---|---|---|---|---|
| | Pt | Na | K | Pt | Na | K | | |
| 0.6Pt-$Al_2O_3$ | 0.6 | | | 1.0 | -- | -- | 176.4 | 5.2±1.6 |
| 2Na-0.6Pt-$Al_2O_3$ | 0.6 | | | | | | 174.7 | |
| 6Na-0.6Pt-$Al_2O_3$ | 0.6 | | | | | | 164.8 | 2.1±0.8 |
| 9Na-0.6Pt-$Al_2O_3$ | 0.6 | | | 0.5 | 18.7 | -- | 146.6 | |
| 2K-0.6Pt-$Al_2O_3$ | 0.6 | | | | | | 168.1 | |
| 6K-0.6Pt-$Al_2O_3$ | 0.6 | | | 0.7 | -- | 7.3 | 154.8 | 2.5±1.2 |
| 9K-0.6Pt-$Al_2O_3$ | 0.6 | | | | | | 131.0 | |
| 0.8Pt-$SiO_2$ | 0.8 | -- | -- | 0.7 | -- | -- | 187 | 4.8 ± 1.2 |
| 1Na-0.8Pt-$SiO_2$ | 0.8 | 1.2 | -- | 0.5 | 1.7 | -- | 171 | 2.2 ± 0.7 |
| 3Na-0.8Pt-$SiO_2$ | 0.8 | 3.1 | -- | 0.5 | 4.2 | -- | 158 | 2.0 ± 0.4 |
| 5Na-0.8Pt-$SiO_2$ | 0.8 | 4.7 | -- | 0.7 | 5.4 | -- | 146 | 1.8 ± 0.3 |
| 1K-0.8Pt-$SiO_2$ | 0.8 | -- | 0.9 | | | | 186 | 2.2 ± 0.5 |
| 3K-0.8Pt-$SiO_2$ | 0.8 | -- | 2.5 | 0.6 | -- | 3.3 | 161 | 1.7 ± 0.3 |
| 5K-0.8Pt-$SiO_2$ | 0.8 | -- | 4.6 | | | | 143 | 1.7 ± 0.3 |
| 1Pt-3Na-$SiO_2$ | | | | 0.3 | 3.9 | -- | 172 | 1.6 ± 0.4 |
| 2Pt-3Na-$SiO_2$ | | | | 0.7 | 3.7 | -- | 148 | |
| 3Pt-3Na-$SiO_2$ | | | | 1.2 | 2.1 | -- | 128 | |

a: Designed concentration confirmed by ICP-OES analyses.

b: determined by XPS.

c: platinum particle size distribution was done from a survey of 50 particles.

*: the sequence of impregnation of Pt and the alkali is denoted by placing the species impregnated first next to the oxide support.

**Table 3.2 $H_2$-TPR of Pt-based catalysts**

| Samples | $H_2$ Consumption ($\mu mol/g_{cat}$) | Reduction Peak Temp. ($^oC$) |
|---|---|---|
| $Al_2O_3$ | -- | No reduction |
| $Al_2O_3$-6Na | 1187 | 510 |
| 0.6Pt-$Al_2O_3$ | 177 | ND |
| 0.6Pt-$Al_2O_3$-2Na | 302 | 240 |
| 0.6Pt-$Al_2O_3$-6Na | 1875 | 185 |
| 0.6Pt-$Al_2O_3$-9Na | 2778 | 176 |
| 0.6Pt-$Al_2O_3$-2K | 292 | 240 |
| 0.6Pt-$Al_2O_3$-6K | 1737 | 250 |
| 0.6Pt-$Al_2O_3$-9K | 3625 | 246 |
| | | |
| $SiO_2$ | -- | No reduction |
| 3Na- $SiO_2$ | 1237 | 510 |
| 0.8Pt-$SiO_2$ | 83 | ND |
| 1Na-0.8Pt-$SiO_2$ | 201 | ND |
| 3Na-0.8Pt-$SiO_2$ | 406 | 227 |
| 5Na-0.8Pt-$SiO_2$ | 717 | 216 |
| 1K-0.8Pt-$SiO_2$ | 281 | ND |
| 3K-0.8Pt-$SiO_2$ | 414 | 245 |
| 5K-0.8Pt-$SiO_2$ | 1145 | 281 |
| 1Pt-3Na-$SiO_2$ | 450 | 180 |
| 2Pt-3Na-$SiO_2$ | 725 | 152 |
| 3Pt-3Na-$SiO_2$ | 470 | 170 |

ND: no discernible peak up to 400$^o$C; broad reduction.

**Table 3.3 Effect of Na-addition on the fraction of surface Pt in various oxidation states**

| Sample | XPS-determined Pt in various oxidation states (%) * | | |
|---|---|---|---|
| | $Pt^{o}$ | $Pt^{2+}$ | $Pt^{4+}$ |
| 3Pt-$SiO_2$ | 40.5 | 35.9 | 23.6 |
| 3Pt-5Na-$SiO_2$ | 11.2 | 40.5 | 48.3 |
| 3Pt-3Na-$SiO_2$ | 26.5 | 34.6 | 38.9 |
| 2Pt-3Na-$SiO_2$ | 10.4 | 33.4 | 56.2 |
| 1Pt-3Na-$SiO_2$ | 2.9 | 39.4 | 57.7 |

*By deconvolution of the $Pt_{4f}$ XP spectra.

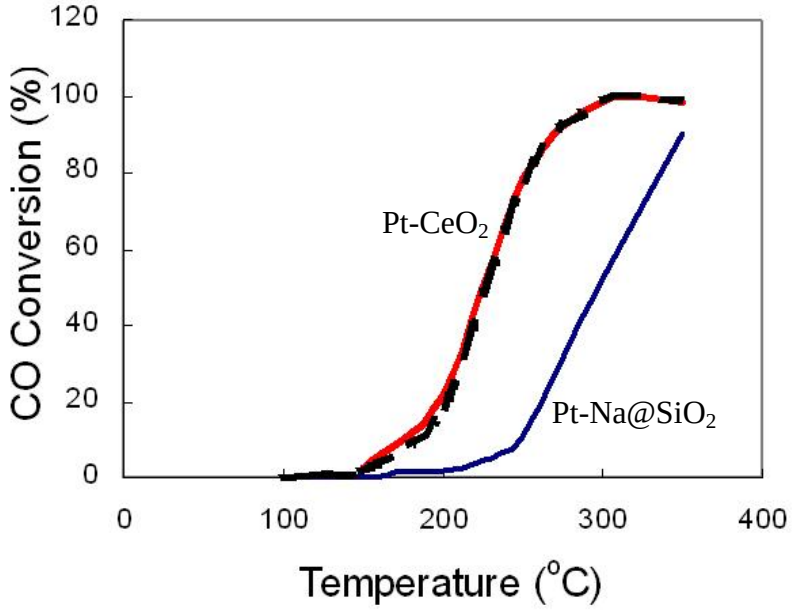


Figure 3.1 WGS light-off-profiles (steady-state data) of Na-modified $Pt@SiO_2$, compared with that of $Pt\text{-}CeO_2$, measured in 2%CO–10%$H_2O$-He gas stream, contact time: 0.09 g.s/cc. [17]

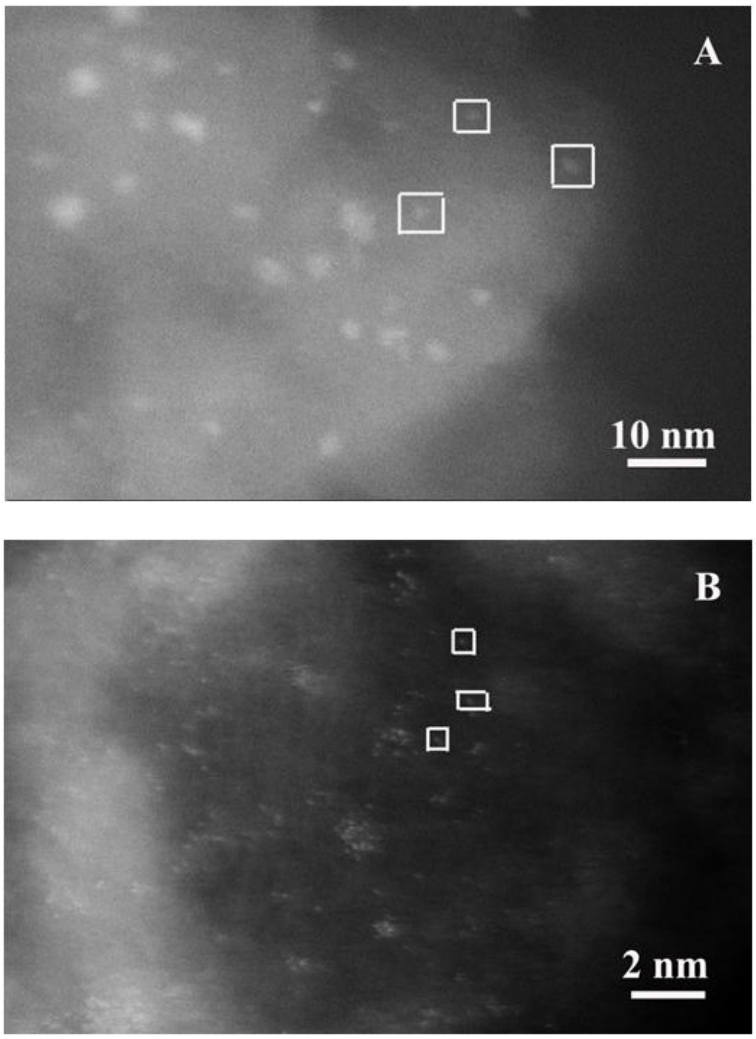


Figure 3.2 HAADF/STEM images of (A) 1Pt-3Na-$SiO_2$ washed and (B) 0.6Pt-6Na-$Al_2O_3$ parent samples. Squared are sub-nm clusters in (A) and Pt ions in (B).

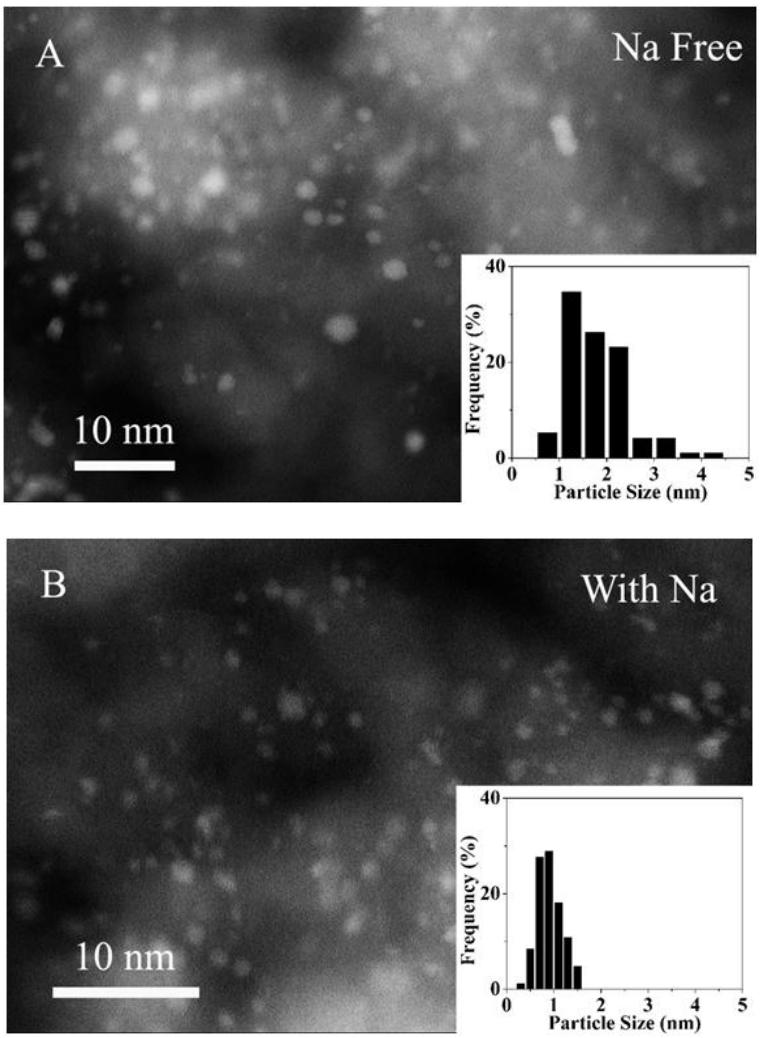


Figure 3.3 HAADF/STEM images and Pt particles size distribution in (A) 1Pt-$SiO_2$ and (B) 1Pt-3Na-$SiO_2$ washed.

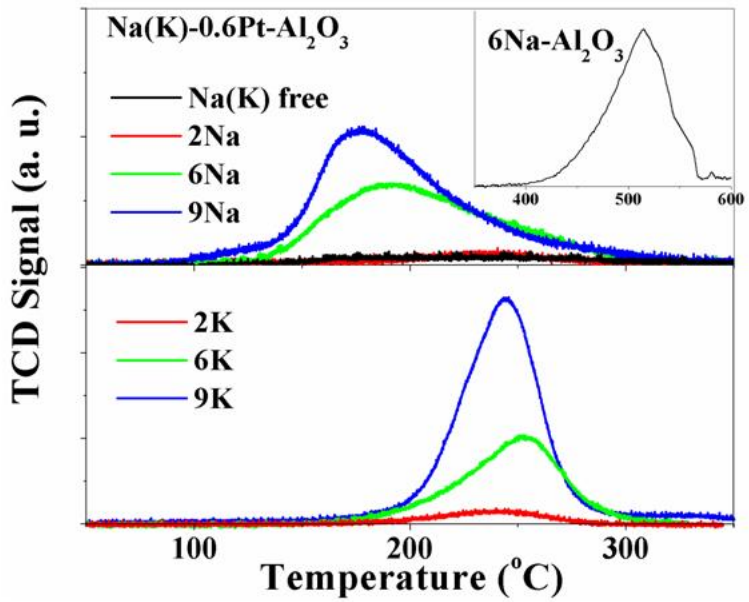


Figure 3.4 $H_2$-TPR of (Na/K)-0.6Pt-$Al_2O_3$ Samples.

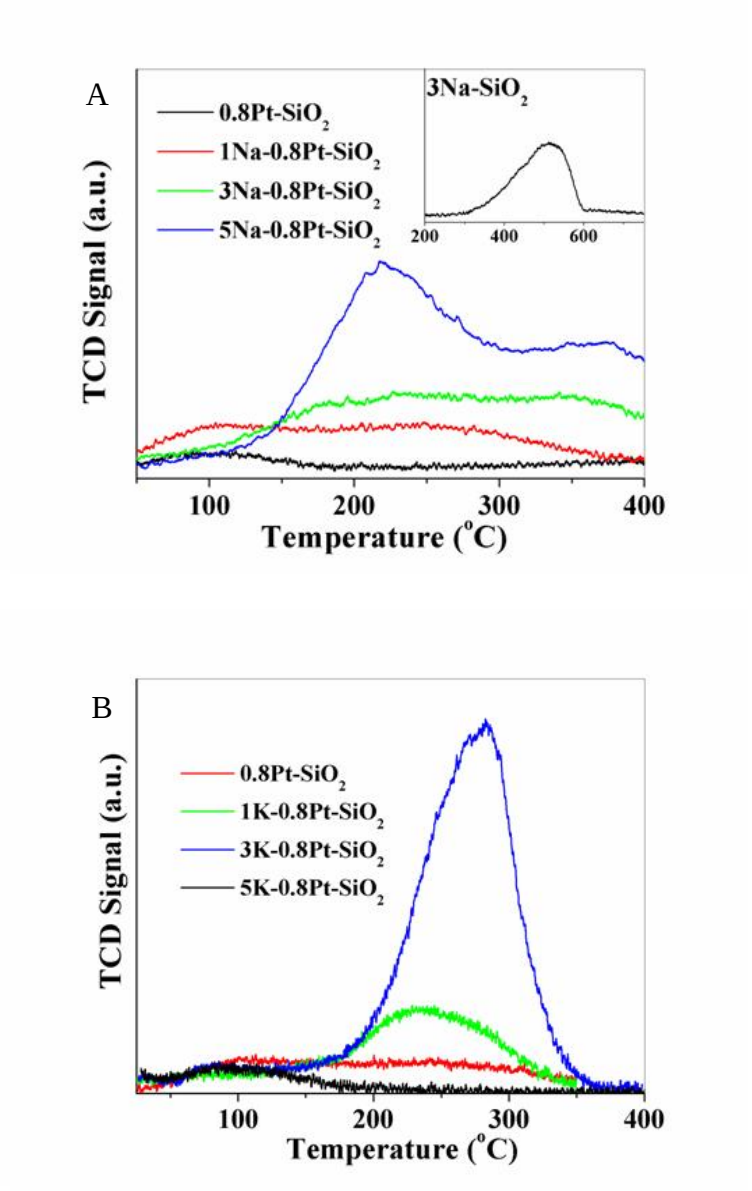


Figure 3.5 $H_2$-TPR of (A) Na-0.8Pt-$SiO_2$ and (B) K-0.8Pt-$SiO_2$ samples

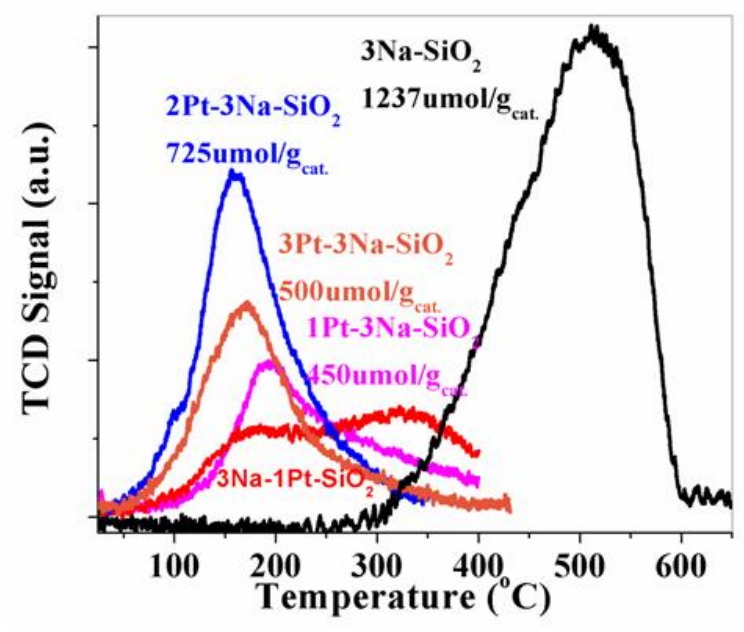


Figure 3.6 $H_2$-TPR of 3Na-$SiO_2$ samples with different Pt loadings.

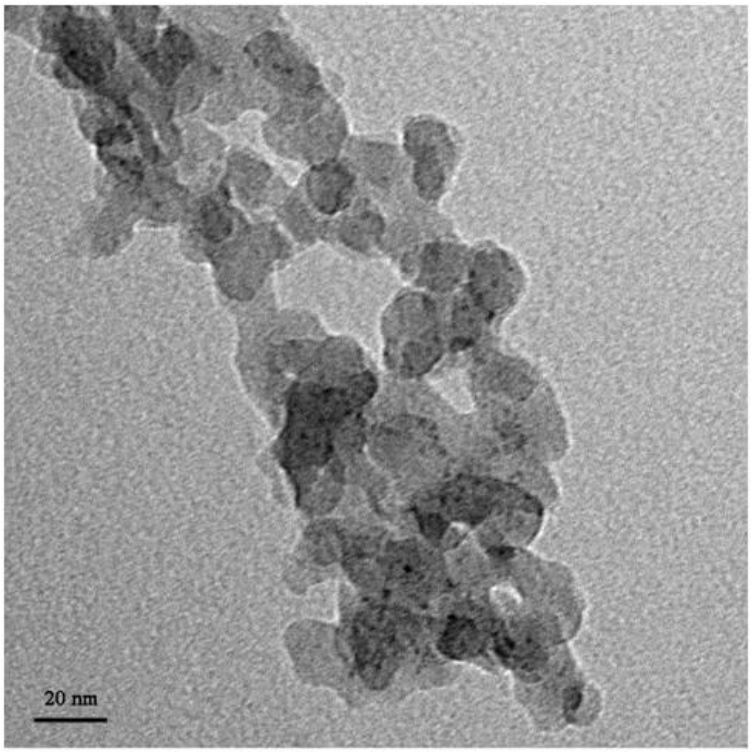


Figure 3.7 TEM image of 3Pt-3Na-$SiO_2$.

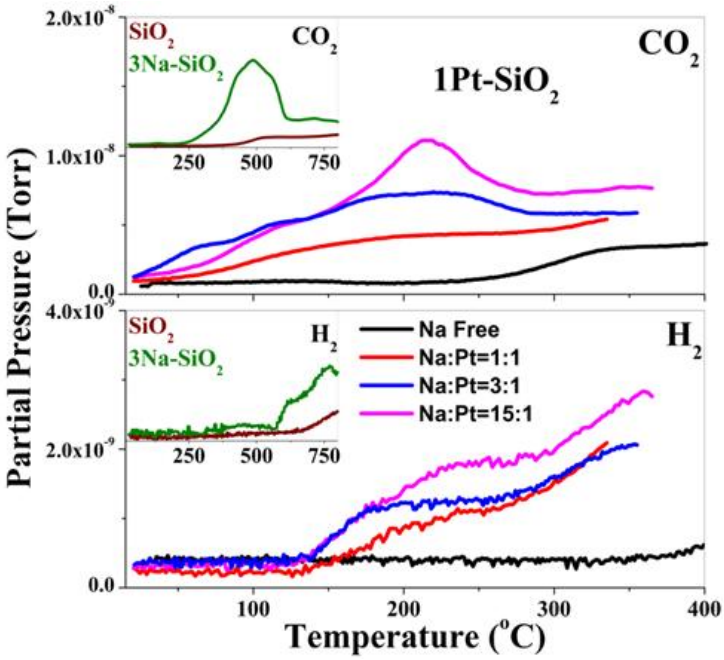


Figure 3.8 CO-TPR of 1Pt-$SiO_2$ catalysts with different Na:Pt ratio in 5%CO-He. The insets are the CO-TPR profiles of Pt-free $SiO_2$ materials.

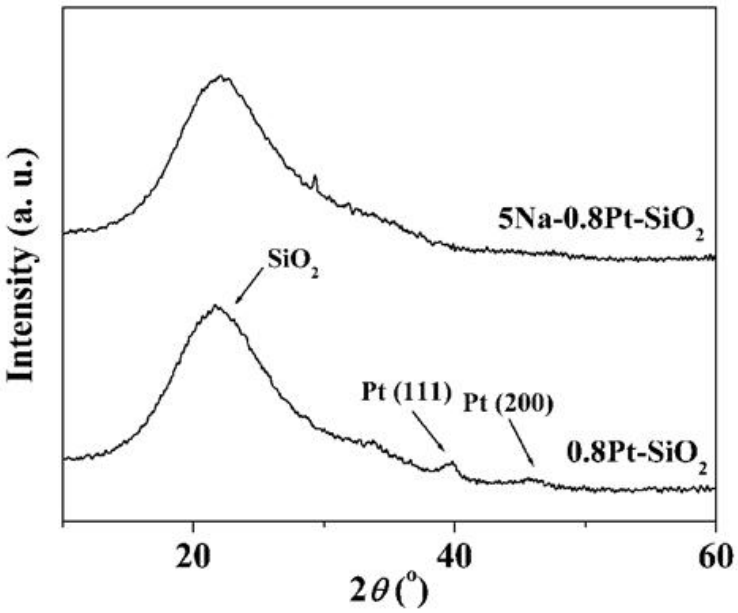


Figure 3.9 XRD patterns of (Na)-0.8Pt-$SiO_2$ samples.

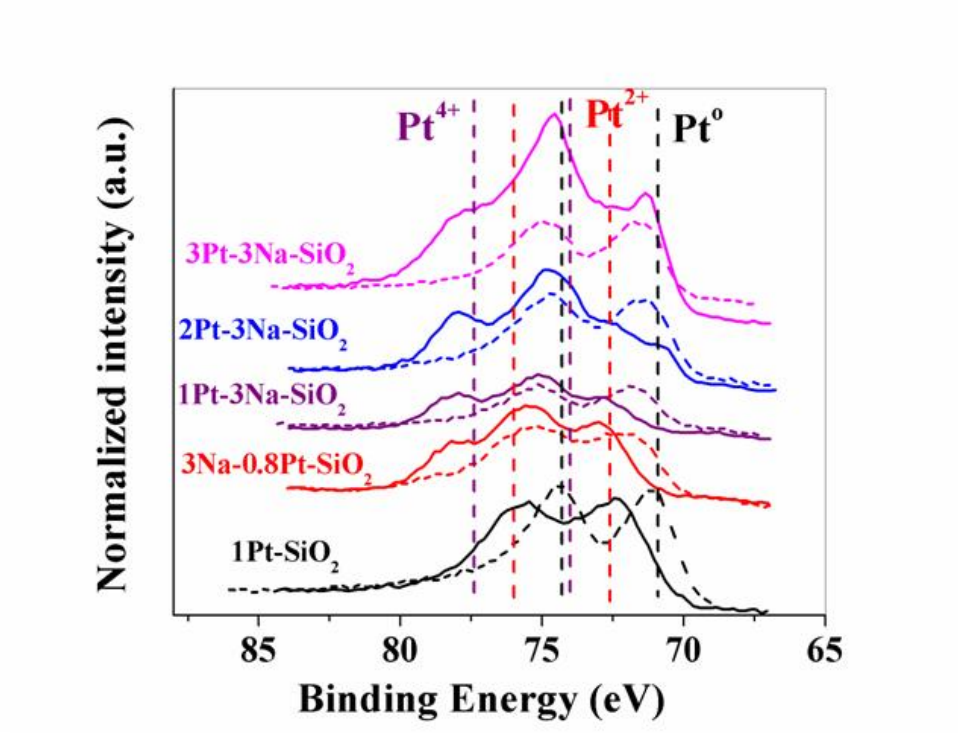


Figure 3.10 $Pt_{4f}$ XP spectra of fresh and used Pt samples. Solid line: fresh sample; dash line: used sample.

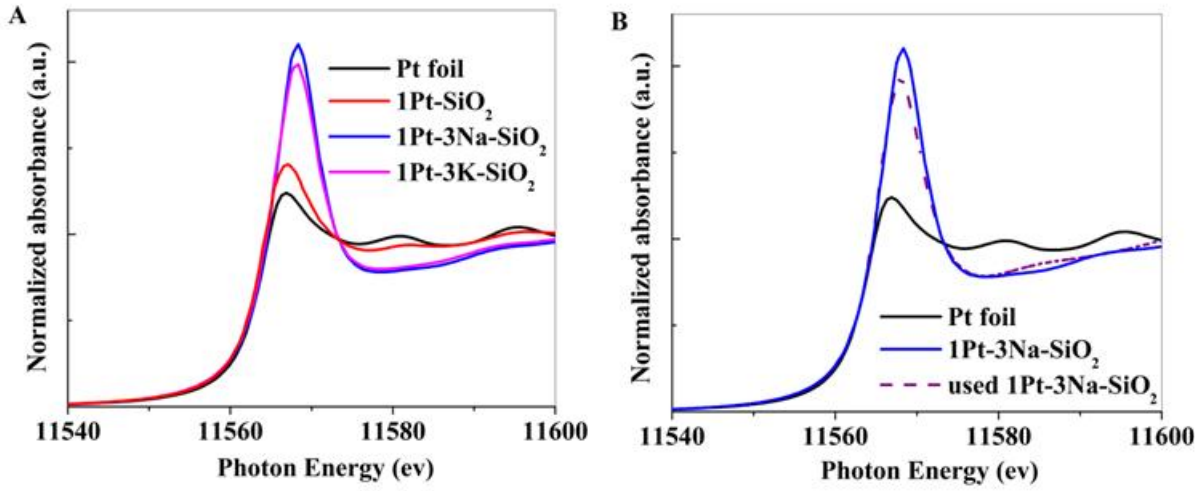


Figure 3.11 XANES spectra at Pt $L_{III}$-edge in fresh and used Pt based samples. (Used 1Pt-3Na-$SiO_2$: after WGS reaction at 275$^{o}$C for 1h in 1%CO-3%$H_2O$-He, 0.09 g.s/cc).

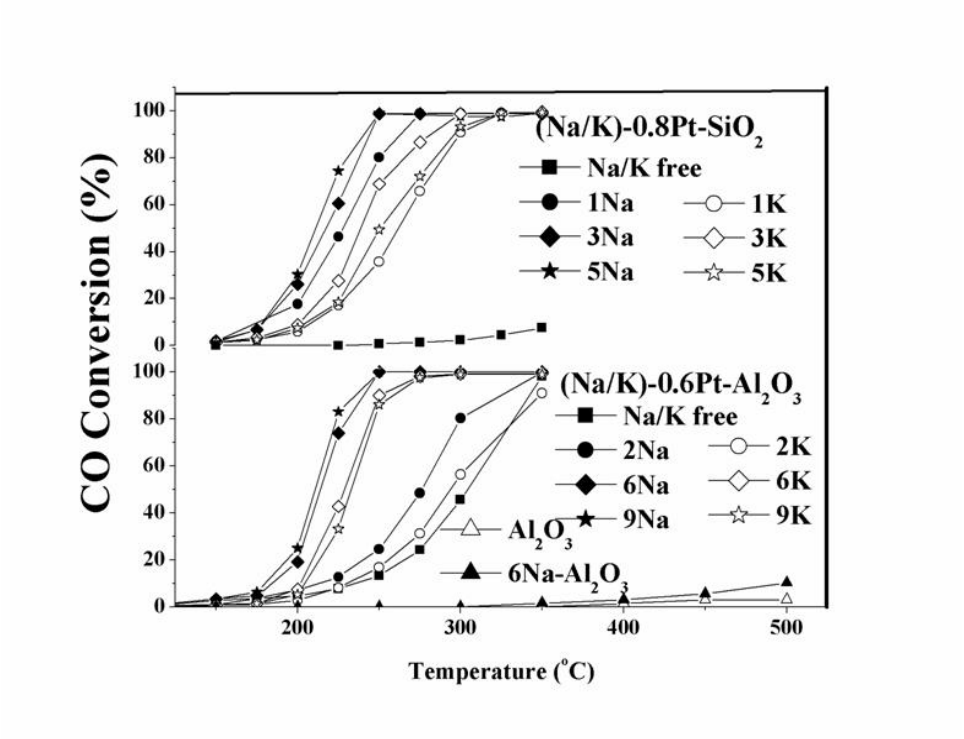


Figure 3.12 WGS steady-state light-off performance of Pt-based samples. Gas composition: 2%CO–10%$H_2O$-He.

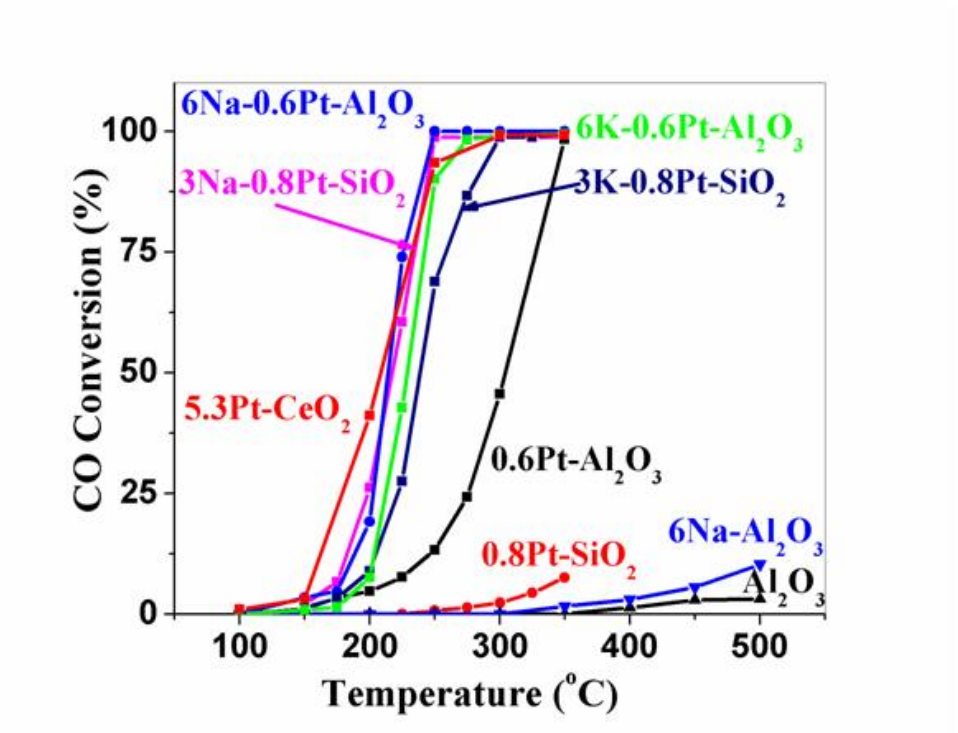


Figure 3.13 Comparison of the WGS reaction light-off performance (steady-state data) measured in a 2%CO–10%$H_2O$-He gas stream at contact time = 0.09 g.s/cc.

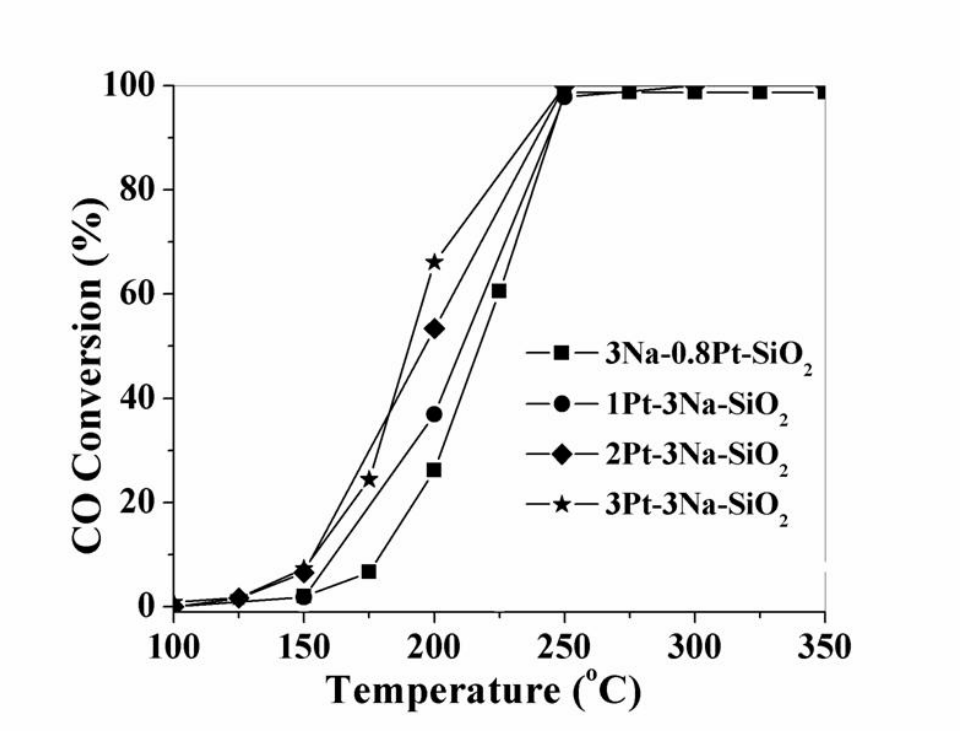


Figure 3.14 WGS steady-state reactivity of Pt-based samples with fixed 3 % Na doping. Gas composition: 2%CO-10%$H_2O$-He.

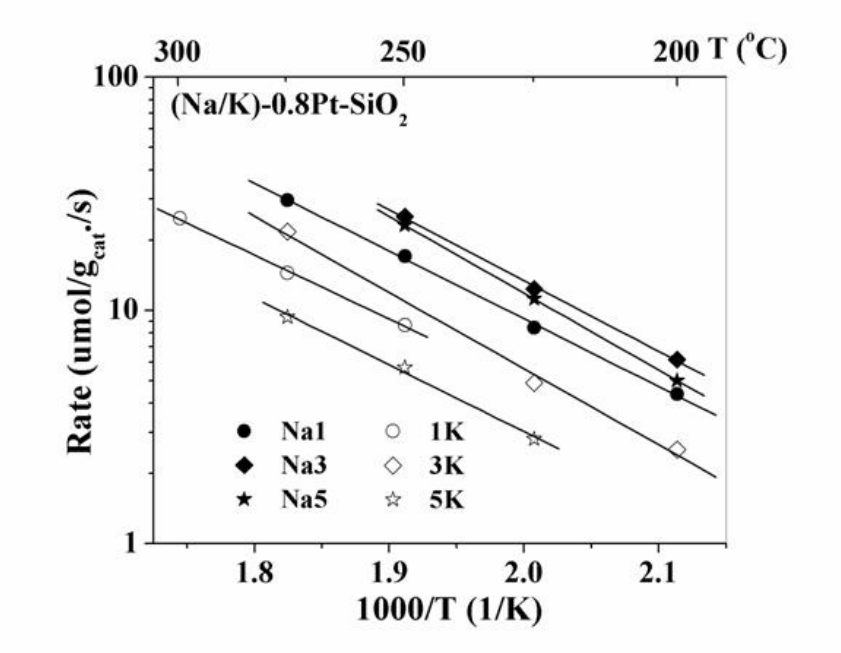


Figure 3.15 WGS reaction rates over Pt supported on silica. Gas composition: 11%CO–26%$H_2O$–26%$H_2$–7%$CO_2$-He.

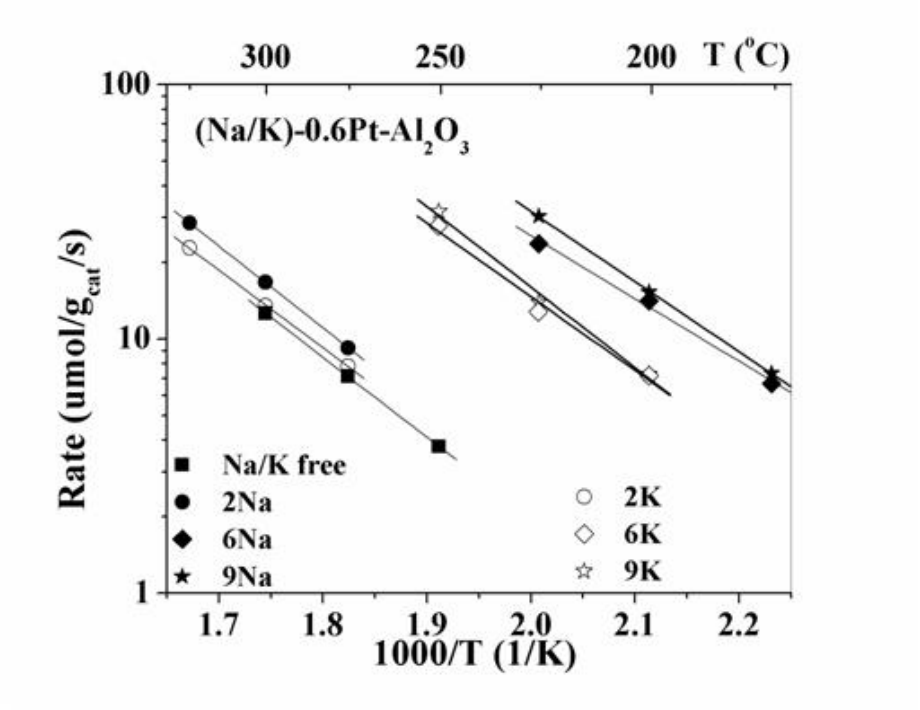


Figure 3.16 WGS reaction rates over Pt supported on alumina. Gas composition: 11%CO–26%$H_2O$–26%$H_2$–7%$CO_2$-He.

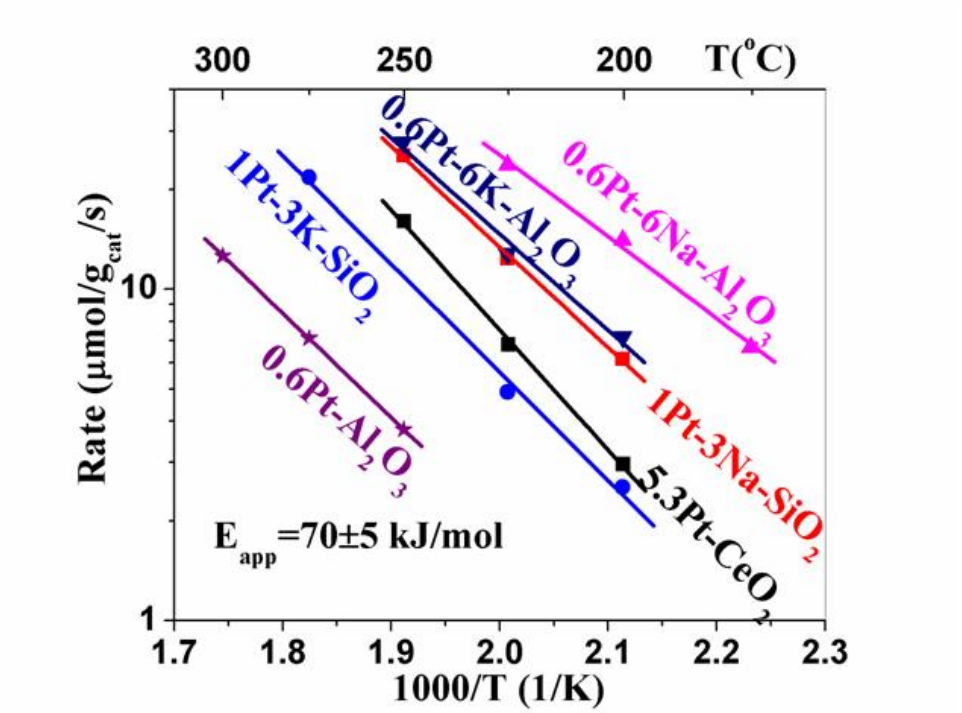


Figure 3.17 Comparison of the WGR reaction rates over Pt-based catalysts measured in 11%CO–26%$H_2O$–26%$H_2$–7%$CO_2$-He.

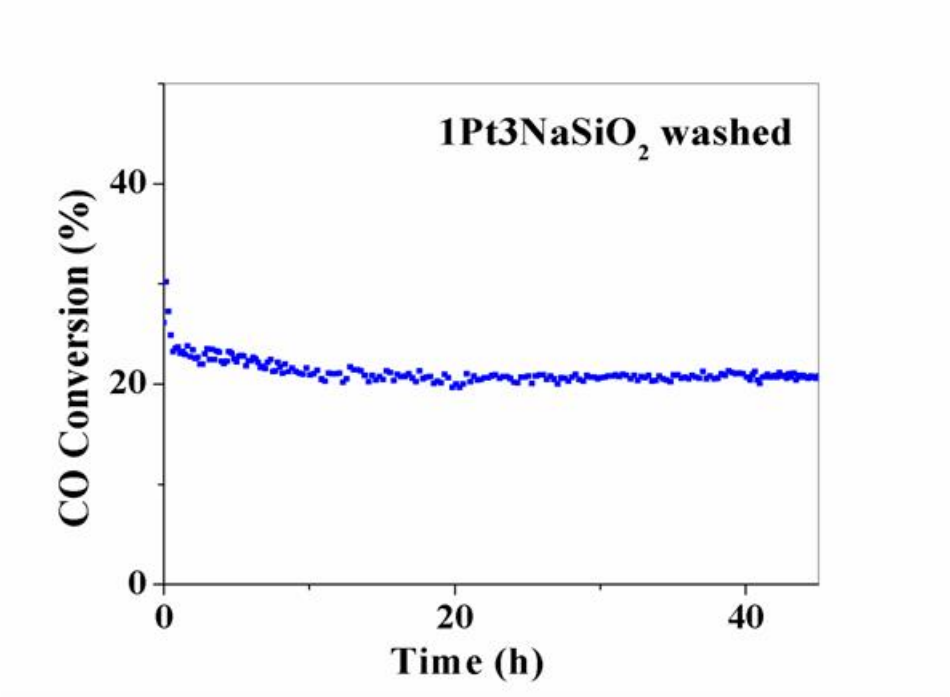


Figure 3.18 Stability test over the washed 1Pt-3Na-$SiO_2$ catalyst. 11%CO-26%$H_2O$-26%$H_2$-7%$CO_2$-He, 207 ml/min, at 275 $^oC$, contact time: 0.03 g.s/cc.

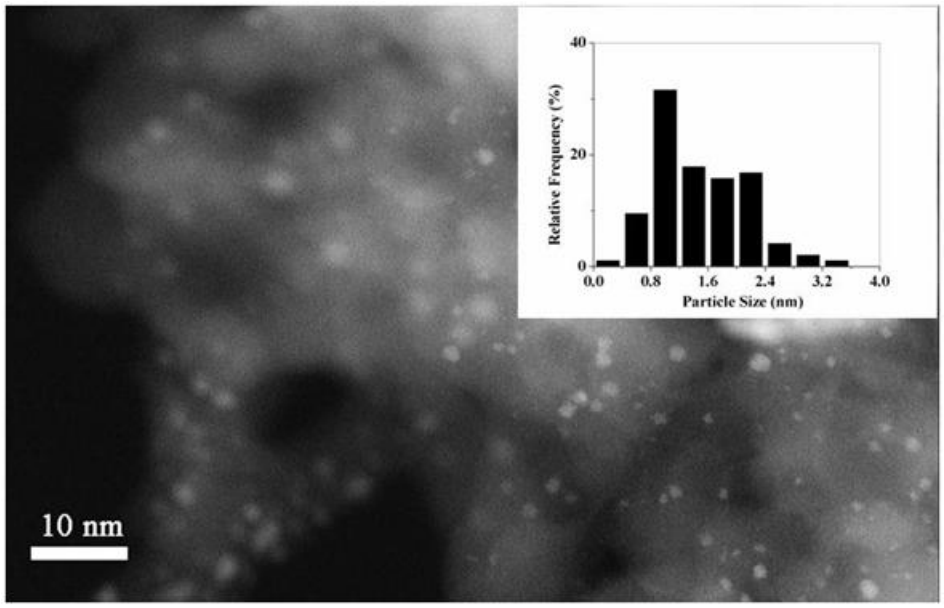


Figure 3.19 HAADF/STEM images of the used washed 1Pt-3Na-$SiO_2$ sample.

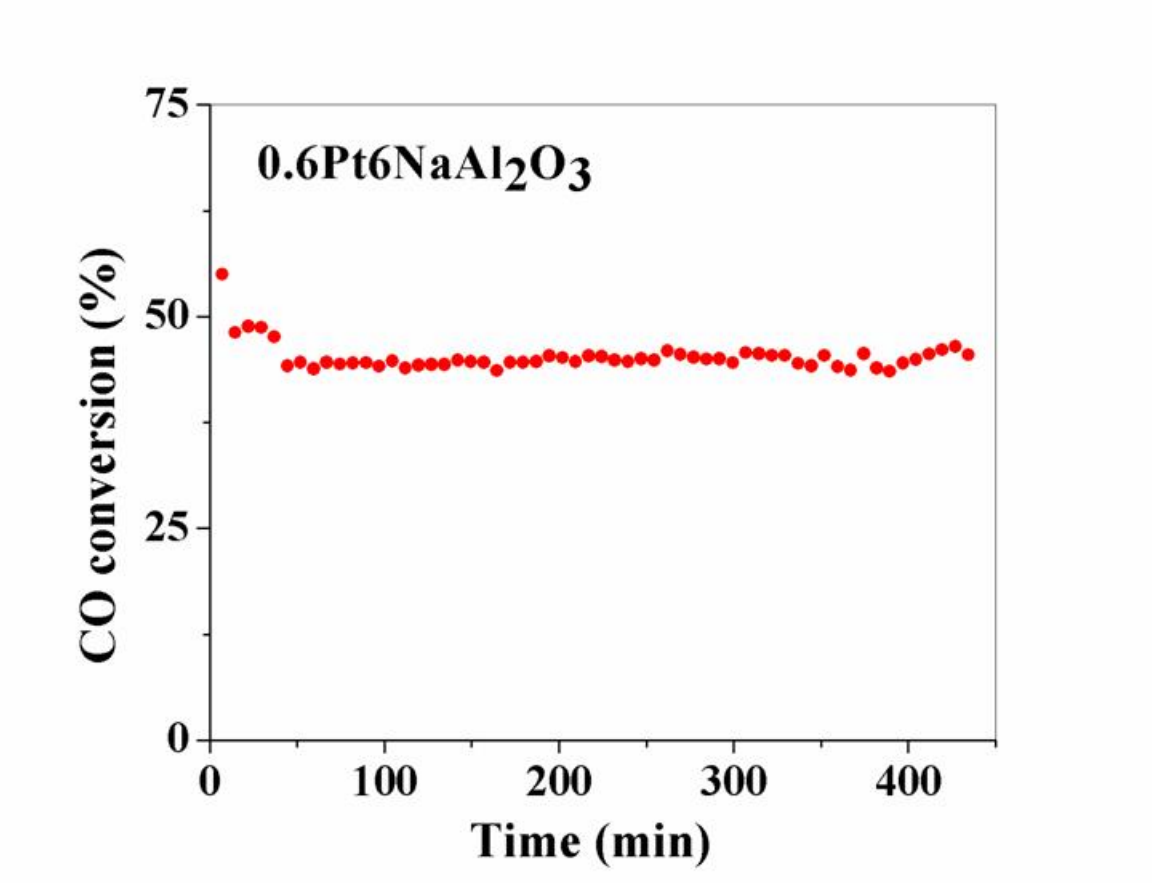


Figure 3.20 Stability test over the 0.6Pt-6Na-$Al_2O_2$ catalyst. 11%CO-26%$H_2O$-26%$H_2$-7%$CO_2$-He, 207 ml/min, at 275 $^oC$, contact time: 0.03 g.s/cc.

## 3.5 References

[1] Q. Fu, H. Saltsburg, M. Flytzani-Stephanopoulos, Science 301 (2003) 935-938.

[2] T. Daniele, G. Alexandre, C.M. Frederic, P.B. John, B. Robbie, chemical communication 14 (2004) 1636-1637.

[3] A. Faur Ghenciu, Curr. Opin. Solid State Mater. Sci. 6 (2002) 389-399.

[4] C. Hardacre, R.M. Ormerod, R.M. Lambert, J. Phys. Chem. 98 (1994) 10901-10905.

[5] S. Golunski, R. Rajaram, N. Hodge, G.J. Hutchings, C.J. Kiely, Catal. Today 72 (2002) 107-113.

[6] K.M.K. Yu, C.M.Y. Yeung, D. Thompsett, S.C. Tsang, J. Phys. Chem. B 107 (2003) 4515-4526.

[7] S. Golunski, R. Rajaram, CATTECH 6 (2002) 30-38.

[8] C.M.Y. Yeung, K.M.K. Yu, Q.J. Fu, D. Thompsett, M.I. Petch, S.C. Tsang, J. Am. Chem. Soc. 127 (2005) 18010-18011.

[9] Y. Amenomiya, G. Pleizier, J. Catal. 76 (1982) 345-353.

[10] X. Zhu, T. Hoang, L. Lobban, R. Mallinson, Catal. Lett. 129 (2009) 135-141.

[11] P. Panagiotopoulou, D.I. Kondarides, J. Catal. 267 (2009) 57-66.

[12] J.M. Pigos, C.J. Brooks, G. Jacobs, B.H. Davis, Appl. Catal., A 319 (2007) 47-57.

[13] H. Evin, G. Jacobs, J. Ruiz-Martinez, U. Graham, A. Dozier, G. Thomas, B. Davis, Catal. Lett. 122 (2008) 9-19.

[14] H. Evin, G. Jacobs, J. Ruiz-Martinez, G. Thomas, B. Davis, Catal. Lett. 120 (2008) 166-178.

[15] J.M. Pigos, C.J. Brooks, G. Jacobs, B.H. Davis, Appl. Catal., A 328 (2007) 14-26.

[16] X. Zhu, M. Shen, L.L. Lobban, R.G. Mallinson, J. Catal. 278 (2011) 123-132.

[17] D. Pierre, M.S., Tufts University, 2006.

[18] D. Pierre, W. Deng, M. Flytzani-Stephanopoulos, Top. Catal. 46 (2007) 363-373.

[19] T. Bunluesin, R.J. Gorte, G.W. Graham, Appl. Catal., B 15 (1998) 107-114.

[20] A.A. Herzing, C.J. Kiely, A.F. Carley, P. Landon, G.J. Hutchings, Science 321 (2008) 1331-1335.

[21] L.F. Allard, A. Borisevich, W. Deng, R. Si, M. Flytzani-Stephanopoulos, S.H. Overbury, J Electron Microsc (Tokyo) 58 (2009) 199-212.

[22] L.F. Allard, M. Flytzani-Stephanopoulos, S.H. Overbury, Microsc. Microanal. 16 (2010) 375-385.

[23] J.H. Kwak, J. Hu, D. Mei, C.-W. Yi, D.H. Kim, *e. al.*, Science 325 (2009) 1670-1673.

[24] M. Konsolakis, N. Macleod, J. Isaac, I.V. Yentekakis, R.M. Lambert, J. Catal. 193 (2000) 330-337.

[25] P. Panagiotopoulou, D.I. Kondarides, J. Catal. 260 (2008) 141-149.

[26] M. Hatanaka, N. Takahashi, N. Takahashi, T. Tanabe, Y. Nagai, A. Suda, H. Shinjoh, J. Catal. 266 (2009) 182-190.

[27] H. Tanaka, M. Kuriyama, Y. Ishida, S.-i. Ito, T. Kubota, T. Miyao, S. Naito, K. Tomishige, K. Kunimori, Appl. Catal., A 343 (2008) 125-133.

[28] C.H. Lee, Y.W. Chen, Ind. Eng. Chem. Res. 36 (1997) 1498-1506.

[29] B.W. Krupay, Y. Amenomiya, J. Catal. 67 (1981) 362-370.

[30] J. Silvestre-Albero, A. Sepúlveda-Escribano, F. Rodríguez-Reinoso, J.A. Anderson, J. Catal. 223 (2004) 179-190.

[31] H. Yoshida, Y. Yazawa, T. Hattori, Catal. Today 87 (2003) 19-28.

[32] W. Deng, M. Flytzani-Stephanopoulos, Angew. Chem. Int. Ed. 45 (2006) 2285-2289.

[33] P. Panagiotopoulou, D.I. Kondarides, Catal. Today 127 (2007) 319-329.

[34] J.C. Brown, E. Gulari, Catal. Commun. 5 (2004) 431-436.

[35] A.A. Phatak, N. Koryabkina, S. Rai, J.L. Ratts, W. Ruettinger, R.J. Farrauto, G.E. Blau, W.N. Delgass, F.H. Ribeiro, Catal. Today 123 (2007) 224-234.

[36] P. Panagiotopoulou, J. Papavasiliou, G. Avgouropoulos, T. Ioannides, D.I. Kondarides, Chem. Eng. J. 134 (2007) 16-22.

[37] K.G. Azzam, I.V. Babich, K. Seshan, L. Lefferts, J. Catal. 251 (2007) 163-171.

# Chapter 4 Mechanistic study of alkali-promoted Pt catalysts for the low-temperature WGS reaction

## 4.1 Introduction

In Chapter 1, it was discussed that oxidized Pt species on ceria are active sites for the low temperature WGS reaction [1, 2]. Both strong metal-support interaction [1] and coordinatively unsaturated sites (cus) on small Pt nano-particles (NPs) [3] have been proposed as crucial to create and stabilize such Pt-O species [4-7], while for (cus) sites on Pt NPs the support would not be important. Reversible changes in the Pt oxidation state and nanostructure on a ceria supported Pt was observed under different treatment atmosphere, oxidizing/reducing conditions, which is evidence of the strong interaction between oxidized Pt and $CeO_2$ that involves the reversible formation of a Pt-O-Ce bond. The bound Pt-O-Ce species stabilize Pt against sintering. Also, aggregated Pt particles formed by destabilization in reducing conditions can be redispersed by treatment in an oxidative atmosphere [6]. The reducible oxides provide superior metal-support interaction than the inert oxides, for example, $CeO_2$ >>$TiO_2$ > $Al_2O_3$ > $SiO_2$ [7]. A lot of effort has been devoted on dispersing and stabilizing the precious metals on the supports by optimizing the synthesis approaches [8-13], modifying the supports by various treatments [14-16] or by additives [11, 17].

Recently, Mavrikakis and co-workers [18, 19] revised the redox mechanism to a carboxyl-mediated mechanism, as CO is proposed to be oxidized by OH groups directly rather than by oxygen atoms adsorbed on Pt (111). While as discussed in Chapter 1, there is still no agreement on the WGS reaction mechanism, the presence of OH is decisively important for both reaction pathways.

Thus, WGS reaction catalysts should contain highly dispersed Pt sites, which are positively charged, and must be able to activate the dissociation of $H_2O$ to generate OH groups for the reaction.

Recently, researchers at the Pacific Northwest National Laboratory [14] have reported that coordinatively unsaturated $Al^{3+}$ Centers were binding sites for active catalyst phases of

platinum on γ-$Al_2O_3$. With low (≤ 1 wt%) Pt loadings, Pt is atomically dispersed on the support surface ($Pt/Al^{3+}_{penta}$ = 1). When the loading of Pt exceeds the number of $Al^{3+}_{penta}$ sites, 2D PtO rafts form. And it was proposed that it was essential to develop synthesis methods that allow for the systematic and controllable variation of the number of $Al^{3+}_{penta}$ sites, ultimately enabling to tailor the dispersion and morphology and, therefore, catalytic activity of active metals on the commonly used γ-$Al_2O_3$ support [14]. It was reported by Yoshida *et al.* [20] that Pt particles could be dispersed and stabilized on a basic support, such as MgO, through the formation of atomically dispersed platinate anions. Panagiotopoulou *et al.* [21] attributed the enhanced low-temperature WGS reaction activity of NM-$TiO_2$ catalysts (NM (noble metal) = Pt, Ru, Pd) promoted with small amounts of alkali metals (X = Li, Na, K, Cs) on the $TiO_2$ support to an increase of the number of the "permanent" strong metal-support interaction sites. Mallinson and co-workers [22, 23] reported that with Na addition, Pt in Pt-$TiO_2$ was more oxidized by Pt electron donation to O in $NaO_x$ through Pt–O–Na linkages. The strong metal–promoter interactions provide highly active sites for the WGS reaction at the periphery of the Pt–$NaO_x$ particles and also inhibit the sintering of Pt particles.

Moreover, alkali additives are known to favor the dissociation of $H_2O$. Campbell and co-workers studied Cs-modified Cu (111) [24] or Cu (110) [25] for the WGS reaction. Promotion by cesium was found and attributed to a mechanism where the surface Cs-O complex participates directly in the dissociation of adsorbed $H_2O$. In other work, Kuriyama *et al.* [26] have reported that potassium doping enhanced the OH coverage on Pt-$Al_2O_3$ with FTIR, which led to the promoted activity for the PROX reaction.

On the basis of the above literature reports, and our own findings of strong promotion of Pt catalysts supported on wither alumina or silica for the WGS reaction, as discussed in Chapter 3 of this thesis, we further investigated the promotion effect here to probe and identify the nature of the active sites, and propose a plausible reaction pathway. The experimental evidence was provided to our collaborators at the University of Wisconsin (Mavrikakis group) who came up with a working structure for the active site that captures all the properties observed experimentally [27]. Our findings are detailed in this chapter.

## 4.2 Materials and methods

The catalyst samples listed in Table 3.1 and examined for their WGS reaction activity in Chapter 3, were further investigated here.

The various alkali (alkaline-earth) ions M-Pt-$SiO_2$ samples were prepared by a two-step IMP method, as described in Chapter 2. In exploratory studies, we found that the Pt loading methods and the sequence of the Pt (Na) impregnation had no effect on either the physical properties or reactivity of the samples. So here to ensure the same Pt loading on all alkali-modified samples, the Pt precursor was added after the M nitrate impregnation. M stands for lithium (Li), sodium (Na), potassium (K), cesium (Cs), magnesium (Mg), calcium (Ca), and barium (Ba). The nitrate salts were used in all cases, and the Pt precursor was $Pt(NH_3)_4(NO_3)_2$.

New samples with a lower Pt loading, 1 wt%Pt-$SiO_2$ (0.3Pt-$SiO_2$) were prepared by the IMP method. Na (K) was added on the dried Pt samples at different Na (K):Pt ratios by sequential IMP using $NaNO_3$ ($KNO_3$) as the precursor.

All the samples were calcined at 400 $^oC$ in air for 4 h before testing. These samples are denoted as αPt-βNa/K-$SiO_2$, where α is the atomic percentage of Pt, and β is the atomic ratio of Na(K) to Pt.

Selected calcined Na-modified samples were washed with D.I. water to remove excess Na, *i.e.* any Na not associated with the Pt. The sample in powder form was suspended in a sufficient amount of D.I. water. To study the influence of washing time on the Na removal, the suspension was stirred at room temperature for 1, 5, 20, or 60 min, respectively. To investigate the influence of temperature on the Na removal, some samples were washed with D.I. water at 70 $^oC$ for 60 min. This was followed by filtering the suspension and drying the solid at 60 $^oC$ under vacuum overnight, further calcining it in static air at 400 $^oC$ for 4 h before testing. A heating rate of 2 $^oC$/min from room temperature to 400 $^oC$ was used.

Catalysts were characterized by ICP, TEM/HRTEM and ac-HAADF/STEM, XPS, CO chemisorption, CO-TPR, DRIFTS (by Professor Frederic Meunier at the University of Caen, France), and XANES, including time-resolved in situ XANES measurements.

Catalyst activities were evaluated for the WGS reaction under various conditions that included product-free and full reformate gas mixtures. Temperature-programmed-surface WGS reaction (TPSR) tests were also conducted to follow the reaction light-off and catalyst activity and stability under dynamic conditions.

## 4.3 Results and discussion

### 4.3.1 Active sites for the WGS reaction

#### 4.3.1.1 Na association on the Pt sites

One of the main questions how alkali ions modify the Pt catalysts. Do they modify the support surface only, making it like a reducible oxide? Or do they modify the Pt species and associate with them in a way that would be similar on any support?

Since alkali nitrate or alkali oxides are all highly soluble, a D.I. water-washing treatment was conducted on selected Na-promoted $SiO_2$ or Pt-$SiO_2$ samples to check how strongly Na bind with the $SiO_2$ or Pt-$SiO_2$ materials.

As shown in Table 4.1, the interaction of $NaO_x$ with $SiO_2$ or $Al_2O_3$ must be a weak one, as Na is easily removed by D.I. water from the modified Pt-free supports (the parent samples had been calcined at 400 $^oC$ in air for 4 h prior to washing). However, when the Na-modified Pt-$SiO_2$ samples, heat-treated the same way, were washed, not all of the $Na^+$ was removed. No Pt was found in the washing solution. Interestingly, we also found that the washing temperature and time had a negligible effect on the concentration of the residual Na (K) on both the Pt-free and Pt-Na (K)-$SiO_2$ or $Al_2O_3$ samples. The residual alkali is then attributed to the interaction of the alkali with the Pt species, *i.e.* to strong Pt-$(ONa)_x$ interaction, resisting washing. This is a direct manifestation of stabilization of both Pt and Na (K) species on the silica or the alumina surfaces. The former was established in Chapter 3, *e.g.* in Figure 3.2 and 3.3 by the Pt clusters and atoms stabilized by the alkali, while the latter is shown by the inability to wash away all the alkali from the surface in the experiments performed here.

Table 4.1 shows the residual amounts of $Na^+$ for the same Pt loading on $SiO_2$ when different atomic ratios of Na:Pt were used. No Pt was lost during the washing of any of the

samples. Clearly, most of the $Na^+$ was associated with the Pt species in the sample with Na:Pt = 1:1, from which only a small portion of the Na ions could be washed off. With higher Na:Pt ratio as 3:1, after washing, the amount of residual Na is bigger, which means that the 1:1 Na:Pt ratio did not provide enough Na to interact with the Pt species. This can explain why the WGS reaction activity of the latter is inferior to the sample with Na:Pt= 3:1, as shown in Figure 4.1. At an even higher Na:Pt ratio, 6:1, the amount of the residual $Na^+$ after washing is close to that in the washed 1Pt-3Na-$SiO_2$. This demonstrates that there is an optimal Na:Pt ratio, which provides efficient interaction between $Na^+$ and Pt species, maximizing the amount of the active sites for the WGS reaction and preventing the loss of Na ions during the washing treatment.

When a fixed amount of Na, 3 at%, was applied, the Pt loading was adjusted to match the maximum Pt-O-Na interaction. However, it was found (Table 4.1) that the residual Na content did not increase with the Pt loading, indicating that there may be a surface saturation for the total amount of metal (Pt and Na) added; alternatively, the limitation may be in the preparation technique (IMP). It was shown in Figure 3.7 that the Pt particle sizes increased with the Pt loading. Therefore we suspect that Na ions may only be able to decorate the small Pt clusters and atoms. The major portion of Pt particles on the 3Pt-3Na-$SiO_2$ sample is thus Na-free.

XPS data in Figure 4.2 shows that the Pt oxidation state in both the parent and washed samples is identical. Therefore the residual Na in the washed samples is enough to keep the Pt species dispersed and in nonmetallic state and the washing process has no effect on the oxidation state of Pt. Thus, there is a certain number of Na ions that interact directly with the Pt, and are non-washable. Above this number, the extra Na in the parent catalyst plays no role, is weakly bound and washable. The extra Na ions could be located on a Pt-free $SiO_2$ region or be close to the Pt species, but at a certain distance. The latter hypothesis can explained by the DFT calculations [27], where alkali ions forming a second shell around Pt atoms do not directly affect the Pt oxidation state and should not play any role on the Pt activity.

As shown by $H_2$-TPR in Table 4.1 and Figure 4.3, the $H_2$ consumption on the washed Na-modified Pt-$SiO_2$ surfaces dropped dramatically. The reduction of surface oxygen in the

washed samples ended at relatively low temperatures (< 300 $^{o}$C), below the onset of the reduction of the Na-$SiO_2$ surface. Apparently, none of that species remained after the washing. Thus, the residual Na must be tightly bound to the Pt-$O_x$ structure, while the associated with just the support is removed after washing.

Figure 4.4 compares the CO-TPR of parent and washed samples. The washing step removed the high-temperature surface oxygen associated with the extra Na. The important feature here is that the onset of $H_2$ production, which is also the onset of the WGS reaction, and the total amount of $H_2$ produced are the same for both the parent and washed catalysts, proving that the active sites are of the type Pt-$O_x(OH)_y$-Na.

The amount of surface oxygen remaining after washing corresponds to the active oxygen and leads to a Na:O atomic ratio=1:1. The surface oxygen amount was measured by CO-TPR, Table 4.1, and is in agreement with the surface oxygen measured by $H_2$-TPR. Because the surface Pt amount measured with XPS (Table 4.1) includes the contribution from Pt nanoparticles along with the atomically dispersed Pt, we cannot use the surface Na:Pt ratio measured by XPS (Table 4.1) as the real optimized Na:Pt atomic ratio. We can only use it as a lower bound; on this basis, the active sites comprise at least 3 Na atoms associated with each Pt atom. By integrating the amount of oxygen reduced in the range of 100-300 $^{o}$C, we calculate a value of OH:Pt between 2 and 3 (Table 4.1).

Considering the same oxidation state of Pt species, the large difference of total surface oxygen amount, but the same active OH amount in the parent and washed samples, we can conclude that washable Na ions (and associated oxygen) in the parent samples are only weakly bound on the $SiO_2$ support and not involved in the WGS reaction pathway. There is a certain Na:Pt ratio, which keeps Na strongly and effectively associated with the Pt-$O_x(OH)_y$ species, and prevents this part of the sodium from washing away, and these sites are the active sites for the WGS reaction.

Notably, the parent and washed samples showed identical WGS reaction activity in a realistic fuel gas stream, as can be seen in Figure 4.1. This result further supports the Pt-$O_x(OH)_y$-Na sites as the active sites for the WGS reaction [27].

#### 4.3.1.2 The oxidation state of Pt in the active sites for the WGS reaction

As discussed above, it appears that only Pt atoms or few-atom clusters can associate with alkali ions to create active sites for the low-temperature WGS reaction. High Pt loading leads to the formation of Pt particles, which are spectator species and most probably would not associate with the added alkali ions. Because of the coexistence of Pt particles with atoms/clusters, it was not possible to precisely follow the reaction-relevant active site structure experimentally and determine the optimum ratio of M:Pt in alkali-promoted Pt samples with high Pt loading, *e.g.* 1 at%.

It was next attempted to lower the amount of Pt and disperse it better on the silica or alumina surfaces. According to a recent publication [14], with mild air-calcination, Pt could be fully dispersed on $\gamma$-$Al_2O_3$ with Pt loading lower than 1 wt%. Here we prepared 0.3 at% (1 wt%) Pt on the fumed silica support.

CO chemisorption was used to characterize the surface Pt dispersion. A linear CO adsorption on Pt (CO:Pt = 1:1) was assumed for the dispersion calculation. The Pt species were fully dispersed on $SiO_2$ even without alkali-modification. Therefore we had an ideal system to begin with. Na ions were applied to modify the well-dispersed Pt species. With Na modification, Pt dispersion was decreased to about 80%, but this decrease could be attributed to the change of the CO adsorption mode on Pt, from linear to bridged adsorption [28], and also possible coverage of Pt by Na instead of the aggregation of Pt particles. As shown in Figure 4.5 with Na promotion, the sample with 0.3% Pt loading is almost as active as the one with 1% Pt loading for the WGS reaction at temperatures higher than 200 $^{o}$C, indicating a more efficient use of Pt in the former. The Na-free 0.3Pt-$SiO_2$ is not active for the reaction up to 350 $^{o}$C even though it contains fully dispersed Pt, at least initially. Hence, the active sites are not just $Pt_n$-O species. Na is needed to provide OH groups and render the Pt active. In Figure 4.5, the corresponding washed samples have the same catalytic activity as their parent samples, which is consistent with the findings in the last section.

The intensity of the white line in XANES directly reflects the electron deficiency of the absorbing atom. In this work in situ XANES and time-resolved Quick-XANES of samples under either WGS reaction or $H_2$-reduction conditions, were applied to identify the

reaction-relevant Pt oxidation state in the alkali-promoted Pt catalysts for the WGS reaction.

The in situ XANES at Pt $L_{III}$-edge was collected in the transmission mode in He at room temperature after different treatment conditions, namely fresh (as prepared), used (after 1 h WGS reaction condition, 1%CO-3%$H_2O$-He, at 275 $^oC$), reduced (the fresh samples were pre-reduced in 5%$H_2$-He at 200 $^oC$ for 2 h), and used reduced (the reduced samples were seen 1%CO-3%$H_2O$-He at 275 $^oC$ for 1 h). The X-ray absorption edge energy was calibrated with Pt foil at 11564 eV. The reported XANES data were the averages of three scans and no changes were detected between the first and last scan.

All fresh samples with 0.3 at% Pt loading have the same white line intensity and Pt species are in more oxidized state, compared with Pt foil, as shown in Figure 4.6 (A). As found by CO chemisorption the 0.3 at% Pt was fully dispersed on the $SiO_2$ support even without K-promotion. Therefore it is reasonable to find oxidized Pt on all samples. Also, the washing procedure did not affect the Pt oxidation state.

In 0.3Pt-$SiO_2$, Pt species are as dispersed as those in K-promoted ones. However, Pt-$SiO_2$ is not active for the WGS reaction up to 350 $^oC$, while the K-promoted sample is activated below 150 $^oC$. Thus, both the oxidized Pt and the K-associated OH groups are both crucial to initiate the reaction. CO-TPR was used to titrate the surface OH groups. The CO-TPR profiles in Figure 4.7 show that even with fully dispersed Pt species on the $SiO_2$ surface, there are no active OH groups, and the reaction does not light-off. On the other hand, $CO_2$ and $H_2$ are readily produced on the K-promoted sample.

Numerous investigations have been carried out to study the $H_2O$ dissociation on metals, such as Cu, Au, Ni, and Pt [29, 30]. $H_2O$ dissociation on Pt is not favorable. Thus, on 0.3Pt-$SiO_2$, even though Pt was fully dispersed on the surface, neither the Pt sites nor the $SiO_2$ surface could dissociate $H_2O$ and supply active OH groups for the WGS reaction pathway. Conversely, because of the hydrophilic properties of the alkali ions, K additives assist the dissociation of $H_2O$ and provide the surface OH groups needed for the reaction pathway. In the presence of Pt, these are activated by CO to give $H_2$ and $CO_2$ at temperatures lower than 100 $^oC$, as shown in Figure 4.7.

After being exposed to the WGS reaction or $H_2$ reduction, the white line intensity of Pt at $L_{III}$-edge decreased. The same trend was observed over all samples, Figure 4.6 (B) and (C) show the plots for K-free and K-promoted samples as examples. But the white line intensities over all the used or reduced samples are still higher than those over Pt foil. Figure 4.6 (D) further compares the XANES over the used catalysts w/o K additives. It is shown that after exposure to the reaction gas at 275 $^oC$ for 1 h, the Pt species in K-promoted catalyst are more electron deficient than those in the K-free sample, which means the reaction or reduction destabilizes and reduces the alkali-free $PtO_x$, species, while the K-promoted Pt-O species are stable and responsible to the long-term catalytic stability shown in Chapter 3, Figure 3.18 and 3.20.

It is also worth mentioning that the white line intensities of Pt in the used samples in Figure 4.6 (C) with or without a $H_2$-pretreatment are the same. Thus the $H_2$-reduction treatment should have no effect on the formation or stability of the Pt active sites. Indeed, activity tests show that the fresh and pre-reduced K-promoted 0.3Pt-$SiO_2$ samples have the same WGS reaction activity. Therefore it is concluded that other than introducing OH groups to the surface, K ions also inhibit the reduction of the oxidized Pt species during reduction or reaction conditions and keep Pt in oxidized state to maintain the catalytic activity for the WGS reaction.

It is also important to follow the Pt active structure evolution during the WGS reaction and various treatments. Time-resolved Quick-XANES was performed to obtain such information.

The time-resolved in-situ Pt oxidation state changes in 0.3Pt-6K-$SiO_2$ during $H_2$-pretreatment was monitored by Quick-XANES at the Pt $L_{III}$-edge, as shown in Figure 4.8. The while line intensity experienced a significant drop below 100 $^oC$ and became constant afterwards, most probably because of the reduction of the adsorbed surface oxygen species, as confirmed by the $CO_2$ production during CO-TPR under 100 $^oC$ (Figure 4.7), while these oxygen species are not involved in the WGS reaction. The stabilized white line intensity is still higher than which of Pt foil, which shows a partially oxidized state of Pt.

A $H_2O$-treatment at 275 $^oC$ for 10 min was able to re-oxidize the Pt species to some extent, as shown in Figure 4.9 with the slightly enhanced white line intensity. The higher but not

constant white line intensity, appearing at the beginning of the test, should be ascribed to the unstable physical adsorption of $H_2O$ on the Pt sites. When the surface was saturated with OH groups from the dissociation of $H_2O$, the white line intensity became constant. Deng *et al.* [31] reported that the oxygen potential in the gas stream controlled the oxidation state of Au in Au-$CeO_2$ catalysts for the WGS reaction. The same may be true for Pt catalysts as well. The $H_2O$-containing gas stream has higher oxidation potential than the $H_2$-containing stream therefore a higher oxidation degree/electron deficiency of Pt is expected with the $H_2O$ treatment.

After CO was introduced into the $H_2O$-He stream, Figure 4.10, the intensity of the while line was not changed, which means the electron deficiency of Pt was maintained during the reaction condition. CO adsorption over alkali-modified samples has been found to be weaker than on unpromoted Pt [32], which means lower electron donation to Pt, *i.e.* less effect on the oxidation state of the Pt species from the CO adsorption, as shown by XANES.

On the basis of the above findings, the dispersed and partially oxidized Pt species with the incorporation of OH groups in the alkali-promoted Pt-$SiO_2$ are the active sites for the WGS reaction. In reducing gases, reduction and sintering of the alkali-free dispersed Pt clusters and atoms takes place, but the Pt-O species associated with alkali ions will be stabilized and exhibit catalytic activity and stability in the WGS reaction, as discussed in Chapter 3.

All this experimental evidence was used to arrive at plausible structures of the active sites by our collaborator, Prof. Manos Mavrikakis and his research group at the University of Wisconsin, Madison. Using ab initio Molecular Dynamics, they modeled the structure as a spherocentric cluster of one Pt atom in the center surrounded by 6 potassium atoms, linked to the Pt with 4 oxygen and 2 OH; $PtK_6O_4(OH)_2$ [27]. This site preserves Pt in an oxidized state, adsorbs CO weakly, and dissociates water with very little energy (almost thermoneutral dissociation). Its properties are similar to Cu (111), one of the best WGS catalysts. One could derive a few other similar structures to fit our data, but the point is that single-site Pt, multinuclear clusters containing the potassium ions and active OH groups are predicted as the active sites without any limitation from the support [27]. This is

an exciting finding that should be pursued further for other alkali and even other metal centers, and is a main recommendation from this thesis work.

#### 4.3.1.3 Regeneration of surface OH groups

Alkali additives are known to favor the dissociation of $H_2O$. Here, we examined the effect of alkali addition to the properties of surface OH groups on the Pt-$SiO_2$ catalysts. Considered as the reactant involved in the WGS reaction pathway, the active OH groups must be regenerated on stream and at low temperatures to have an effective low-temperature shift catalyst. As mentioned above, being highly hydrophilic, alkali ions should be able to facilitate the adsorption and the dissociation of $H_2O$. At high temperatures (>300 $^oC$) they can do this without a metal, *e.g.* on the alumina surfaces studied by Amenomiya and co-workers [33]. Pt addition shifts the activation to low temperatures, as shown by Pierre [34] and in this thesis, *e.g.* Figure 3.4. To investigate this further, cyclic CO-TPR with intermittent $H_2O$ treatment was performed. Temperature-programmed WGS reaction was carried out as well to confirm the regeneration of OH groups on-stream.

To eliminate the influence of adsorbed surface oxygen species, a pre-reduction was carried out before the cyclic CO-TPR. It was shown in Figure 4.7, that there are no active surface OH groups on the alkali-free 0.3Pt-$SiO_2$. With Na-promotion, the surface OH groups were introduced and begin to react with CO at around 100 $^oC$, as can be seen in Figure 4.11. Cooling the sample in He to room temperature, a second cycle of the CO-TPR begun without any treatment, which checked that the surface OH groups had been almost completely depleted during the first cycle, and neither $CO_2$ nor $H_2$ was produced in the second cycle. However, if a water-vapor treatment at room temperature for 30 min preceded the second cycle, a complete recovery of the $CO_2$ and $H_2$ production was observed as shown in Figure 4.11. Therefore, the alkali additives do favor the adsorption and dissociation of $H_2O$ at low temperatures, rendering quick regeneration of the active OH reactant for the reaction. As is evident in the WGS-TPSR measurement, Figure 4.12, the onset of the reaction is the same as the onset of $H_2$ production in CO-TPR. In addition

with on-stream supply of $H_2O$, OH groups were regenerated simultaneously and the catalytic activity of alkali-promoted Pt-$SiO_2$ was maintained.

Therefore, we have shown that other than keeping the Pt in oxidized state, alkali ions also facilitate the adsorption and dissociation of $H_2O$ to provide the OH groups for the WGS reaction.

### 4.3.2 Comparison of promotion effects with different alkali/alkaline-earth ions

We have noticed that when the Pt loading is fixed, when the same ratio of alkali ion to Pt, Na:Pt or K:Pt is used, the reducible surface oxygen species on the Na-modified sample are less than K-modified sample over the entire temperature range, while it is more reducible at lower temperatures. In turn, Na-promoted catalysts are more active than the K-promoted ones for the WGS reaction. This is shown in Figure 3.4, 3.5, and 3.12 in Chapter 3. Potentially it could be due to sub-optimal ratios used or they may derive from the different nature of each promoter. Panagiotopoulou et al. [21] investigated the different promotion of Li, Na, K, and Cs on Pt-$TiO_2$ and found the promotion effect was in the order of Na>K≈Li>Cs. A volcano-type dependence of intrinsic reaction rate on the chemisorption strength of the active sites toward hydrogen was proposed. When alkaline-earth metals were applied, the promotion effect followed the order of CaO > SrO > BaO > MgO [35]. It was claimed that the additives did not alter the reaction mechanism or the rate determining step, but mainly favored the formation of active sites for the WGS reaction, $Pt–□_s–Ti^{3+}$. From both the fundamental and the practical viewpoint, it would be interesting to evaluate and rank order of the promotion effects from other alkali or alkaline-earth ions to find the most efficient additives for the Pt-based catalysts used in this work.

M-promoted 1Pt-$SiO_2$ samples were prepared by the two-step impregnation method described in Chapter 2, where M= Li, Na, K, Cs, Mg, Ca, Ba. A fixed atomic ratio M:Pt = 3 was used here for the 1 at.% Pt loading. It is important to point out that the D.I. water washing treatment has no effect on the Pt oxidation state and reactivity of the M-modified samples. And from our earlier work described above, the residual (non washable) Na or K ions associated and stabilized by Pt-O are the active promoters; the excess Na plays no role in the reaction. Hence, the following discussion is focused on the washed M-modified

samples only. Figure 4.13 displays the steady-state WGS reaction rate over the washed M-modified 1Pt-$SiO_2$ samples. Clearly all the M ions boost the 1Pt-$SiO_2$ for the low-temperature WGS reaction. The apparent activation energies over all samples are in the same range, 70 ± 5 kJ/mol, which indicate that the same WGS reaction pathway is shared by all Pt-based catalysts. The difference in the reaction rates may be merely due to the different concentration of the active sites on each sample.

In Chapter 3, it was noted that the WGS active site in Pt-based catalysts may not depend on the support or the type of promoter used. The zero activity of Pt-$SiO_2$ allows us to count the active sites created by each additive without interference of Pt-support interaction. Finding the same turnover frequency (TOF) for the WGS reaction over various M-modified Pt-$SiO_2$ would be a more convincing way to claim a support- or additive-independent active site for the Pt catalysts. Due to the difficulty in measuring the Pt dispersion by chemisorption or XPS, as mentioned in Chapter 3 and since the OH groups are part of the active site [27], the active sites were estimated here in terms of the amount of active OH groups in the low temperature range.

As discussed in Chapter 3, K-modified Pt-$SiO_2$ behaves a little differently from the Na-modified ones, as the same amount of K ions leads to more reducible surface oxygen on $SiO_2$, but the center of the reduction peak shifts to higher temperatures. K-modified samples show lower catalytic activity for the WGS reaction, which indicates that only the low-temperature (< 200 $^oC$) reducible surface oxygen is relevant to the removal of CO by $H_2O$.

$H_2$-TPR profiles over the washed M-Pt-$SiO_2$ materials were collected and are shown in Figure 4.14. The reducibility of 1Pt-$SiO_2$ apparently differs with different additives. As just mentioned, only the low-temperature (<200 $^o$) reducible surface oxygen species are relevant to the removal of CO by $H_2O$ in this WGS application. Based on the CO-TPR over the washed 1Pt-3Na-$SiO_2$ in Figure 4.4, the reducible surface oxygen at temperatures lower than 100 $^oC$ is mostly probably responsible for just the dry CO oxidation, while the oxygen reduced above 100 $^oC$ comprises the active OH groups for the WGS reaction. Therefore deconvolution of the reduction peaks in $H_2$-TPR (Figure 4.14) was carried out to separate different kinds of oxygen species. The amount of reducible oxygen species

centered between 100-150 $^{o}$C, which contains the active OH groups, is listed in Table 4.2. These OH groups are counted as active sites for the WGS reaction and the reaction rate was normalized by the amount of these OH groups to calculate the TOF over Pt-$SiO_2$ samples with various additives. Figure 4.15 shows that normalizing the reaction rate by the active OH groups, brings the Arrhenius plots over M-Pt-$SiO_2$ samples into a single line. The TOFs over M-Pt-$SiO_2$ materials for the WGS reaction at 250 $^{o}$C are compared in Table 4.2. Similar TOF is found over Pt-$CeO_2$ [2], which further demonstrates that the alkali or alkaline-earth additives as well as ceria create similar active sites on Pt catalysts for the WGS reaction, and the structure of the active site, Pt-$O_x(OH)_y$ appears to be both support- and additive-independent.

Using the total OH as a scaling factor may be inaccurate, of course, as perhaps not all of the OH is regenerable (*i.e.* active) on the catalyst surface. But after washing, and after a reduction step (followed by room temperature rehydration), counting the active OH by the CO-TPR technique is proposed as a good, complementary method to IR and other spectroscopies that could be used for the same purpose.

It is clear that with the same M:Pt ratio, different alkali or alkaline-earth ions associate with the Pt sites differently, creating different amounts of active sites in the investigated temperature range. As these additives are different in size, electronegativity, or basicity, the optimum ratio of M:Pt, providing the most effective promotion for creating active sites, should be different for each additive. Since they are all highly hydrophilic, the dissociation of $H_2O$ and regeneration of OH groups over alkali/alkaline-earth modified Pt sites should not be an essential concern in the design of new catalysts. However, to find the optimum M:Pt ratio, which efficiently decorates all the Pt sizes and stabilizes them, is a major undertaking recommendation to be addressed in future work.

In this thesis work, some preliminary work was done to check the effect of various additives on the Pt oxidation state. XPS and XANES measurements were conducted to check the effect of additives on the oxidation state of Pt species. Figure 4.16 shows the XP spectra at $Pt_{4f}$ in some of the modified samples. In the presence of the promoter, the Pt peaks shifted to higher binding energies compared to those of the bare Pt-$SiO_2$, indicating a higher oxidation state of the promoted Pt species. Such effect is confirmed by XANES, in

Figure 4.17. The XANES was taken over the fresh samples in He. All the additives enhance the electron deficiency of the Pt species supported on silica, as shown by higher white line intensity at Pt $L_{III}$ edge, compared with that of bare Pt-$SiO_2$. The different promoters modify the Pt oxidation state to a different extent, while currently available data are not enough to provide a solid plausible explanation. More careful synthesis and characterization are required to obtain detailed information about the difference of Pt oxidation states caused by the additives. The following discussion provide some thoughts regarding the different effect of various additives on the Pt oxidation state, and it also give a possible explanation for why the promoter-stabilized $PtO_x$ is more stable than $PtO_x$ alone.

In 2003 Hattori and co-workers [36] claimed that the total electrophilic/electrophobic properties of the support and additive controlled the oxidation state of platinum, *i.e.* higher electrophobic property provided more oxidized platinum. The mechanism of the support/additive effect on the oxidation-stability of precious metals was discussed as it came from the variation of the stability of the binary oxide containing the precious metals. These binary oxides containing precious metals were more stable than precious metal oxide such as $PtO_2$, and the conjugation with alkali and alkaline earths is especially effective for stabilization [37].

$$Pt + MO_x + O_2 \xrightarrow{oxidation} PtO_2 + MO_x \xrightarrow{binary\ oxide\ formation} MPtO_\alpha$$

The decomposition temperature of the binary oxide containing platinum is listed in Table 4.3 [36]. From this table we can deduce that the lower the electronegativity of the additives/supports, the more stable the binary oxide containing platinum. The electronegativities of all studied alkali and alkaline-earth metals are shown in Table 4.4. K, Cs, and Ba are the metals with lower electronegativity than that of Na, which are supposed to give more stable binary oxide and thus theoretically provide more stable active sites for the WGS reaction. However, this deduction is not consistent with the experimental reactivity data shown in Figure 4.13.

To explain this discrepancy, firstly as discussed above, the M-doping may modify the electron property of Pt species, keeping Pt species more dispersed and in more oxidized state, which may in turn influence the CO adsorption binding strength and then the WGS reaction activity. Additives with very low electronegativities may over-compensate the

properties of the Pt sites. The *"good"* stability of the *"binary oxide"* may negatively affect the ability of Pt species to serve as catalytically active sites for the WGS reaction. DFT calculations are required to test this hypothesis and guide further design of the new catalysts.

### 4.3.3 Reaction intermediates for the WGS reaction

As mentioned in Chapter 1, Davis and co-workers [21-23, 38-41]investigated the alkali-promoted Pt on $ZrO_2$, $CeO_2$, or $TiO_2$ catalysts and explained the alkali promotion as a weakening of the C-H bond of formate species, the breaking of C-H bond in the formate proposed to be the rate-limiting step of the low temperature WGS reaction. In-situ SSITKA-DRIFTS techniques were used to draw these conclusions. However, while formate species exist on these surfaces, they may not be the reaction intermediates. The formate mechanism for the WGS reaction on these Pt-based catalysts has been challenged by others [42-44].

Here we tried briefly to use in situ DRIFTS to examine the alkali-promoted 0.3Pt-$SiO_2$ samples and see what species dominated the surface under in situ conditions. The experiments were carried out by Professor Frederic Meunier at the University of Caen, France. When 2%CO-6%$H_2O$-He was passed over the washed 0.3Pt-Na-$SiO_2$ at 250 $^oC$, various Pt species were found, with distinct carbonyl bands as shown by the different peaks in Figure 4.18. The peaks at 2049 $cm^{-1}$ and 1736 $cm^{-1}$ are assigned to linearly-bonded CO to $Pt^o$, the peak at 2180 $cm^{-1}$represents the CO adsorbed on $Pt^{3+}$, and the peak at 1938 $cm^{-1}$ is either due to CO adsorption on low-coordinated Pt or a bridged CO-adsorption [45, 46]. With time-on-stream, the carbonyl on oxidized Pt readily vanishes, the carbonyl of $Pt^o$ increases a lot, while the carbonyl on low coordination number $Pt^o$ increases a bit in Figure 4.18. Of course, we need also to differentiate the OH groups on the surface, but this was not easy to do from the present data. Interestingly, no formate species were found on this sample during the course of the reaction.

Correlating the dynamic DRIFTS results with the reaction activity, as shown in Figure 4.19, the oxidized Pt species appear to have the highest activity for the WGS reaction. However they are not stable, and will vanish rapidly under the reaction condition. Such rapid

deactivation at the beginning of the test was reported in Chapter 3, Figure 3.18 and 3.20, when the stability test was conducted in the reformate gas stream. And the Q-XANES shown in Figure 4.8 also confirms a quick loss of part of the oxidized Pt species as soon as the sample was exposed to the reducing gas stream. The quick reduction of the oxidized Pt species could be attributed to the reduction of alkali-free $PtO_x$ sites, which are unstable as just discussed in the last section, or the reduction of alkali-lean $PtO_x$ sites, as suggested by the DFT calculations [27], the charge of the Pt atom is stabilized only when there are more than 6 potassium atoms around it. Therefore, optimizing the M:Pt ratio is crucial for good catalyst design, avoiding Pt overloading to efficiently stabilize the oxidized Pt sites.

In Figure 4.6 (D) it is seen that the Pt species in the used alkali-modified samples are still more electron deficient than those in the alkali-free sample. It is believed that these are the sites stabilized by the alkali ions. In Figure 4.18 & 4.19, it is shown that the "low-coordinated" Pt species are stable throughout the activity test. Are they involved in the reaction? It is unclear. The assignment of the carbonyl peak at 1938 $cm^{-1}$, now given as CO adsorbed on low-coordinated Pt species, needs more investigation in future work. Kuriyama *et al*. [26] have reported that with the alkali-modification the Pt species on $Al_2O_3$ were in a electron deficient state and the CO adsorption would be weakened over these sites, leading to bridged CO-adsorption, which are more active than the linearly adsorbed CO molecules. The metallic $Pt^o$ is not active for the WGS reaction, based on the data of Figure 4.18 and 4.19.

26%$H_2$ was added into the reaction gas stream to force the depletion of $Pt^{3+}$. Figure 4.20 compares the DRIFTS spectra of Pt-$SiO_2$ without any Na additives. At the steady-state, 0.3Pt-$SiO_2$ gave a very low CO conversion as 0.3%. From the spectra, it is clear that there is only one peak, carbonyl on $Pt^o$, which is not the active site for the reaction. While over the Na-promoted sample, a CO conversion of 3.6% was recorded, and a peak assigned to carbonyl on "low-coordinated" Pt was captured.

As mentioned above, both Figure 4.18 and Figure 4.20 show no evidence of formate over this $SiO_2$–supported Pt sample, which clearly shows that formate species are not the intermediates for the WGS reaction. Potentially the formate species found on other supports are bound to the support, but are spectator species for the WGS reaction, unlike

what has been proposed by other groups [39, 47]. The carboxyl reaction pathway proposed by Mavrikakis and co-workers for Pt catalysts [18, 19] may be invoked to explain the Na-promotion effect. Accordingly, CO is oxidized by the OH groups and the alkali ions facilitate the dissociation of $H_2O$ to generate active OH groups for the reaction. The energetic of carboxyl formation is more favorable than that of a formate [18, 19]. Additional IR evidence needs to be gathered focusing also on the active (regenerable) OH species and their depletion during reaction; and regeneration with properly designed experiments.

## 4.4 Summary

The strong Pt-O/OH-Na association in the Na-promoted Pt-$SiO_2$ samples was determined by a D.I. water treatment. D.I. water was effective to wash away the Na part weakly associated with the support from parent catalysts after the 400 $^oC$-air calcination, any residual alkali is then attributed to the interaction with Pt species, *i.e.* to strong Pt-$(ONa)_x$ interaction. Pt oxidation states in the washed and parent samples are the same. The total reducible oxygen amount on the washed sample is decreased compared with which on the corresponding parent sample, while the onset of $H_2$ production, which is also the onset of the WGS reaction, and the total amount of $H_2$ production are the same for both the parent and washed catalysts. The parent and washed samples showed identical WGS reaction activity in a realistic fuel gas stream. These evidences highly express that the non-washable Pt-$O_x(OH)_y$-Na sites serve as the active sites for the WGS reaction.

With the study on 0.3Pt-$SiO_2$ samples by the detail Quick-XANES and cyclic CO-TPR analysis, it is concluded that the dispersed and electron positive Pt species with the incorporation of OH groups are the active sites for the WGS reaction. The reducing atmosphere will reduce and sinter the alkali-free Pt clusters, while those associated with alkali ions will be stabilized and corresponding to the good stability as discussed in Chapter 3. The presence of alkali-ions also facilitates the dissociation of $H_2O$ and thus the regeneration of OH groups, which in turn lasts the reaction.

Other than Na and K ions, alkali-promotion effect was also found by other alkali/alkaline-earth ions, $Li^+$, $Cs^+$, $Mg^{2+}$, $Ca^{2+}$, and $Ba^{2+}$. A significantly enhanced catalytic activity is

reported over all modified Pt catalysts on $SiO_2$. An support- or additive-independent Pt active site, Pt-$O_x(OH)_y$, is proposed in the Pt-based materials for the WGS reaction. The presence of the alkali or Ce ions is important to stabilize the active Pt sites, but the host oxide does not participate in the reaction.

No formate species were observed over the $SiO_2$-supported catalysts by DRIFTS. The carboxyl reaction pathway is applied to explain the Na-promotion effect. The additional Na ions keep the Pt in an oxidized or electron deficient state, as the active sites for the WGS reaction, and facilitate the dissociation of $H_2O$ to regenerate active OH groups. CO is oxidized by OH groups, and this step is the rate limiting step for the WGS reaction over Pt-$SiO_2$ samples.

**Table 4.1 Physical properties and reducibility of parent and washed[a] Pt-O-Na-$SiO_2$ samples.**

| Sample | Bulk Composition (at.%) [b] | | Surface concentration (at.%) [c] | | Surface [O] ($\mu mol/g_{cat}$)[d] | Surface Na/Pt | Surface Na/O | Surface [OH]/Pt[e] |
|---|---|---|---|---|---|---|---|---|
| | Pt | Na | Pt | Na | | | | |
| 3Na-$SiO_2$ | 0 | 3.0 | 0 | | 500 | -- | | |
| 3Na-$SiO_2$ Washed | | -- | | trace | -- | -- | | |
| 1Pt-1Na-$SiO_2$ | | 1.0 | 0.3 | 0.9 | 210 | -- | | |
| 1Pt-1Na-$SiO_2$ washed | 1 | 0.7 | 0.4 | 0.5 | 185 | 1.2:1 | 1:1.5 | 2:1 |
| 1Pt-3Na-$SiO_2$ | | 3.0 | 0.3 | 3.9 | 450 | -- | | |
| 1Pt-3Na-$SiO_2$ washed | 1 | 1.6 | 0.4 | 1.2 | 245 | 3:1 | 1:1 | 3:1 |
| 1Pt-6Na-$SiO_2$ | | 6.0 | 0.5 | 4.4 | 1744 | -- | | |
| 1Pt-6Na-$SiO_2$ washed | 1 | 2.1 | 0.7 | 2.2 | 305 | 3:1 | 1:1 | 3:1 |
| 2Pt-3Na-$SiO_2$ | | 3.0 | 0.5 | 4.5 | 634 | | | |
| 2Pt-3Na-$SiO_2$ washed | 2 | 2.0 | 0.7 | 1.7 | 295 | | | |
| 3Pt-3Na-$SiO_2$ | | 3.0 | 1.2 | 2.1 | 470 | | | |
| 3Pt-3Na-$SiO_2$ washed | 3 | 2.1 | 0.8 | 1.2 | 353 | | | |

a: DI-water-washed samples were calcined at 400 $^oC$ in air before testing.

*b:* Measured by ICP-OES.

*c*: measured by XPS.

*d*: By CO-TPR in 5%CO-He, from RT to 400$^oC$, at 10$^oC$/min.

e: [OH]--calculated from CO-TPR by peak deconvolution. Pt amount was measured by XPS.

**Table 4.2 WGS TOF of Pt-$SiO_2$ modified by various additives.**

| Sample | OH (μmol/g) * | TOF ($s^{-1}$) # |
|---|---|---|
| 1Pt-Li-$SiO_2$ | 189 | 0.1 |
| 1Pt-Na-$SiO_2$ | 245 | 0.13 |
| 1Pt-K-$SiO_2$ | 172 | 0.05 |
| 1Pt-Cs-$SiO_2$ | 29 | 0.05 |
| 1Pt-Mg-$SiO_2$ | 27 | 0.05 |
| 1Pt-Ca-$SiO_2$ | 118 | 0.05 |
| 1Pt-Ba-$SiO_2$ | 69 | 0.2 |
| 0.8Pt-$CeO_2$ | NA | 0.13 & |

*: The amount of OH groups was estimated from deconvolution of the $H_2$-TPR profiles and integration of the $H_2$ reduction peak centered between 100-150 $^oC$.

#: The TOF was calculated by normalizing the reaction rate by the OH amount. Values are for 250 $^oC$, in 11%CO-26%$H_2O$-26%$H_2$-7%$CO_2$-He at atmosphere pressure.

&: The reaction rate was normalized by the surface Pt amount, which was measured by XPS [2].

**Table 4.3 Decomposition temperature of binary oxides containing platinum [37]**

| Oxide | Electronegativity of $MO_x$ in $MPtO_\alpha$ | Decomposition temperature (K) |
|---|---|---|
| $PtO_2$ | --- | 896-933 |
| $CdPt_3O_4$ | 2.44 | 978-1162 |
| $ZnPt_3O_4$ | 2.37 | 982-1165 |
| $CaPt_3O_4$ | 1.87 | 1053-1307 |
| $LiPt_3O_4$ | 1.52 | 1042-1135 |
| $NaPt_3O_4$ | 1.41 | 1071-1241 |

**Table 4.4 Electronegativities of alkali and alkaline-earth metals**

| Metal | H | Li | Na | K | Cs | Mg | Ca | Ba |
|---|---|---|---|---|---|---|---|---|
| Electronegativity | 2.20 | 0.98 | 0.93 | 0.82 | 0.79 | 1.31 | 1.00 | 0.89 |

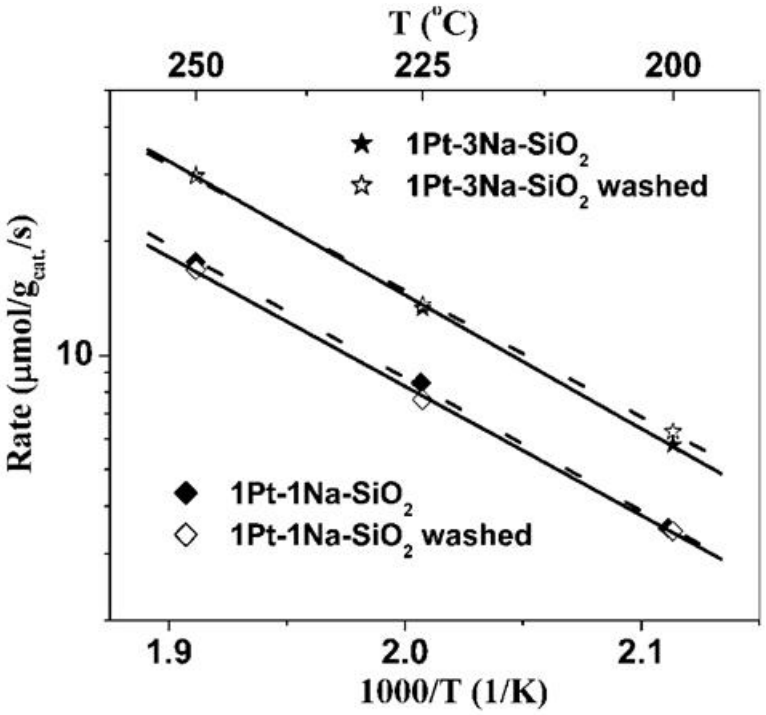


Figure 4.1 Steady-state WGS reaction rates measured on parent and D.I.-water washed samples in a fuel gas mixture: 11%CO-26%$H_2O$-26%$H_2$-7%$CO_2$-He.

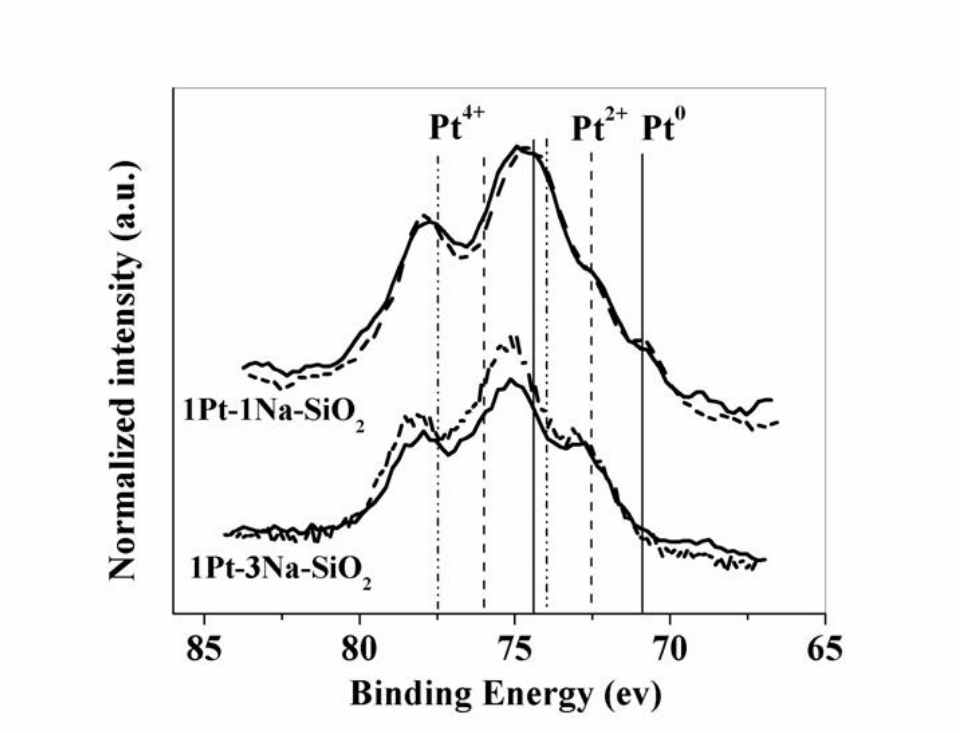


Figure 4.2 $Pt_{4f}$ XP spectra of parent and washed Na- promoted Pt samples.

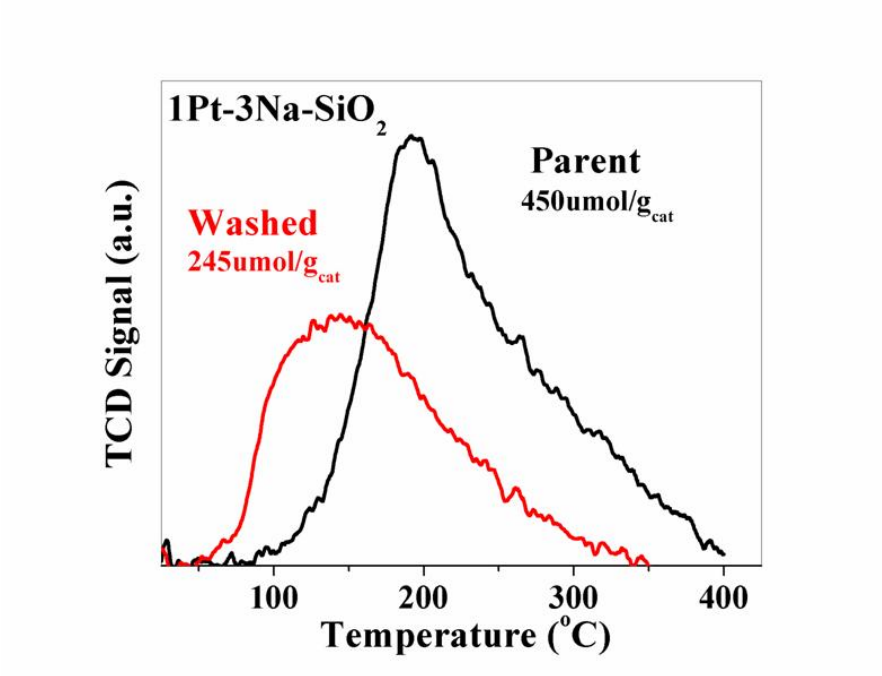


Figure 4.3 Comparison of $H_2$-TPR profiles of parent and washed 1Pt-3Na-$SiO_2$.

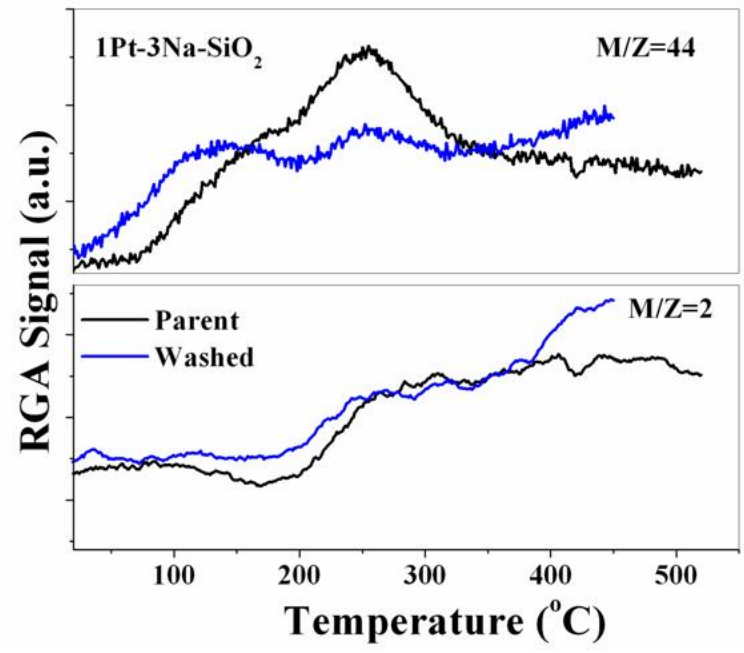


Figure 4.4 Comparison of CO-TPR profiles of both parent and washed 1Pt-3Na-$SiO_2$ catalysts.

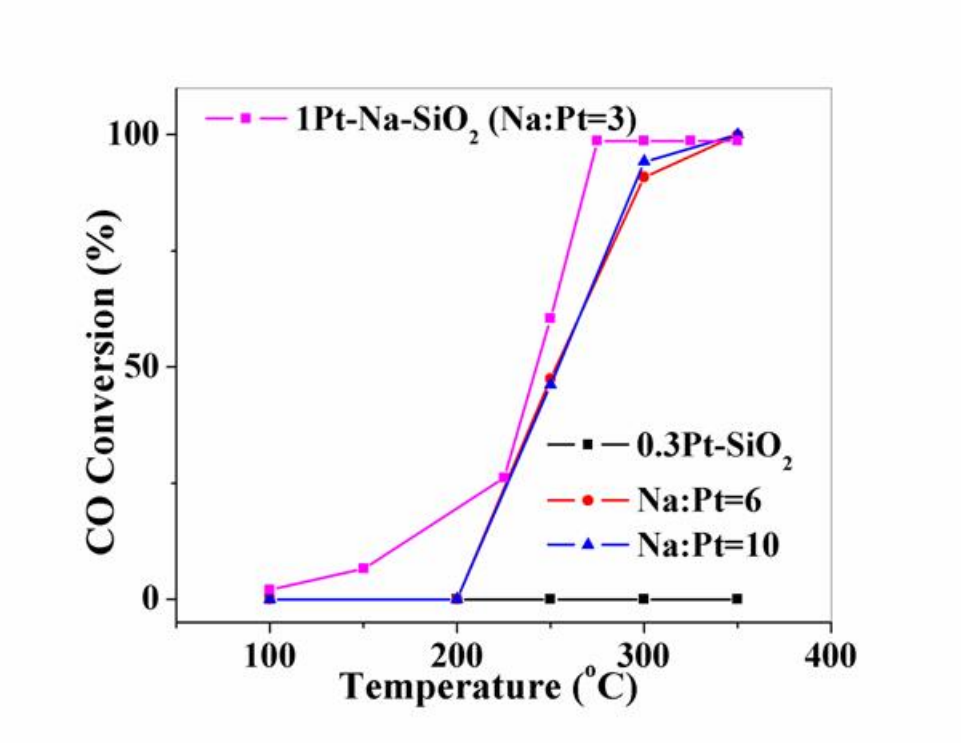


Figure 4.5 WGS steady-state light-off activity of Na-promoted Pt-$SiO_2$ catalysts. Gas composition: 2%CO-10%$H_2O$-He.

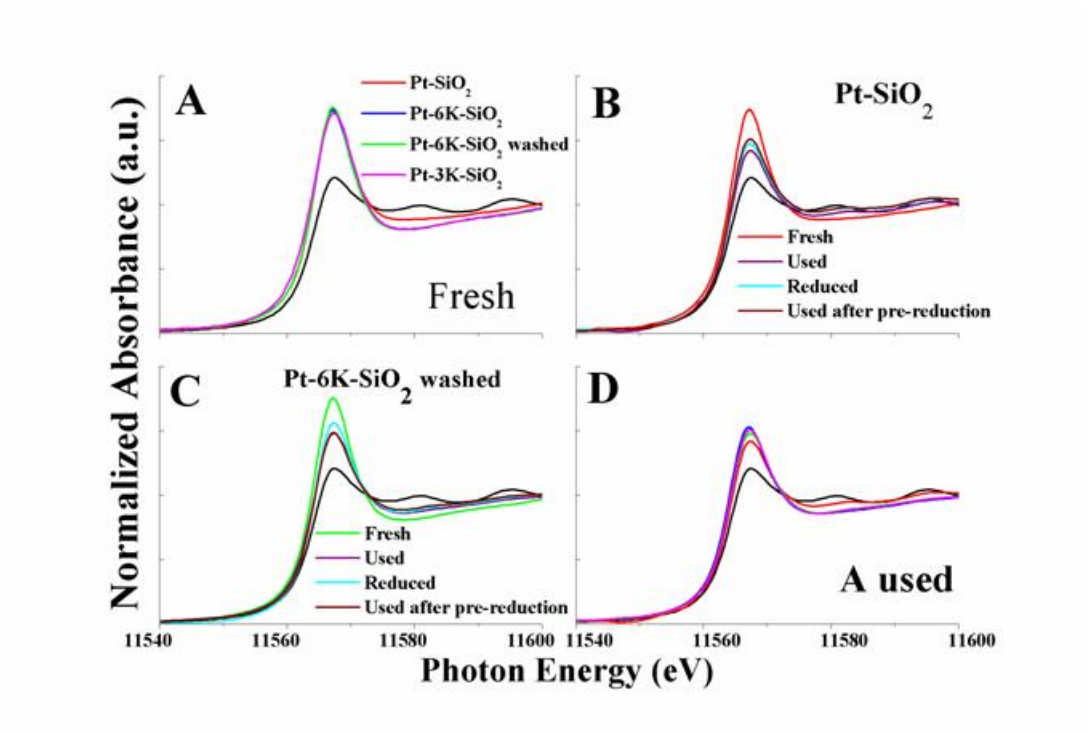


Figure 4.6 XANES spectra at Pt $L_{III}$-edge in (alkali)-promoted 0.3Pt-$SiO_2$ samples.

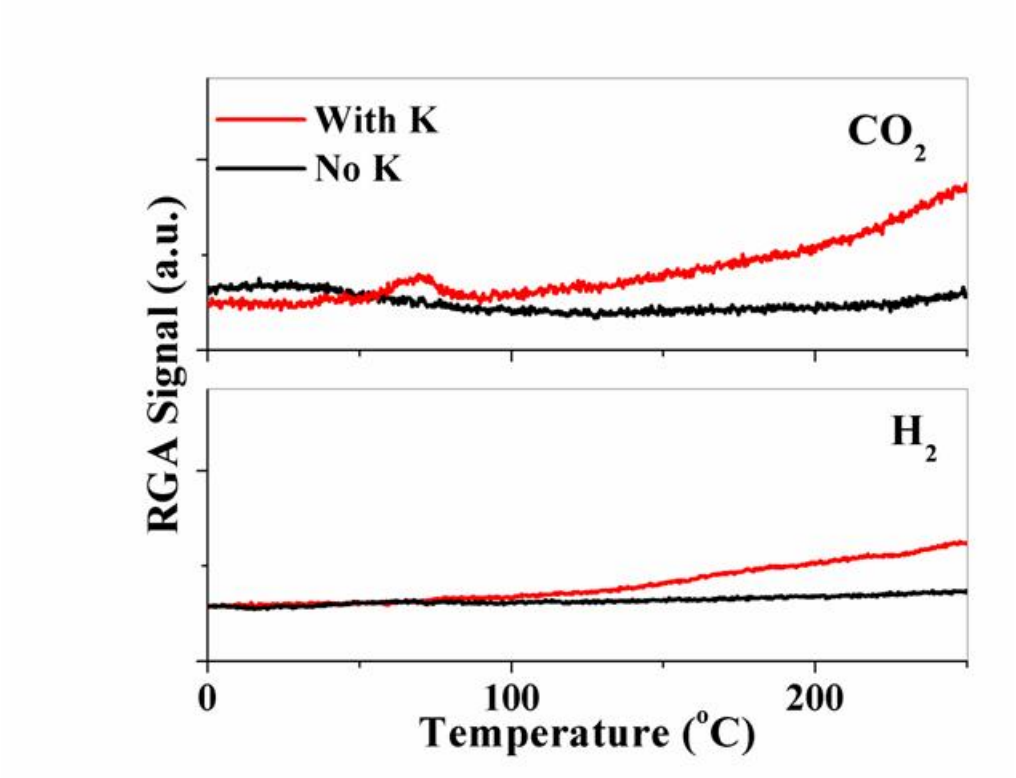


Figure 4.7 CO-TPR of 0.3Pt-$SiO_2$ with and without K-promotion.

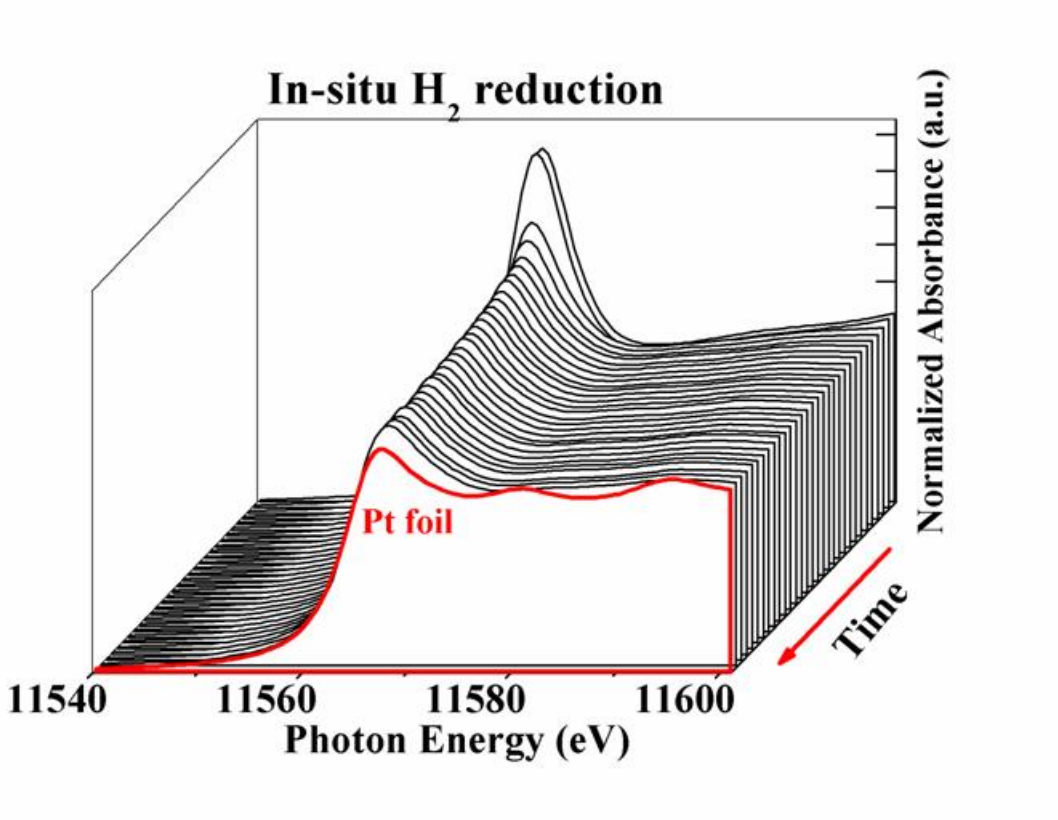


Figure 4.8 Q-XANES spectra at Pt $L_{III}$-edge in 0.3Pt-K-$SiO_2$ during the $H_2$-treatment. 5%$H_2$-He at 200 $^oC$ for 2 h, at 5 $^oC$/min.

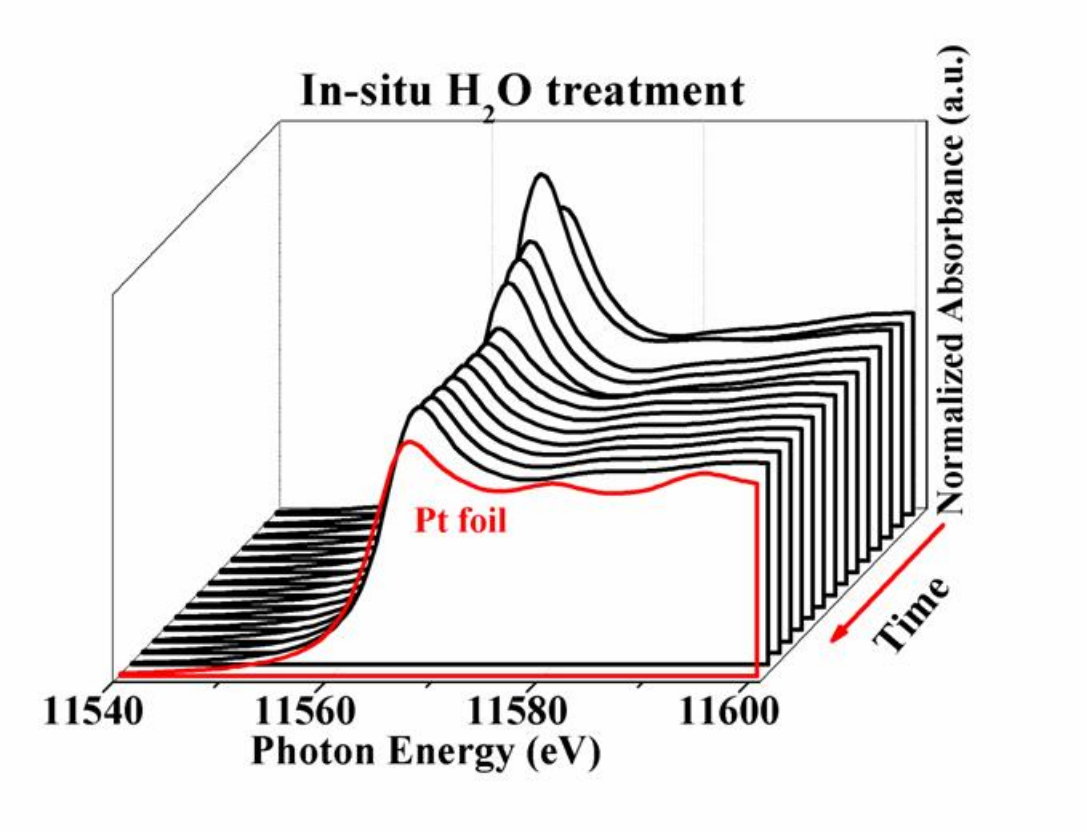


Figure 4.9 Q-XANES spectra at Pt $L_{III}$-edge in 0.3Pt-K-$SiO_2$ during the $H_2O$-treatment. The prereduced sample was exposed to 3%$H_2O$-He at 275 $^oC$ for 10 min.

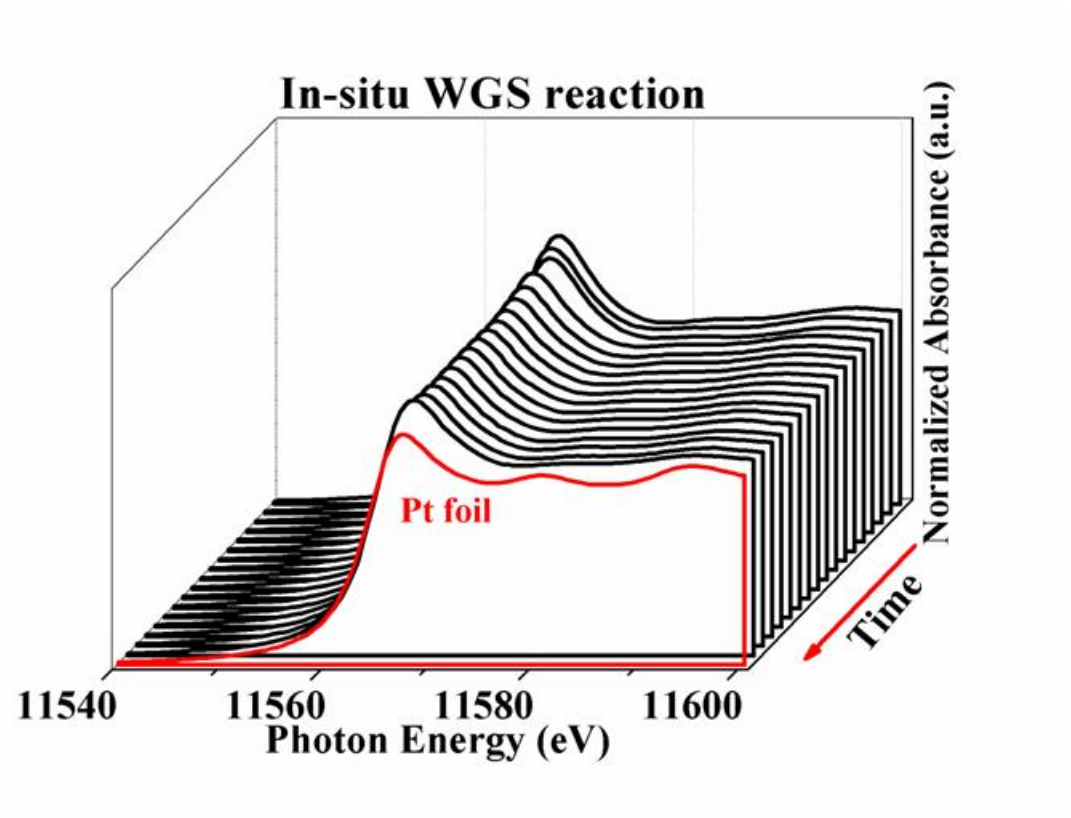


Figure 4.10 Q-XANES spectra at Pt $L_{III}$-edge in 0.3Pt-K-$SiO_2$ during the WGS reaction. 1%CO-3%$H_2O$-He at 275 $^oC$ for 1 h.

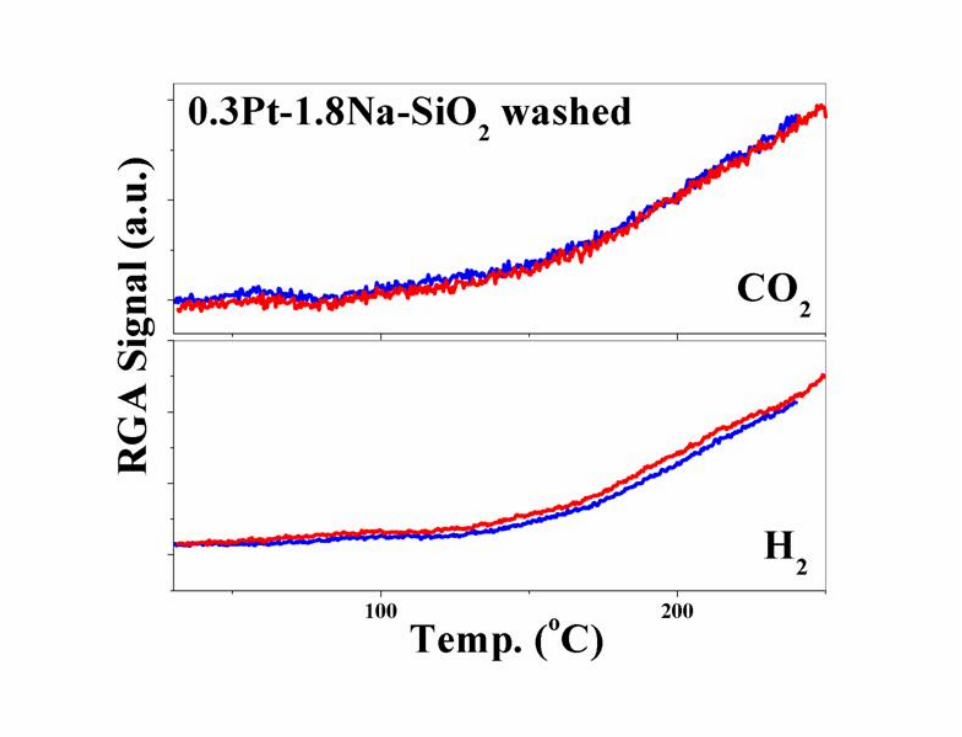


Figure 4.11 Cyclic CO-TPR of Na-promoted 0.3Pt-$SiO_2$ catalysts in 5%CO-He.

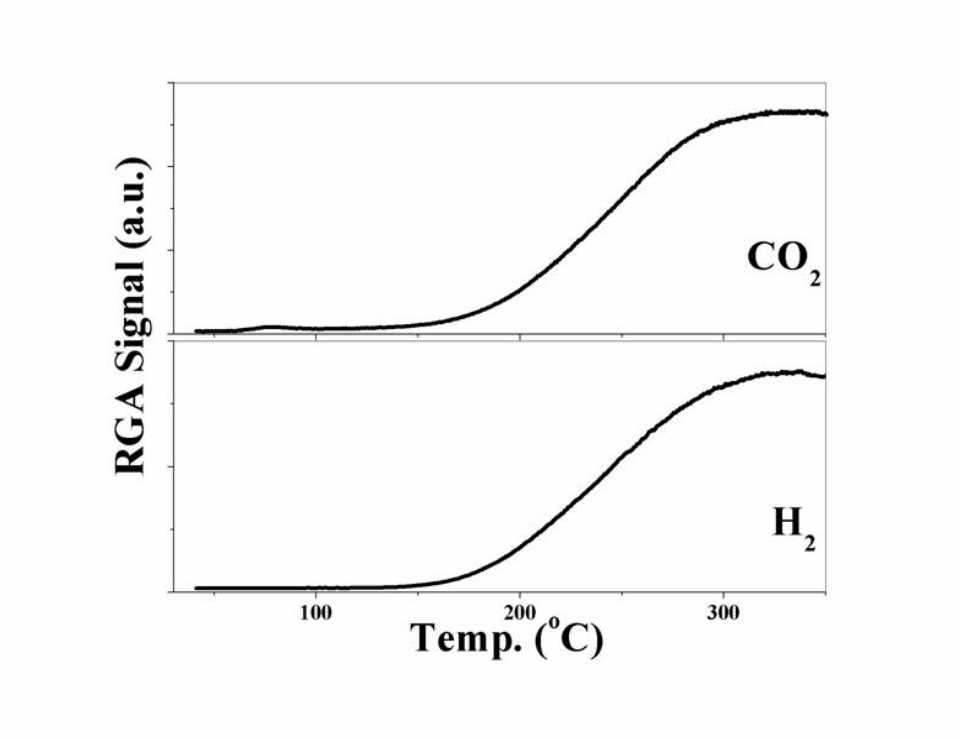


Figure 4.12 WGS-TPSR over 0.3Pt-Na-$SiO_2$ sample. Gas composition: 5%CO-3%$H_2O$-He.

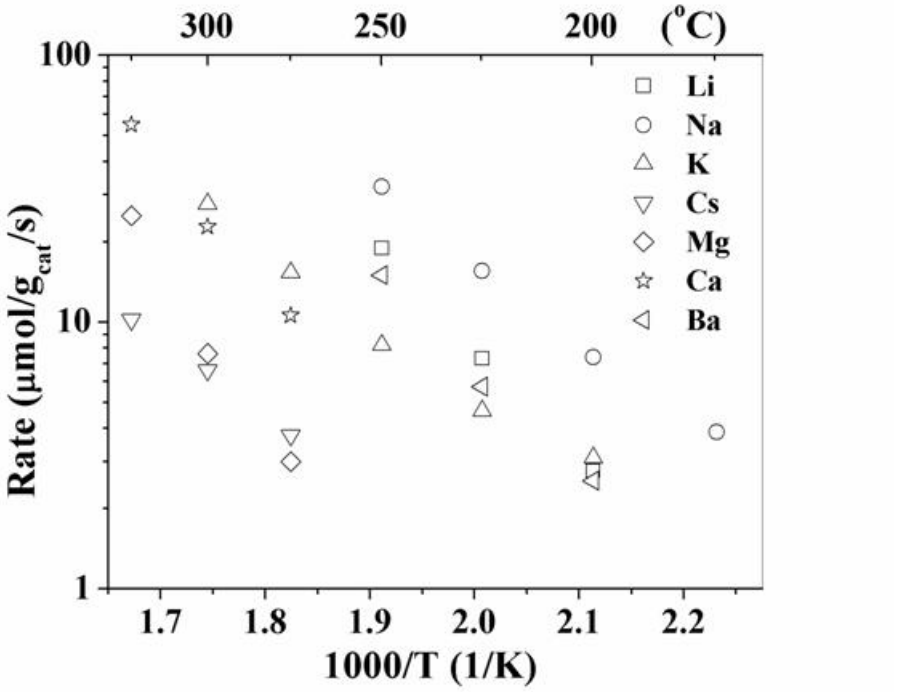


Figure 4.13 WGR reaction rates over $SiO_2$-supported Pt catalysts with different additives, measured in 11%CO–26%$H_2O$–26%$H_2$–7%$CO_2$-He.

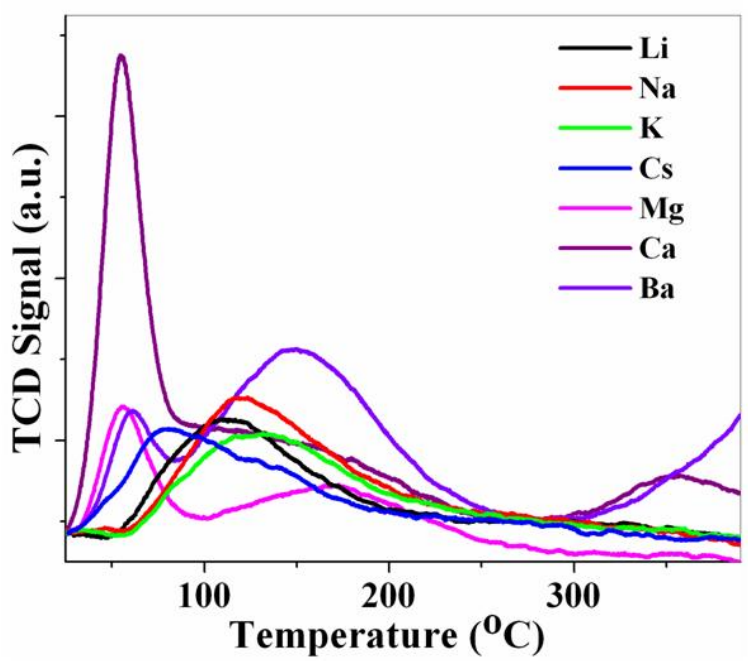


Figure 4.14 $H_2$-TPR of alkali and alkaline-earth modified 1Pt-$SiO_2$ Samples.

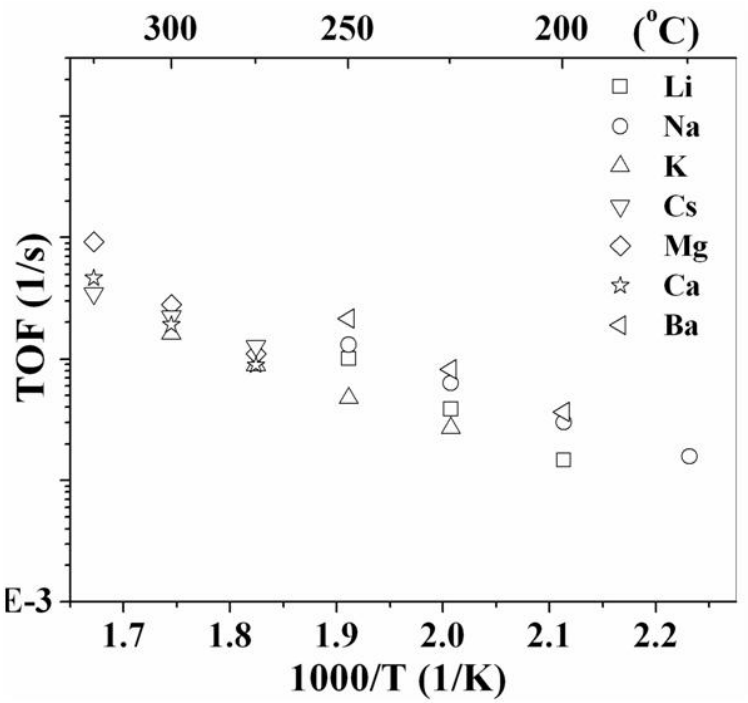


Figure 4.15 TOF of WGS reaction over 1Pt-$SiO_2$ catalysts with different additives, measured in 11%CO–26%$H_2O$–26%$H_2$–7%$CO_2$-He.

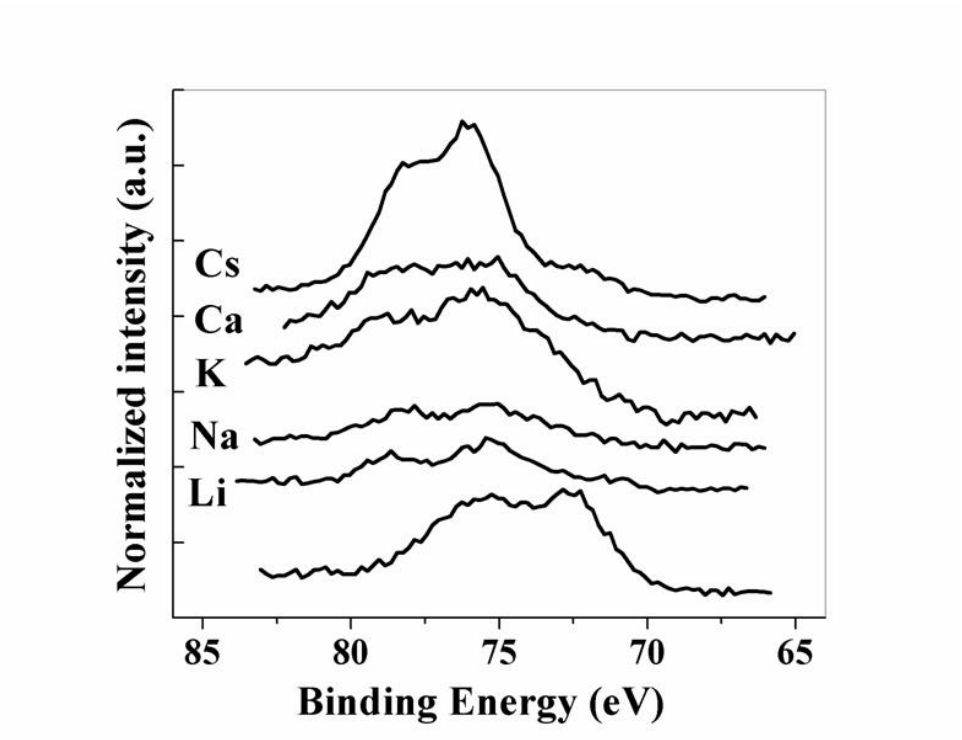


Figure 4.16 $Pt_{4f}$ XP spectra of 1Pt-$SiO_2$ with different additives.

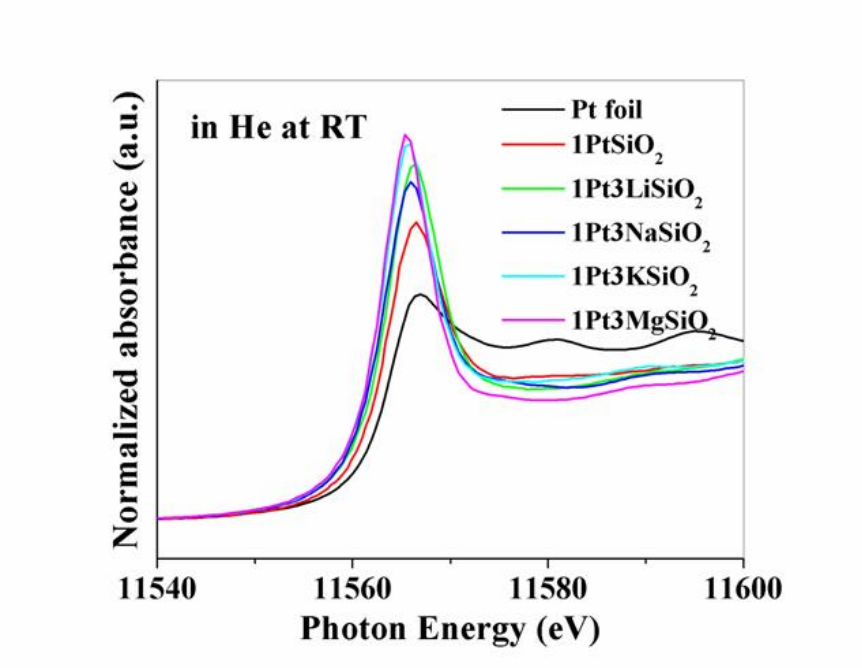


Figure 4.17 XANES analysis at the Pt $L_{III}$-edge of 1Pt-$SiO_2$ with various additives.

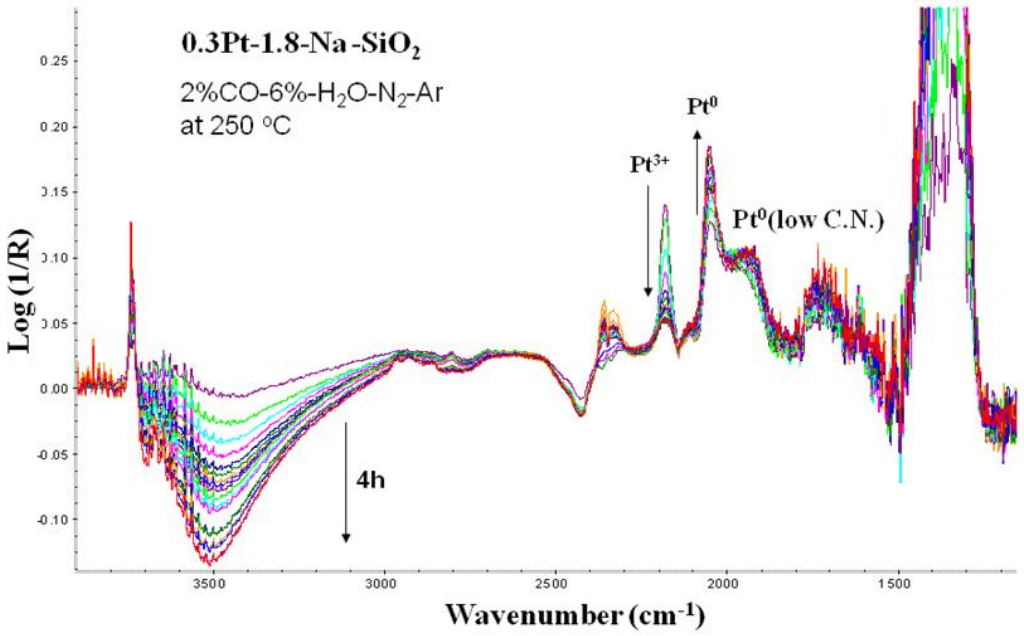


Figure 4.18 Dynamic DRIFTS on 0.3Pt-Na-$SiO_2$ at 250 $^oC$ in 2%CO-6%$H_2O$-$N_2$-Ar.

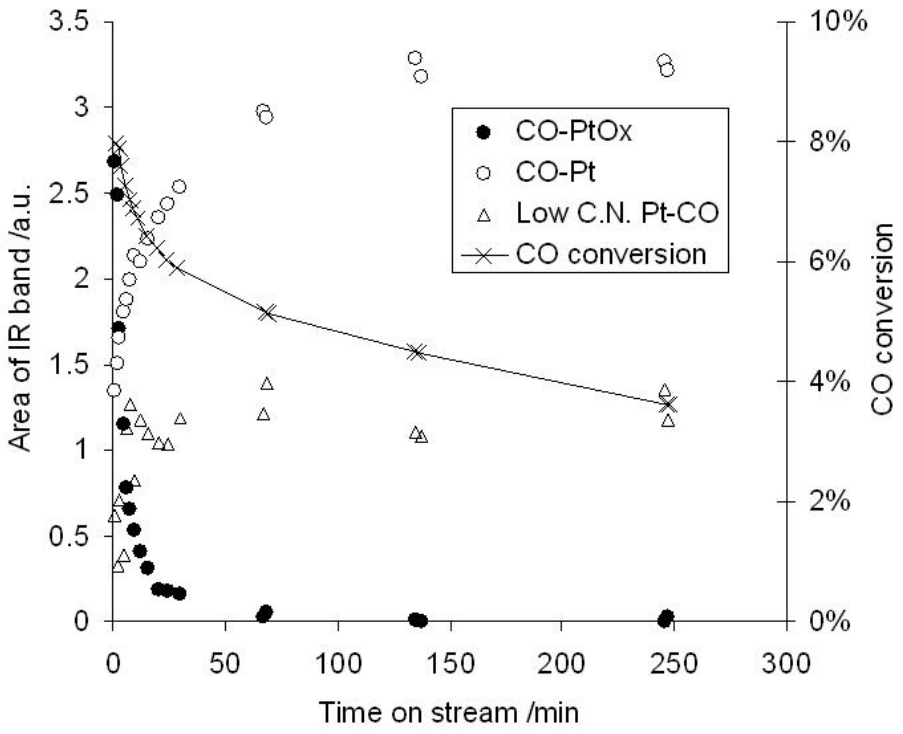


Figure 4.19 Correlation of the IR spectra in Figure 4.18 and the reaction activity of 0.3Pt-Na-$SiO_2$ at 250 $^oC$ in 2%CO-6%$H_2O$-$N_2$-Ar.

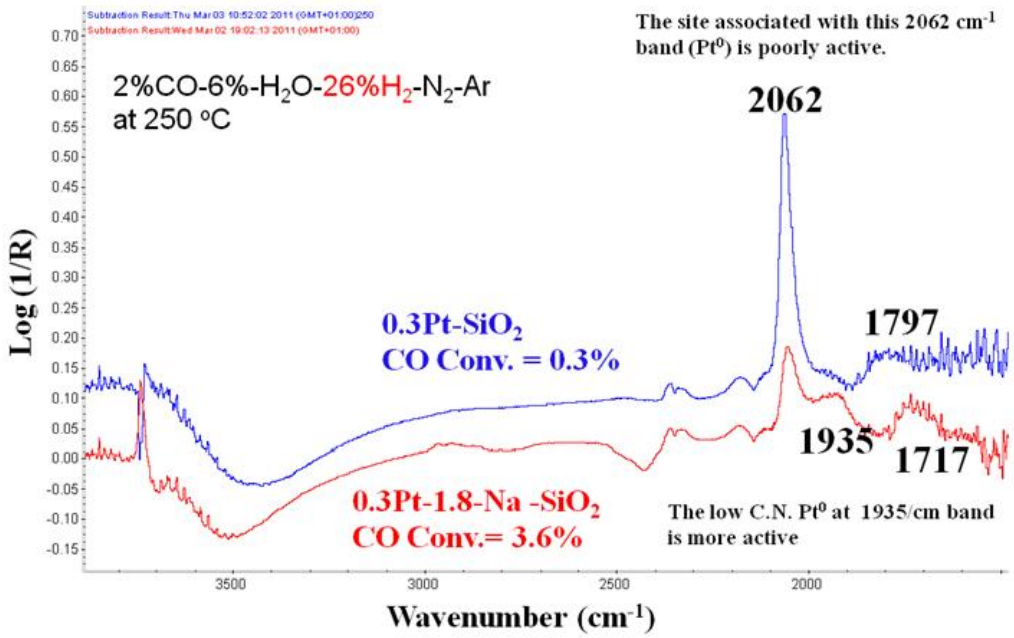


Figure 4.20 DRIFTS of Na-free and Na-promoted 0.3Pt-$SiO_2$ at 250 $^oC$ in 2%CO-6%$H_2O$-$N_2$-Ar.

## 4.5 References

[1] Q. Fu, H. Saltsburg, M. Flytzani-Stephanopoulos, Science 301 (2003) 935-938.

[2] D. Pierre, W. Deng, M. Flytzani-Stephanopoulos, Top. Catal. 46 (2007) 363-373.

[3] I.N. Remediakis, N. Lopez, J.K. Nørskov, Angew. Chem. 117 (2005) 1858-1860.

[4] S.J. Tauster, S.C. Fung, R.L. Garten, J. Am. Chem. Soc. 100 (1978) 170-175.

[5] L.L. Murrell, S.J. Tauster, D.R. Anderson, F.S. L. Guczi, T. P, Stud. Surf. Sci. Catal., Elsevier, 1993, pp. 681-690.

[6] M. Hatanaka, N. Takahashi, N. Takahashi, T. Tanabe, Y. Nagai, A. Suda, H. Shinjoh, J. Catal. 266 (2009) 182-190.

[7] W. Lin, A.A. Herzing, C.J. Kiely, I.E. Wachs, J. Phys. Chem. C 112 (2008) 5942-5951.

[8] R. Zanella, L. Delannoy, C. Louis, Appl. Catal., A 291 (2005) 62-72.

[9] R. Zanella, C. Louis, Catal. Today 107-108 (2005) 768-777.

[10] A.K. Medina-Mendoza, M.A. Cortes-Jacome, J.A. Toledo-Antonio, C. Angeles-Chavez, E. Lopez-Salinas, I. Cuauhtemoc-Lopez, M.C. Barrera, J. Escobar, J. Navarrete, I. Hernandez, Appl. Catal., B 106 (2011) 14-25.

[11] D. Andreeva, I. Ivanov, L. Ilieva, M.V. Abrashev, R. Zanella, J.W. Sobczak, W. Lisowski, M. Kantcheva, G. Avdeev, K. Petrov, Appl. Catal., A 357 (2009) 159-169.

[12] C.M.Y. Yeung, F. Meunier, R. Burch, D. Thompsett, S.C. Tsang, J. Phys. Chem. B 110 (2006) 8540-8543.

[13] J. Radnik, L. Wilde, M. Schneider, M.M. Pohl, D. Herein, J. Phys. Chem. B 110 (2006) 23688-23693.

[14] J.H. Kwak, J. Hu, D. Mei, C.-W. Yi, D.H. Kim, *e. al.*, Science 325 (2009) 1670-1673.

[15] F. Menegazzo, F. Pinna, M. Signoretto, V. Trevisan, F. Boccuzzi, A. Chiorino, M. Manzoli, ChemSusChem 1 (2008) 320-326.

[16] J. Hua, K. Wei, Q. Zheng, X. Lin, Appl. Catal., A 259 (2004) 121-130.

[17] Z. Ma, H. Yin, S. Dai, Catal. Lett. 136 (2009) 83-91.

[18] L.C. Grabow, A.A. Gokhale, S.T. Evans, J.A. Dumesic, M. Mavrikakis, J. Phys. Chem. C 112 (2008) 4608-4617.

[19] A.A. Gokhale, J.A. Dumesic, M. Mavrikakis, J. Am. Chem. Soc. 130 (2008) 1402-1414.

[20] H. Yoshida, S.-i. Nonoyama, Y. Yazawa, T. Hattori, Catal. Today 153 (2010) 156-161.

[21] P. Panagiotopoulou, D.I. Kondarides, J. Catal. 267 (2009) 57-66.

[22] X. Zhu, T. Hoang, L. Lobban, R. Mallinson, Catal. Lett. 129 (2009) 135-141.

[23] X. Zhu, M. Shen, L.L. Lobban, R.G. Mallinson, J. Catal. 278 (2011) 123-132.

[24] C.T. Campbell, B.E. Koel, K.A. Daube, J. Vac. Sci. Technol., A 5 (1987) 810-813.

[25] J.M. Campbell, J. Nakamura, C.T. Campbell, J. Catal. 136 (1992) 24-42.

[26] M. Kuriyama, H. Tanaka, S.-i. Ito, T. Kubota, T. Miyao, S. Naito, K. Tomishige, K. Kunimori, J. Catal. 252 (2007) 39-48.

[27] Y. Zhai, D. Pierre, R. Si, W. Deng, P. Ferrin, A.U. Nilekar, G. Peng, J.A. Herron, D.C. Bell, H. Saltsburg, M. Mavrikakis, M. Flytzani-Stephanopoulos, Science 329 (2010) 1633-1636.

[28] H. Tanaka, M. Kuriyama, Y. Ishida, S.-i. Ito, T. Kubota, T. Miyao, S. Naito, K. Tomishige, K. Kunimori, Appl. Catal., A 343 (2008) 125-133.

[29] A.A. Phatak, W.N. Delgass, F.H. Ribeiro, W.F. Schneider, The Journal of Physical Chemistry C 113 (2009) 7269-7276.

[30] M.A. Henderson, Surf. Sci. Rep. 46 (2002) 1-308.

[31] W. Deng, A.I. Frenkel, R. Si, M. Flytzani-Stephanopoulos, J. Phys. Chem. C 112 (2008) 12834-12840.

[32] N. Guo, B.R. Fingland, W.D. Williams, V.F. Kispersky, J. Jelic, W.N. Delgass, F.H. Ribeiro, R.J. Meyer, J.T. Miller, PCCP 12 (2010) 5678-5693.

[33] Y. Amenomiya, G. Pleizier, J. Catal. 76 (1982) 345-353.

[34] D. Pierre, M.S., Tufts University, 2006.

[35] P. Panagiotopoulou, D.I. Kondarides, Appl. Catal., B 101 (2011) 738-746.

[36] H. Yoshida, Y. Yazawa, T. Hattori, Catal. Today 87 (2003) 19-28.

[37] D.V.B.a.R. Kohlhaas, Z. Anorg. Allg. Chem 401 (1973) 15.

[38] J.M. Pigos, C.J. Brooks, G. Jacobs, B.H. Davis, Appl. Catal., A 319 (2007) 47-57.

[39] H. Evin, G. Jacobs, J. Ruiz-Martinez, G. Thomas, B. Davis, Catal. Lett. 120 (2008) 166-178.

[40] H.G.K.K. Kaisha, WO 2004/058635 (2004).

[41] E. Chenu, G. Jacobs, A.C. Crawford, R.A. Keogh, P.M. Patterson, D.E. Sparks, B.H. Davis, Appl. Catal., B 59 (2005) 45-56.

[42] D. Tibiletti, A. Goguet, D. Reid, F.C. Meunier, R. Burch, Catal. Today 113 (2006) 94-101.

[43] F.C. Meunier, A. Goguet, C. Hardacre, R. Burch, D. Thompsett, J. Catal. 252 (2007) 18-22.

[44] F.C. Meunier, D. Reid, A. Goguet, S. Shekhtman, C. Hardacre, R. Burch, W. Deng, M. Flytzani-Stephanopoulos, J. Catal. 247 (2007) 277-287.

[45] M. Kappers, J. Maas, Catal. Lett. 10 (1991) 365-373.

[46] E. Ivanova, M. Mihaylov, F. Thibault-Starzyk, M. Daturi, K. Hadjiivanov, J. Mol. Catal. A: Chem. 274 (2007) 179-184.

[47] J.M. Pigos, C.J. Brooks, G. Jacobs, B.H. Davis, Appl. Catal., A 328 (2007) 14-26.

# Chapter 5 Formation and stabilization of active sites in Au-based catalysts for the WGS reaction

## 5.1 Introduction

Au-$CeO_2$ catalysts have been reported to be highly active for the low-temperature WGS reaction which makes them interesting candidates for a range of applications including hydrogen upgrade (CO cleanup) for low-temperature fuel cells. However, the commercial application of these catalysts has been hindered by their tendency to deactivate rapidly under reaction conditions. The long-term stability is an important property if catalysts are to be developed for commercial WGS applications. Therefore, an understanding of the deactivation mechanism is critical in designing new catalysts/processes able to achieve close to CO-free hydrogen production via the WGS reaction. Deng *et al.* [1], using in situ EXAFS started from a fully dispersed state of gold on ceria to examine the gold structural evolution under reaction conditions and see if this would correlate with the loss of the WGS reaction activity. Indeed they found that loss of bound (oxidized) gold species in the used samples correlated well with gold cluster formation and growth and with catalyst activity loss. Results from $H_2$-TPR corroborated the loss of oxidized gold in the used samples. They also found that this is a reversible structural change, whereby re-dispersion of gold in the used Au-ceria surface was observed after 400 $^oC$ oxidation in 20%$O_2$-He gas mixture, accompanied by surface oxygen and catalytic activity recovery. These findings further confirm that the Au-O-Ce species are the active sites for the low-temperature WGS reaction.

$Fe_2O_3$ supported Au catalysts [2, 3] have also been reported to be very active for the WGS reaction. Andreeva et al. were the first to report the Au-$FeO_x$ system as a low-temperature WGS catalyst [4]. The Andreeva group also reported in a later study that the iron oxide surface played an important role and $FeO(OH)_x$ surfaces were very good to prepare active Au-$FeO_x$ catalysts [5]. Further understanding of the WGS activity of the Au-$FeO_x$ system has been obtained in more recent work carried out by our group at Tufts [2, 6-9]. The areal reaction rates, which are reaction rates normalized by the sample surface area, were about

the same on both $CeO_2$ and $Fe_2O_3$ supported Au catalysts, and dependent only on the number of available Au-O-Ce or Au-O-Fe sites [2]. Thus, the atomic distribution of gold on these oxides is important, and should be possible to capture by various techniques. By using atomic-resolution electron microscopy at Oak Ridge National Lab, Allard *et al.* [7], examined NaCN-leached Au-$Fe_2O_3$ materials prepared at Tufts, and found them to contain a preponderance of gold ions. The same group also showed that the Au-$FeO_x$ interaction is very strong [7, 8]. By a series of in-situ heating tests in the microscope up to 700 $^oC$, sintering did not begin below 500 $^oC$ and even at 700 $^oC$, the Au NPs were below 2 nm size.

Isolated Au cations on $Fe_2O_3$ surface have been observed also by Herzing et al. [10] with atomic resolution microscopy in their analysis of several iron oxide-supported Au catalyst samples, ranging from those with little or no activity to others with high activities. High catalytic activity for carbon monoxide oxidation is correlated with the presence of bilayer Au clusters that are ~0.5 nm in diameter and contain only ~10 gold atoms. More recently Yates *et al.* [11] observed a dual catalytic site, Au-Ti, at the perimeter of 3-nanometer Au particles supported on $TiO_2$ during CO oxidation with transmission infrared spectroscopy and DFT calculations. Ribeiro *et al.* [12] used a physical model of Au-$TiO_2$ to claim that corner atoms with fewer than seven neighboring gold atoms are the dominant active sites for the low-temperature WGS reaction. The number of corner sites does not vary as particle size increases above 1 nm, giving the surprising result that the rate per gold cluster is independent of size.

The atomic–scale interaction of Au with $Fe_3O_4$ (111) single crystal surface was recently demonstrated by STM/STS work carried out at George Flynn's lab at Columbia University [6]. A sub-monolayer of Au adatoms was vapor deposited on a Fe-terminated $Fe_3O_4$ (111) crystal. Even after 500 $^oC$ annealing the Au atoms were isolated and "bound" preferentially on uncovered O sites on the surface, surrounded by Fe ions. They formed equivalent "unit cell" structures similar in size (0.56 nm x 0.56 nm) to the $Fe^{2+}$-$Fe^{3+}$ unit cell. The Au adatoms were positively charged. Interestingly, CO adsorption on this Au-$Fe_3O_4$ (111) surface at 260 K was atop up the Au atoms, exclusively. In following work, the same group showed that adsorbed OH from water dissociation takes place on the iron sites

surrounding the uncovered O sites [13]. These studies clearly demonstrate that an ensemble of [Au-$O_x(OH)_y$] sites is bound onto the $FeO_x$ surfaces, and this may be where all the active sites for the WGS reaction reside.

To further understand the reaction-relevant gold structure evolution under reaction conditions, in this thesis, we followed the gold structural evolution as a function of gas composition using in situ XANES and EXAFS. The regenerability of these structures was also evaluated and compared to the Au-$CeO_x$ system. This result can guide the design of the gold-based catalysts, and of the processing conditions, *e.g.* addition of small amounts of oxygen in the reformate gas, to control catalyst deactivation and prolong the catalyst lifetime.

Recent studies have focused on the modification of supports to keep the Au dispersed, primarily for the dry CO oxidation reaction, where Au destabilization, *e.g.* on $TiO_2$, takes place even with storage [14]. Veith *et al.* [14, 15] found that the surface hydroxyl groups were essential for stabilizing the gold clusters on $TiO_2$ against coarsening under ambient conditions. Haruta *et al.* [16] found a hydroxide, $AuLa_2(OH)_9$, which was prepared by co-precipitation, showed markedly high catalytic activity for CO oxidation (100% conversion) at a temperature as low as 193 K after reduction at 373 K. The catalyst mainly consists of $Au^0$ clusters smaller than 1.5 nm, which are well-mixed with $La(OH)_3$ containing isolated $Au(OH)_3$ species. In other work, Nieuwenhuys and co-workers [17] used alkali/alkaline earth metals as structural promoters to stabilize gold clusters in the preferential oxidation of CO reaction in $H_2$-rich gas stream.

However, not everyone agrees on the role of hydroxyl groups or alkali and alkaline-earth metals on dispersing gold species on oxide supports. For example, Hutchings and co-workers [10] have reported that surface hydroxyl groups on FeOOH enhanced the coarsening of the gold particles.

Since OH groups are also deemed as reactants in the WGS reaction, in this part of the thesis work different approaches were used to control the concentration of surface OH groups and examine if the OH groups, other than serving as reactants in the reaction pathway, also stabilize the active Au sites.

One approach was using OH-rich oxides, such as $LaO(OH)_x$, as supports and compare the different activity/stability of Au supported on these surfaces as a function of the surface OH concentration. Still another approach will be to boost the performance of Au-based catalysts with alkali ions as we did for the Pt base-catalysts. For this purpose, inert oxides will be used.

## 5.2 Materials and methods

### 5.2.1 $SiO_2$-supported Au catalysts

Au-$SiO_2$ was prepared by a deposition precipitation method. Firstly, 4.75 g fumed $SiO_2$ powder was stirred in 500 mL D.I. water at room temperature. The pH value of the slurry was adjusted to 8.5 by adding 1M ammonium carbonate. 0.5 g $HAuCl_4$ was dissolved in 100mL D.I. water at RT, and the $HAuCl_4$ solution was added drop wise into the slurry keeping constant pH=8.5 with 1M ammonium carbonate. The slurry was aged for 1 h at room temperature to allow for adequate deposition. Filtering and washing the precipitate three times with D.I. water at 60-70 °C was used to remove excess chloride, followed by drying in vacuum at 70 $^oC$. Na-modified Au-$SiO_2$ was prepared by IMP with $NaNO_3$ as the Na precursor. The sample was dried in vacuum at 70 $^oC$. Both Na-free and Na-modified Au-$SiO_2$ were calcined in static air at 400 $^oC$ for 4 h before testing.

### 5.2.2 $Fe_2O_3$/$CeO_2$-supported Au catalysts

The 2 at%Au-$Fe_2O_3$ catalyst used in this work was obtained from the World Gold Council. It was prepared by co-precipitation (CP) and had been calcined at 400 $^oC$. Au on $CeO_2$ was prepared by the DP method following the same procedure as for the preparation of Au-$SiO_2$. Ceria was first prepared by the urea-gelation-coprecipitation (UGC) method [18], dried in a vacuum oven at 60 °C overnight and calcined at 400 $^oC$ for 10 h. This method produces a well-dispersed ceria, nano-crystallized and with relatively high surface area, 130 $m^2/g$, as can be seen in Table 5.3.

Another series of Au-$Fe_2O_3$ was prepared by a two-step method. $Fe_2O_3$ was prepared by precipitation, by adding an iron nitrate aqueous solution drop wise into D.I. water

containing sodium carbonate at pH=8. The precipitate was washed with D.I. water at 60$^{o}$C three times, dried in a vacuum oven at 60°C overnight and calcined at 400$^{o}$C for 4h. Au was loaded on this $Fe_2O_3$ by the DP method following the same procedure for the preparation of Au-$SiO_2$.

Leaching of weakly bound gold from calcined Au-$CeO_2$ and Au-$Fe_2O_3$ samples took place in an aqueous solution of 2% NaCN at room temperature with pH=12 [19]. After washing by D.I. water, the leached catalysts were dried in a vacuum oven at 60 °C overnight and calcined at 400 $^{o}$C for 4 h.

Na (K) modified catalysts were prepared by further impregnating dried samples (Au-$CeO_2$, Au-$Fe_2O_3$, both parent and leached samples) without prior calcination, with aqueous solution of $NaNO_3$ ($KNO_3$) and drying them again in a vacuum oven at 60 °C overnight. All the modified samples were calcined at 400 $^{o}$C for 4 h at a heating rate of 2 $^{o}$C/min.

### 5.2.3 $La_2O_3$-supported Au catalysts

$La_2O_3$ was prepared by hydrolysis [20] with a medium-high surface area of 75 $m^2$/g. In the hydrolysis method, precipitation of the lanthanum nitrate took place by a highly concentrated NaOH (2.5 M) aqueous solution under stirring at *ca.* 100 °C for about 6 h. The suspension was cooled to room temperature, separated and washed by centrifugation with D.I. water until the pH dropped below 8, and finally dried under vacuum at 80 °C overnight. The dried powders were crushed and sieved (<53 μm), and then calcined in air at 400 °C for 4 h (2 °C/min). Commercial $La_2O_2SO_4$ was bought from Sigma-Aldrich with surface of 60 $m^2$/g.

Au-$La_2O_3$ /Au-$La_2O_2SO_4$ was prepared by following the same DP procedure for gold as when preparing Au-$SiO_2$.

### 5.2.4 Characterization and reactivity measurements

Catalysts were characterized by BET, ICP, TEM, HRTEM, XPS, $H_2$/CO-TPR, and in-situ XANES/EXAFS measurements. Catalyst WGS reaction activities were evaluated at steady-state under various conditions that included product-free and full reformate gas

mixtures. Temperature-programmed surface WGS reaction was also applied to evaluate and compare the various catalysts.

The CO oxidation reaction was carried out over some of the $SiO_2$-supported Au catalysts in steady-sate experiments, using a feed gas mixture of 2%CO-1%$O_2$-He at 75 ml/min. A typical load of 0.1 g catalyst was used, and the contact was 0.1 g.s/cc.

## 5.3 Results and discussion

### 5.3.1 Reaction-relevant Au structure changes in Au-$Fe_2O_3$ catalysts

To exclude the influence of weakly bound metallic gold particles, a leached Au-$Fe_2O_3$ (WGC) sample, 0.7Au-$Fe_2O_3$ was used. As has been reported [9], the parent and the leached samples have the same catalytic performance for the WGS reaction. Also, the areal reaction rates are the same for Au-$Fe_2O_3$ and Au-$CeO_2$. Moreover, the apparent activation energy is the same over these two Au catalysts, 49 ± 7 kJ/mol, which indicate that the same active sites are operating for the WGS reaction. The results also demonstrate that leachable metallic gold nanoparticles present in the parent catalysts do not participate in the WGS reaction.

XP spectra [2] found no Au species on the surface of the 400 $^oC$-calcined, leached 0.7Au-$Fe_2O_3$. The ac-HAADF/STEM image [7], in Figure 1.2 shows that Au is actually atomically dispersed throughout the bulk of $Fe_2O_3$ in this fresh sample. A reduction treatment gradually brings the gold to the iron oxide surface, as verified by XPS [2], and as can be seen in Figure 1.3. Migration of gold and sintering of Au clusters is caused by the $H_2$ reduction at 400 $^oC$. However, small Au particles (1-2 nm), clusters (< 1 nm) and atoms are all present on the support surface. The existence of Au atoms after such harsh treatment indicates a strong Au-$Fe_2O_3$ interaction, as discussed in the introduction of this chapter.

In this thesis work, in situ XANES was employed to examine the oxidation state of Au in 0.7Au-$Fe_2O_3$, which initially comprised of fully dispersed Au species. EXAFS was conducted at room temperature over the sample after the WGS reaction, and re-oxidation conditions. The local coordination environment of gold with oxygen and with gold

obtained from the EXAFS analysis will be correlated with the WGS reaction activity, catalyst reducibility and surface oxygen amount.

#### 5.3.1.1 WGS reaction-induced structural effect

In Figure 5.1 the high white line intensity of the fresh 0.7Au-$Fe_2O_3$ sample shows a high oxidation state of the Au species. This observation is consistent with the R-space EXAFS data in Figure 5.2 and Table 5.1. Fits were performed with FEFF model of Au-O, Au-Au, and Au-Fe interactions for all the samples. The fresh sample only has Au-O contribution, and adding Au-Au or Au-Fe contributions, did not improve the fit after comparing different models. This is also consistent with the HAADF/STEM image, in Figure 1.2, where almost all the Au species are atomically dispersed throughout the bulk of the iron oxide. And the first cycle of the $H_2$-TPR over the fresh 0.7Au-$Fe_2O_3$ material, in Figure 5.3 (A), shows a strong interaction between Au species and iron oxide. A large $H_2$ consumption takes place at temperatures above 150 $^oC$, which is attributed to the reduction of strongly interacting Au-O-Fe species, and the reduction of $Fe_2O_3$ to $Fe_3O_4$ at a much lower temperature (~200 $^oC$) than in the absence of gold (350 $^oC$) [9]. During this heating in $H_2$, gold ions from the bulk diffused to the surface and were reduced. A second cycle of $H_2$-TPR after re-oxidation would then be more representative of the surface reducibility of the material. The second cycle of the $H_2$-TPR after 20%$O_2$–He treatment at 350 $^oC$ for 30 min, shows that there are two main peaks, *i.e.* two different oxygen species on the surface. The first is probably due to adsorbed oxygen species on gold nanoclusters, the second due to the Au-O-Fe interaction, in the temperature range where the water-gas shift reaction lights off. Similar results were reported for Au-$CeO_2$ catalysts [19, 21, 22].

The WGS reaction was conducted over 0.05 g fresh 0.7Au-$Fe_2O_3$ at 250 $^oC$ in a gas mixture of 5%CO-3%$H_2O$-He at a total flow of 20 ml/min. XANES spectra were taken after 2-h-on-stream, when deactivation was observed, as can be seen from Figure 5.4 by the decreasing $H_2$ production. The lower while line intensity at Au $L_{III}$ edge in the sample after reaction, in Figure 5.1, shows that the O-rich environment for the fresh sample no longer exists. EXAFS of the sample were taken under the same condition. Oxidized gold is reduced; Au-Au contribution is now dominant as shown in the R-space (Figure 5.2) with

Au-Au coordination number of 7.2. The coordination number of Au-O decreased from 2.3 to 0.5. From these results, it is clear that gold clusters and nanoparticles (1-2 nm) formed in the reaction atmosphere at 250 $^{o}$C.

According to the gradually decreasing profile of $H_2$ production with time-on-stream in Figure 5.3, it is predicted that the Au-O coordination will continue to decrease, while the Au-Au coordination will increase, leading to the appreciable sintering of the Au particles after some time. The ac-HAADF/STEM image of a 2-h used sample under the same condition as for the XANES/EXAFS testing, in Figure 5.5, shows that the reaction gas mixture and temperature have caused a considerable change of the dispersion of gold, compared to Figure 1.2. Au clusters (< 1 nm) and atoms still exist on this sample, but Au nano-particles (1-2 nm) were also formed during the reaction at 250 $^{o}$C.

The reduced interaction between Au and the support is confirmed also by the loss of surface oxygen by $H_2$-TPR, in Figure 5.3 (B), compared to the fresh sample (using the second cycle of $H_2$-TPR from Figure 5.3 (A), also shown in Figure 5.3 (B). Over the used sample, only small amount of reducible oxygen was detected. The loss of the surface oxygen should be attributed to the loss of the Au-O-Fe interaction as indicated by the XANES and EXAFS analysis.

These studies illustrate that Au-O-Fe species comprise the WGS reaction-relevant active sites in 0.7Au-$Fe_2O_3$. The fresh sample, after heating to ~ 175 $^{o}$C in the reaction mixture, to allow for gold ion migration to the surface [2, 7] has the highest concentration of such Au-O-Fe species (Figure 5.3), and the highest activity (Figure 5.4). With time-on-stream, the strongly bound Au-O species are destabilized and loss of reducible surface oxygen and reactivity ensues.

#### 5.3.1.2 Re-oxidizing the used catalyst

Here, we follow the same approach as used to regenerate the deactivated Au-$CeO_2$ samples [1], namely, the used sample was exposed to an oxidizing gas stream, 20 %$O_2$-He at 250 $^{o}$C or 350 $^{o}$C, respectively, for 1 h.

Figure 5.1 shows that after the used sample was re-oxidized at 250 $^{o}$C for 1 h, the white line intensity of Au at the $L_{III}$ edge was increased compared with the used sample, while it was still much lower than that in the fresh sample. With the EXAFS analysis, in Figure 5.2 and Table 5.1, an increasing Au-O coordination number was observed as 1.3 ± 0.7. This means that a small portion of the Au particles was redispersed and is in oxidized state. Increasing the $O_2$-treatment temperature to 350 $^{o}$C was able to further enhance the intensity of the white line at the Au $L_{III}$ edge in XANES, Figure 5.1. In the EXAFS analysis, the higher temperature $O_2$-treatment has little effect on the Au-O coordination number; however the Au-Au contribution disappeared, indicating no metal gold was present. Figure 5.5 (B) compares the $H_2$-TPR profiles of the fresh, used and the 350 $^{o}$C-re-oxidized samples. Obviously the $O_2$-treatment was able to re-oxidize and re-disperse most of the reduced and sintered Au species onto the iron oxide surface, and the reducibility of the used sample after oxidization is the same as that of the fresh sample during the second $H_2$-TPR cycle.

Further checking the reactivity of the $O_2$-treated 0.7Au-$Fe_2O_3$ sample for the WGS reaction, we found that the $O_2$-treatment recovers the initial reactivity of the fresh sample, Figure 5.4, although with time-on-stream deactivation happens again. But it is also worth noticing that after an initial loss of the activity, the sample is now more stable than the fresh one over longer times. This requires further investigation.

From this and the previously reported work on Au-$FeO_x$ [2, 6-8, 13] and Au-$CeO_2$ [1, 19], the atomically dispersed Au species, $Au_n$-O-Fe, $Au_n$-O-Ce, on these types of surfaces, are found to be the active sites for the WGS reaction. Highly reducing gas mixtures can destabilize these Au-O-Fe/Ce sites and cause the formation and sintering of Au clusters and particles, and further lead to catalyst deactivation. The $Au_n$-O-Fe/Ce active sites can be restored, at least partially, by $O_2$-treatment, which in turn recovers the activity of the catalyst for the WGS reaction.

#### 5.3.1.3 $O_2$-stabilized catalytic performance

Since the post $O_2$-treatment can restore the oxidized Au species for the WGS reaction and recover activity, it is natural to consider whether $O_2$-assisted WGS reaction may help to

stabilize the Au-O species on these catalysts. This could be a way to prevent the reduction of oxidized Au and the sintering of gold clusters, and it maybe the best approach for practical applications of gold catalysts.

Deng *et al.* [23], have reported a small amount of gaseous oxygen (air) added to the feed gas can stabilize nanostructured Au-$CeO_2$ and Pt-$CeO_2$ catalysts for the WGS reaction in $H_2$-rich gases and shutdown-restart operation.

Here, we extended this approach to the Au-$FeO_x$ catalysts. $O_2$-assisted reactivity and stability measurements were conducted with the 0.7Au-$Fe_2O_3$ material. The stability test was carried out in reformate gas mixture, 11%CO-26%$H_2$-26%$H_2O$-7%$CO_2$-He at 325 $^oC$. Different concentrations of $O_2$ gas were added to examine the effect of oxygen potential on the reactivity and stability of the catalyst.

Figure 5.6 shows the details of the stability tests. At the beginning, only the reformate gas mixture was passed over the sample. A significant drop of the activity took place at the very beginning. As discussed above, this was due to the reduction of the oxidized Au species, such deactivation increasing with time-on-stream. After about 30 h-stability test, 0.5%$O_2$ was added into the gas stream. However neither the activity nor the stability was improved. After another 5 h-on-stream with 0.5%$O_2$, the $O_2$ was removed, and the deactivation continued just like that before the $O_2$ was introduced.

Since the reformate gas mixture has a high concentration of $H_2$, 26%, the oxygen potential, even with 0.5%$O_2$ added in the mixture, may still be too low to preserve the active oxidized structure of Au. Therefore, 1%$O_2$ was added. An immediate promotion of the CO conversion was observed. This enhanced CO conversion corresponds to contribution from the CO oxidation. The significant finding here is the improved catalyst stability. With 1%$O_2$ on, the CO conversion was maintained, which indicates the active sites for the WGS reaction were stabilized by the additional $O_2$. When the 1%$O_2$ was removed from the gas stream, the CO conversion gradually decreased to a level even lower than before the introduction of 1%$O_2$. The oxygen potential of the gas mixture with 1%$O_2$ was able to stabilize the available oxidized Au species. However it is still not enough to re-disperse the Au clusters/particles formed from the previous tests. When $O_2$ was removed, the oxidized Au species were destabilized again. The highly reducing reformate gas mixture will further

destabilize the sites and gradually bring down the CO conversion. When the 1%$O_2$ was switched back to the gas stream, as shown in Figure 5.6, the promoted CO conversion was lower than before, which indicates further loss of active sites for the WGS reaction during the period when $O_2$ was off.

To confirm the above explanations, a new set of in-situ XANES spectra were taken to clarify the Au structure changes with $O_2$ on or off.

The catalyst, fresh 0.7Au-$Fe_2O_3$ with fully dispersed Au, was tested under two different reaction gas mixtures at 250 $^oC$. One gas mixture was 5%CO-3%$H_2O$-He (WGS), and the second one included 1%$O_2$ ($O_2$-assisted WGS). The CO conversions under the two different reaction conditions are plotted in Figure 5.7. In $O_2$-free conditions, an initial fast drop of the activity was observed and a slower deactivation continued, similar to what we had previously observed. A decreased while line intensity at Au $L_{III}$ edge confirms the loss of oxidized Au species, in Figure 5.8.

With 1%$O_2$ added in the gas stream, enhanced CO conversion was found, due to both the WGS and CO oxidation reactions. Most importantly, the stability of the catalyst was significantly enhanced. Other than a small drop of the CO conversion at the beginning of the test, the CO conversion kept constant over the 6-h long test. The $O_2$ on stream was only partially consumed as tracked by GC, which indicates that the CO oxidation reaction does not consume all the oxygen and the remaining $O_2$ species stabilizing the oxidized Au species for the WGS reaction. The high while line intensity at Au $L_{III}$ edge in Figure 5.8 reflects the high oxidation state of Au, which is about the same as that of the fresh sample. Therefore the active Au structure was maintained during the $O_2$-assisted WGS reaction. Deng reported similar findings for the $O_2$-assisted operation on Au-$CeO_2$ catalysts [9, 23]. $O_2$-assisted operation of Au catalysts for the WGS reaction may also effectively stabilize gold on other supports.

As was discussed above, adding $O_2$ in the gas mixture after some time-on-stream can not achieve re-dispersion of the sintered Au particles/clusters. It can only preserve whatever gold has not yet being lost. So to maintain the reactivity of Au-$FeO_x$ at its highest level, $O_2$ must be added at the very beginning of the test to stabilize most of the active sites. Hence, $O_2$-assisted WGS reaction is recommended to stabilize the active Au-O-Fe species.

### 5.3.2 Re-generable OH groups as active species for the WGSR

An approach that has been proposed in the recent literature to stabilize nanoclusters of Au is via modification of the support oxide surface. For instance, Veith *et al.* [14, 15] have reported that the surface hydroxyl groups are essential on the surface of $TiO_2$ for stabilizing gold clusters against coarsening under ambient conditions, hence a base-treated $TiO_2$ surface was used and gold was sputter-deposited on it. A natural fumed titania was hydroxylated at pH= 10. The gold oxide clusters grown on the hydroxylated surface were at least 180 times more catalytically active and stable for the oxidation of CO than those grown on the native oxide surface. Haruta *et al.* [16] found that a gold lanthanum hydroxide, $AuLa_2(OH)_9$, which was prepared by co-precipitation, showed very markedly high catalytic activity for CO oxidation (100% conversion) at a temperature as low as 193 K after it was first mildly reduced at 373 K. The catalyst mainly consists of $Au^0$ clusters smaller than 1.5 nm, which are well-mixed with $La(OH)_3$ containing isolated $Au(OH)_3$ species.

Surface OH groups not only stabilize dispersed Au species as reported in literature, but also serve as a key reactant in the WGS reaction pathway, similar to the case of Pt-based and other WGS catalysts. This is of interest to this thesis. We can use CO-TPR to titrate the OH on the surface of supported Au catalysts. As an example, we consider here the CO-TPR of Au on three different supports, having surface –OH groups. In Figure 5.9 CO-TPR profiles over Au-$CeO_2$, Au-$La_2O_3$, and Au-$Fe_2O_3$ are displayed. Comparing the three sets of plots, the similarity is clear. There is a $CO_2$ production peak at temperatures lower than 100 $^oC$ in all the cases, which should be assigned to the reduction of the surface oxygen species to produce $CO_2$. A second $CO_2$ production peak traced by an identical $H_2$ production peak follows, which indicates the reaction between CO and surface OH groups, releasing products $CO_2$ and $H_2$. The onset of the $H_2$ production is about 100 $^oC$, which is the same as for the WGS reaction over the Au-based catalysts, illustrating that OH groups are the reactants involved in the WGS reaction pathway. This is the same conclusion we got from the first part of the thesis.

Therefore we try to use OH-rich oxide surface to create and possibly stabilize the active gold species for the WGS reaction. Using oxides with high OH-content without promoters is one approach, but motivated by the alkali-effect on the Pt-based catalysts, we also examined how alkali additives affect the stability of surface OH species.

#### 5.3.2.1 Au on OH-rich supports (Au-LaO(OH)x)

Lanthanum has been widely investigated as a promoter to improve the redox properties of $CeO_2$ [18, 24, 25]. Because of its irreducibility, $La_2O_3$ is not a good choice as a support for noble metals to keep the noble metals dispersed. However, it was recently reported that ionic Au could be obtained on $La_2O_3$ [26], especially on a high surface area $La_2O(OH)_x$ prepared by a hydrolysis method [27].

We have prepared lanthana samples in the lab both by hydrolysis and by precipitation/gelation with urea (UGC method). Compared with the low-surface area $La_2O_3$ (5 $m^2$/g after calcination in air at 800 $^oC$ [20] prepared by UGC with lanthanum carbonate as the precursor, the high surface area $La_2O_3$ (75 $m^2$/g after calcination in air at 400 $^oC$), has probably more OH groups on the surface. However because of the big difference in surface area this becomes another variable when studying the role of OH in the dispersion of Au on $La_2O_3$. Calcining the hydrolysis-prepared $La_2O_3$ at different temperatures to control the available OH population is another approach, while again it introduces the change of the surface area as another variable, 75 $m^2$/g (400 $^oC$) *vs.*23 $m^2$/g (800 $^oC$).

To exclude other variables and focus mainly on understanding how OH groups affect the dispersion of Au species and the reactivity for the WGS reaction, we also used lanthanum oxysulfate, $La_2O_2SO_4$ with surface area of 60 $m^2$/g, which is irreducible at temperatures lower than 400 $^oC$, and barely has any OH groups on the surface [20].

Of course we can use CO-TPR and IR techniques as well as XPS ($O_{1s}$) [28] to check for OH presence on the catalyst surfaces. Here we used CO-TPR. Figure 5.10 shows the CO-TPR profiles of $La_2O_3$ (prepared by hydrolysis method and calcined at 400 $^oC$ for 4 h), and commercial $La_2O_2SO_4$. As expected, there is only a negligible amount of OH on $La_2O_2SO_4$,

and CO consumption begins at temperatures above 400 $^{o}$C and is very high above 500 $^{o}$C, which is due to the bulk reduction of the oxysulfate [29].

$$La_2O_2SO_4 + CO \leftrightarrow La_2O_2S + CO_2$$

The reaction is reversible; $H_2O$ can also be used to reoxidize the oxysulfide to the oxysulfate form [20]. This redox property of $La_2O_2SO_4$ renders it a good catalyst for the high temperature reverse WGS reaction [20]. On the other hand, a significant amount of $H_2$ production along with $CO_2$ production was observed on $La_2O_3$, above 300 $^{o}$C, which indicates the existence of surface OH groups and the possibility to use material as a high-temperature WGS catalyst.

5 at%Au was loaded on both $La_2O_3$ and $La_2O_2SO_4$ by the DP method. The ICP measurement confirms the actual Au loading was the same as the designed.

The TEM image of 5Au-$La_2O_3$, Figure 5.11, shows that small Au particles/clusters (1-2nm) were well dispersed on the support surface, while only big Au particles (>3nm) were observed on $La_2O_2SO_4$. This may be explained as the Au species bind stronger on $La_2O_3$, most probably through OH groups, than on $La_2O_2SO_4$.

CO-TPR profiles over these two Au-based samples, in Figure 5.12, further proves that the OH groups on lanthanum oxide can be activated by the presence of well-dispersed Au species and the catalyst is now good for the low-temperature shift. To be activated by the Au species at the lower temperatures, OH groups must be in close proximity to the Au species. We can then propose that such Au-O-OH-La sites stabilize the sub-nm Au clusters and ions and prevent gold particle growth and sintering during the preparation and calcination steps. On the other hand, due to lack of surface OH groups, the lanthanum oxysulfate can not disperse the gold and does not show any low-temperature activity for the WGS reaction. The high-temperature activity is there, as Figure 5.12 shows, but this reaction is independent of the presence of Au species [20].

The steady-state WGS reactivity of these catalysts is shown in Figure 5.13. In agreement with the CO-TPR results, 5Au-$La_2O_3$ shows good catalytic activity for the WGS reaction, while Au-$La_2O_2SO_4$ is almost inactive for the reaction. However it should be noticed that

during the cool down testing, decreased activity was observed for both samples, which means the Au species are not stable on both supports under the reaction conditions.

Because of the good activity of 5Au-$La_2O_3$, we further investigate the storage effect on this sample. After one-month storage, the sample was tested under the same condition, and only half of its previous activity was found. This reveals that OH groups help to create Au-O-OH sites on the surface, active for the WGS reaction. However, the Au-O-OH association is not strong enough to inhibit the mobility of Au effectively.

These findings argue strongly in favor of a similar active structure in the Au-based catalysts, Au-$O_x(OH)_y$. Novel synthesis methods, aiming at depositing atomically dispersed metals on supports, are also recommended for future work. Potentially all of these catalysts can be prepared with a stabilizing agent, such as the alkali additives used in this thesis to promote the activity and stability of Pt-$O_x(OH)_y$ catalysts. This was examined briefly in the last part of the thesis and is presented below.

#### 5.3.2.2 Alkali-promoted Au catalysts for the WGS reaction

##### 5.3.2.2.1. Au catalysts supported on reducible oxides

To date, no promotion effect on Au-based catalysts by alkali additives has been reported in literature for the WGS reaction. However, Deng [9] found if small amount of Na impurity from the synthesis process remained in Au-$CeO_2$ samples, the activity of the latter increased, as shown in Table 5.2 [9].

This was confirmed here by adding Na into Au-$CeO_2$ in a second step by IMP method. The physical properties of the related Au-$CeO_2$ samples are listed in Table 5.3. Figure 5.14 shows the steady-state WGS reaction activity of the $CeO_2$-supported catalysts. Obviously the Au-$CeO_2$ was boosted by the addition of Na ions, at atomic ratio of Na:Au = 1:1. $H_2$-TPR shows that the Na-promoted sample has more reducible oxygen, in Figure 5.15 and Table 5.4. But the catalytic activity of Au-$CeO_2$ is very sensitive to the Na:Au ratio; when the Na:Au is increased to 3, a negative effect was observed. This may be due to the coverage of the active sites by the excess Na ions. A further washing treatment is recommended to check this hypothesis in future work.

Also when Na was added onto the leached Au-$CeO_2$ (before calcination) the reactivity remains unaltered. We suspect that this is because the Au species in the leached sample are strongly bound onto the $CeO_2$ support and the added Na has little effect. A higher amount would then have a negative effect by coverage of the active sites. More in-depth investigation of this effect is recommended.

Promoted catalytic activity for the WGS reaction is observed on both parent and leached Au-$Fe_2O_3$ catalysts, and the effect is more significant on the parent sample, as shown in Figure 5.16. The physical properties of the Au-$Fe_2O_3$ samples are listed in Table 5.3. A clear promotion effect of K doping is evident on the leached Au-$Fe_2O_3$.

The electronegativities of Na, K, Ce, and Fe are 0.93, 0.82, 1.12, and 1.83 respectively. Ce and Na have similar electronegativities, which mean they have similar ability to hold $O^{2-}$ or $OH^-$, so the promotion of Na ions will be significant only when there are "inert" Au species available, as in the parent sample. While the electronegativities of K and Fe are so different, K ions can hold $O^{2-}$ or $OH^-$ much stronger, so compared with Fe ions K ions should have better ability of dissociating $H_2O$ and creating active sites for the WGS reaction.

Although the alkali-promotion on the Au-based catalysts is not well understood, the Arrhenius plots for the WGS reaction over Au-$CeO_2$, in Figure 5.17 and Au-$Fe_2O_3$, in Figure 5.18, show that all the alkali-free or alkali-promoted Au catalysts have similar apparent activation energies (45 ± 5 kJ/mol), as listed in Table 5.5, which indicates that when the proper amount of alkali ions is added in Au catalysts, supported on reducible oxides, it will promote the activity for the WGS reaction, but it does not change the reaction pathway, or the structure of the active sites for the reaction. A common active site, Au-$O_x(OH)_y$, is thus proposed for the WGS reaction on Au-based catalysts.

#### 5.3.2.2.2. Au catalysts supported on inert oxides

Because of the good WGS reaction activities of alkali-free Au-$CeO_2$ or Au-$Fe_2O_3$, it is difficult to define the real role of alkali ions on the Au-based catalysts. So here we also want to investigate the alkali-effect on an inert oxide-supported Au, such as Au-$SiO_2$, which is known to be completely inactive for the low temperature WGS reaction.

Figure 5.19 clearly shows the significantly enhanced WGS reaction activity by addition of Na ions or La ions on Au-$SiO_2$. Au-$SiO_2$ is not active up to 300 $^oC$, but with the addition of $Na^+$ or $La^{3+}$, Au-$SiO_2$ becomes active and has the same light-off temperature, around 100 $^oC$, as Au-$CeO_2$, which means all Au-based catalysts probably share the same active sites, Au-$O_x(OH)_y$, for the WGS reaction.

The different promotion by Na ions and La ions may due to their different electronegativities, 0.93 and 1.1 for Na and La respectively. Similar to the case of the Pt-based catalysts, there must be an optimum M:Au ratio to achieve the best promotion effect. In Figure 5.19 the 3%La-promoted sample is similar, if not slightly inferior to the 1 %La-promoted one. This could be due to the coverage of the active sites as discussed above or to different effective surface basicity as discussed briefly below.

Doping by alkali or alkaline-earth ions definitely will change the surface basicity of the support. Choudhary *et al.* reported that the alkaline-earth modified catalysts contain a larger number of strong basic sites [30]. During the solution-based preparation of Au catalysts, the high pH of the solution leads to the reduction of Au species and relatively big particles will be formed. Also Hutchings and co-workers [10] have reported that surface hydroxyl groups on FeOOH enhanced the coarsening of the gold particles. Therefore it is possible that a large amount of the alkali doping leads to the high concentration of surface OH groups and enhances the surface basicity of the support, which favors the reduction of Au species to metallic gold and then the sintering of gold particles.

Since we discovered the significantly promoted Au-$SiO_2$ for the WGS reaction by alkali additives, we have tried to characterize it. We found these samples were very sensitive to storage conditions, to the beam energy during TEM measurements, and to $H_2$ treatment, all these conditions leading to particle growth and the sintering of Au particles. No activity was detected over the most active 1%Na-Au-$SiO_2$ sample after it has been stored in a sealed vial for a month.

When kinetics measurements were carried on these promoted samples in the reformate gas stream, which contains 26%$H_2$, a quick deactivation was observed over the promoted samples. Thus, the alkali ions and La promoters were able to create active sites over $SiO_2$, however, they were not able to stabilize these sites, especially in reducing atmospheres.

Since it has been reported that the alkali-ions promote Au-$SiO_2$ catalysts for the CO oxidation reaction [31], we checked the activities for the CO oxidation reaction of the samples prepared in this work to ensure these samples at least behave as well as has been reported. Figure 5.20 shows the steady-state CO conversion plots of all the $SiO_2$-supported catalysts for the CO oxidation reaction. Clearly all the additives promote the Au-$SiO_2$ catalysts for the CO oxidation reaction even when they were inactive for the WGS reaction. The activity is stable in ramping up and down the temperature. The oxidative atmosphere may have a beneficial effect on the activity and stability. More detailed work is needed to probe and understand the different catalytic activity/stability in the two reactions.

## 5.4 Summary

The evolution of the Au active structures in Au-$Fe_2O_3$ was followed by XANES and EXAFS analysis and compared with that in Au-$CeO_2$. It was found that atomically dispersed gold as [Au-O-Ce] and [Au-O-Fe] species catalyze the WGS reaction. Highly reducing gas mixtures destabilize the [Au-O-Ce, Fe] sites and cause gold cluster/particle formation and deactivation. Activity recovery is possible by re-oxidation (350-400 $^oC$). Catalyst stability is improved if gas mixtures with higher oxygen potential are used. Therefore oxygen-assisted WGS operation is recommended.

OH-rich oxide supports were applied to create and stabilize Au-O active sites for the reaction. By comparing the catalytic performance of $La_2O_3$ or $La_2O_2SO_4$ supported Au catalysts it was further shown that OH-rich surfaces can stabilize the dispersed Au species during the synthesis and thermal treatment steps, and provide reactant for the reaction pathway.

An alkali-promotion effect was observed on all Au catalysts, whether supported on reducible oxides, *e.g.* $CeO_2$, $Fe_2O_3$, or inert oxides, *e.g.* $SiO_2$. The alkali-free and alkali-promoted Au-$CeO_2$ or Au-$Fe_2O_3$ have the same apparent activation energy, which indicates that the proper amount of additional alkali ions can enhance the activity for WGS reaction, but it does not change the reaction pathway, or the structure of the active sites for the reaction. A common active site, Au-$O_x(OH)_y$, is proposed for the Au-based catalysts for the WGS reaction.

However, the stability of the Au species is not good either in the OH-rich or the alkali-modified surfaces, especially with inert oxide as the support. The electronegativity of the oxide or promoter metal seems to play an essential role on the stability of the Au active sites. And a large amount of the alkali doping leads to the high concentration of surface OH groups and enhances the surface basicity of the support, which favors the reduction of Au species to metallic gold and then the sintering of gold particles.

Though the effect of alkali ions on the Au-based catalysts is not well addressed in this thesis work it should be aware that the properties of the oxide supports/additives, e.g. electronegativity and basicity, play an important role in the formation and stabilization of the active sites, which will guide the choice of supports/additives and the optimization of the synthesis condition of the catalysts.

**Table 5.1 EXAFS fitting data for the 0.7Au-$Fe_2O_3$ sample**

| Sample | Au-O | | | Au-Au | | |
|---|---|---|---|---|---|---|
| | CN | R (Å) | $\sigma^2$ (Å$^2$) | CN | R(Å) | $\sigma^2$ (Å$^2$) |
| Fresh | 2.3±0.5 | 2.01±0.07 | 0.004±0.002 | — | — | — |
| 250 °C WGS[a] | 0.5±0.2 | 1.97±0.02 | 0.000±0.006 | 7.2±1.3 | 2.77±0.11 | 0.013±0.002 |
| 250 °C re-oxidation[b] | 1.3±0.7 | 1.98±0.04 | 0.009±0.008 | 9.5±3.0 | 2.79±0.10 | 0.022±0.005 |
| 350 °C re-oxidation[c] | 1.4±0.8 | 2.03±0.08 | 0.003±0.007 | — | — | — |

a after 1 h WGS reaction at 250 $^oC$ in 5%CO-3%$H_2O$-He;

b after re-oxidation of a at 250 $^oC$ in 5%$O_2$-He for 1 h;

c after oxidation of b at 350 $^oC$ in 5%$O_2$-He for 1 h.

**Table 5.2 Na-promotion effect on Au-$CeO_2$ for the low temperature WGS reaction [9].**

| Sample | Au content (at.%) | Na content (at.%) | WGSR rate at 240°C (umol/g/s)[#] |
|---|---|---|---|
| #1 Au-$CeO_2$ | 4.86 | 0.88 | 104 |
| #2 Au-$CeO_2$ | 5.04 | 0 | 22 |

# measured in 11%CO-26%$H_2O$-26%$H_2$-7%$CO_2$-He gas mixture.

**Table 5.3 Physical properties of Au-based materials**

| Sample | Preparation | Bulk Composition[a] (at%) | | | BET Surface Area ($m^2/g$) |
|---|---|---|---|---|---|
| | | Au | Na | K | |
| $CeO_2$ | UGC | -- | -- | -- | 131.6 |
| Au- $CeO_2$ | DP | 1.0 | -- | -- | 123.3 |
| 1Na-Au- $CeO_2$ | DP+IMP | 0.9 | 0.9 | -- | 118.8 |
| 3Na-Au- $CeO_2$ | DP+IMP | 0.9 | 2.6 | -- | 112.0 |
| 0.4Au- $CeO_2$ | DP, leached | 0.4 | -- | -- | 114.6 |
| 0.8Na-0.4Au- $CeO_2$ | DP, leached, IMP | 0.4 | 0.8 | -- | 117.8 |
| $Fe_2O_3$ | CP | -- | -- | -- | |
| 1.7Au-$Fe_2O_3$ | DP | 1.7 | -- | -- | |
| 1.5K-1.7Au-$Fe_2O_3$ | DP+IMP | 1.7 | -- | 1.5 | 38.1 |
| 0.1Au- $Fe_2O_3$ | DP, leached | 0.1 | -- | -- | 40.4 |
| 0.8K-0.1Au- $Fe_2O_3$ | DP, leached, IMP | 0.1 | -- | 0.8 | 37.0 |

a: Bulk composition was determined by ICP-OES.

**Table 5.4 $H_2$ consumption in $H_2$-TPR of Au-$CeO_2$-(Na) samples**

| Samples | $H_2$ Consumption ($\mu mol/g_{cat}$) | Reduction Temp ($^oC$) |
|---|---|---|
| 1Au-$CeO_2$ | 918 | 156 |
| 1Na-1Au-$CeO_2$ | 1202 | 159 |

**Table 5.5 $E_{app}$ for the WGS reaction over Au catalysts**

| Catalyst | $E_{app}$ # (kJ/mol) |
|---|---|
| 1.0Au- $CeO_2$ | 49.9 |
| 1Na-1Au- $CeO_2$ | 40.7 |
| 3Na-Au- $CeO_2$ | 49.7 |
| 0.4Au- $CeO_2$ | 49.2 |
| 0.8Na-0.4Au- $CeO_2$ | 49.4 |
| 1.7Au-$Fe_2O_3$ | 46.1 |
| 1.5K-1.7Au-$Fe_2O_3$ | 41.9 |
| 0.1Au- $Fe_2O_3$ | 50.5 |
| 0.8K-0.1Au- $Fe_2O_3$ | 39.7 |

# measured in11%CO-26%$H_2O$-26%$H_2$-7%$CO_2$-He gas mixture.

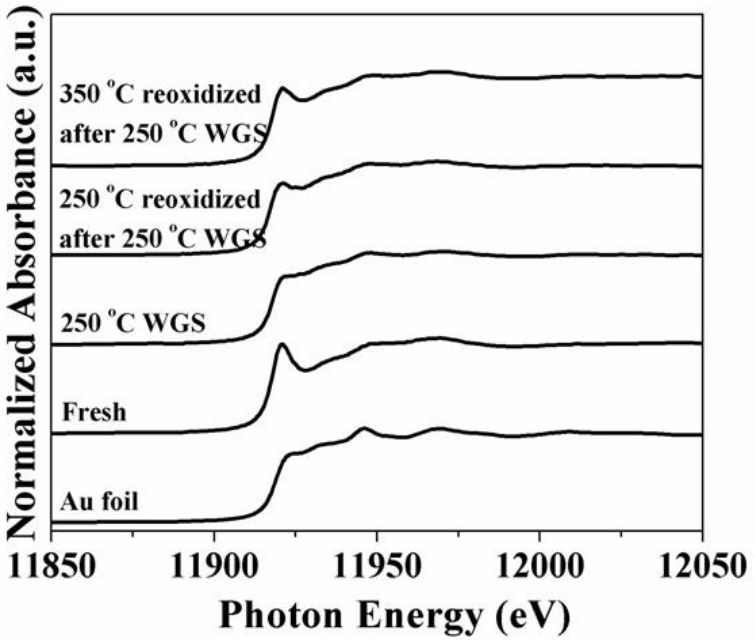


Figure 5.1 Au $L_{III}$-edge XANES spectra of 0.7Au-$Fe_2O_3$ under various conditions. a) fresh; b) a after 1 h WGS reaction at 250 $^oC$ in 5%CO-3%$H_2O$-He; c) b after re-oxidation at 250 $^oC$ in 5%$O_2$-He for 1 h; d) b after oxidation at 350 $^oC$ in 5%$O_2$-He for 1 h.

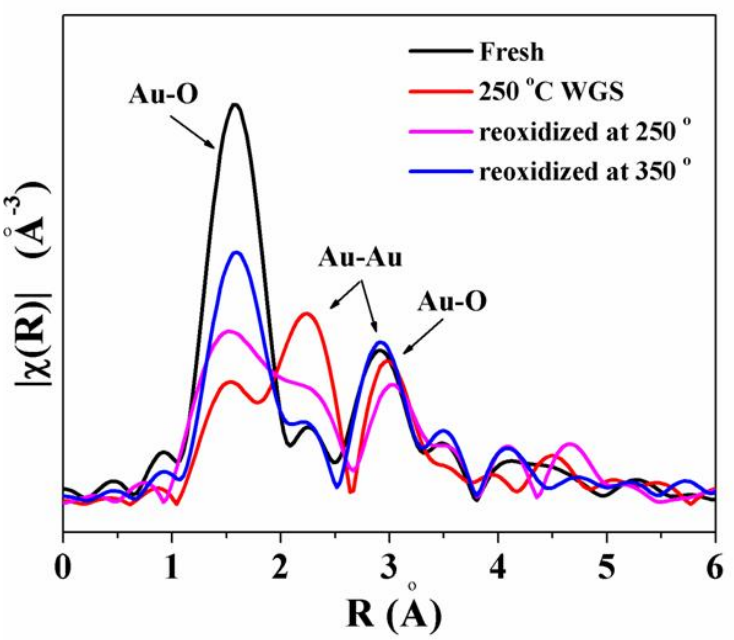


Figure 5.2 EXAFS spectra in R-space of 0.7Au-$Fe_2O_3$ under different conditions, a) fresh; b) a after 1 h WGS reaction at 250 $^oC$ in 5%CO-3%$H_2O$-He; c) b after re-oxidation at 250 $^oC$ in 5%$O_2$-He for 1 h; d) b after re-oxidation at 350 $^oC$ in 5%$O_2$-He for 1 h.

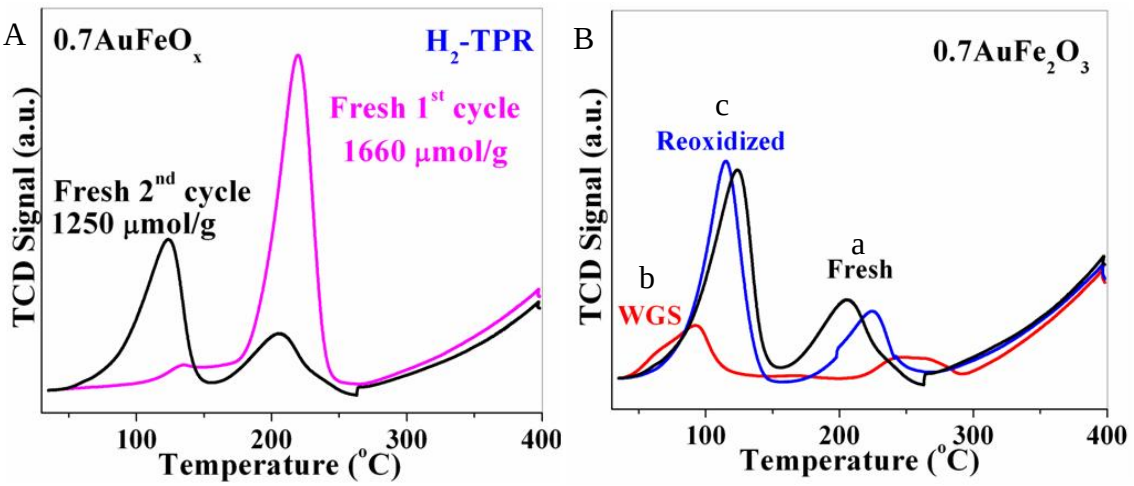


Figure 5.3 $H_2$-TPR over 0.7Au-$Fe_2O_3$ sample under various conditions. A: Cyclic $H_2$-TPR over fresh 0.7Au-$Fe_2O_3$; B: a) fresh; b) a after 1 h WGS reaction at 250 $^oC$ in 5%CO-3%$H_2O$-He; c) b was re-oxidized at 350 $^oC$ in 5%$O_2$-He for 1 h.

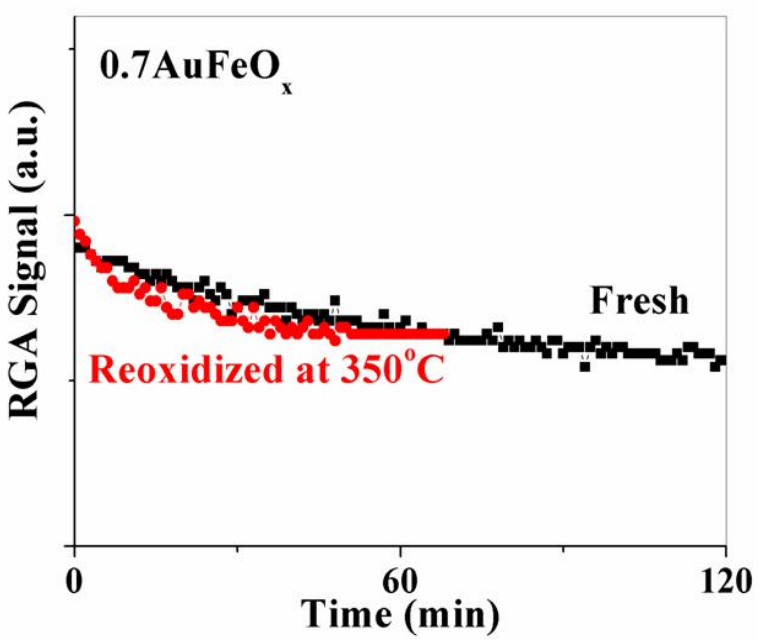


Figure 5.4 $H_2$-production during isothermal WGS reaction over 0.7Au-$Fe_2O_3$ at 250 $^oC$ in 5%CO-3%$H_2O$-He. Black line: fresh 0.7Au-$Fe_2O_3$; Red line: the used sample (black line) after oxidation at 350 $^oC$ for 1 h in 5%$O_2$-He.

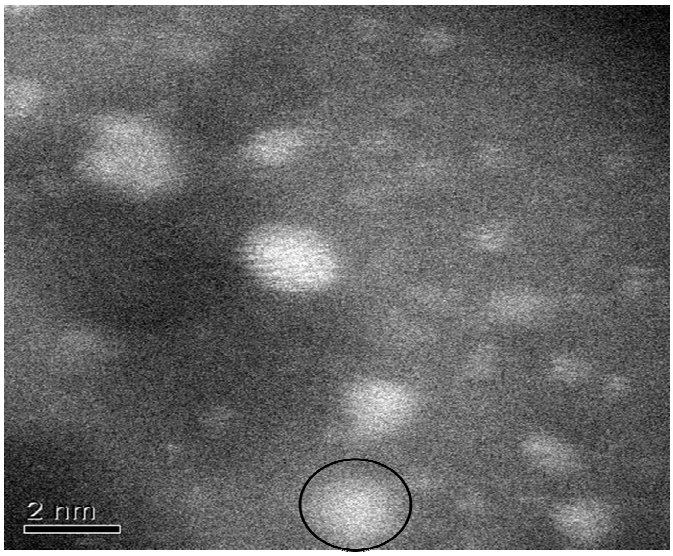


Figure 5.5 Aberration-corrected HAADF-STEM image of used 0.7Au-$FeO_x$ catalyst. [7]. After 2h at 250 $^oC$ in 5%CO-3%$H_2O$-He.

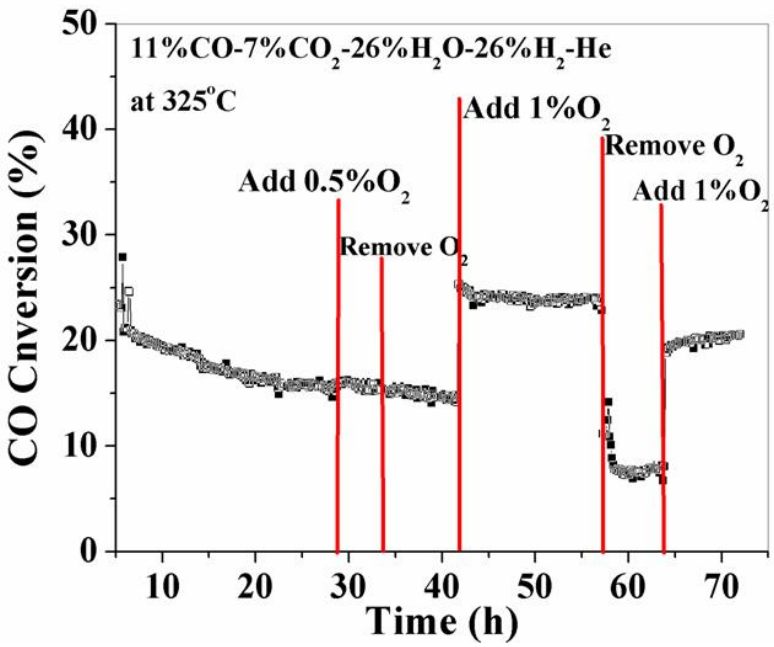


Figure 5.6 $O_2$-free and $O_2$-assisted WGS reaction stability test over 0.7Au-$Fe_2O_3$ catalyst, measured in 11%CO-26%$H_2O$-26%$H_2$-7%$CO_2$-He, contact time 0.03 g.s/cc.

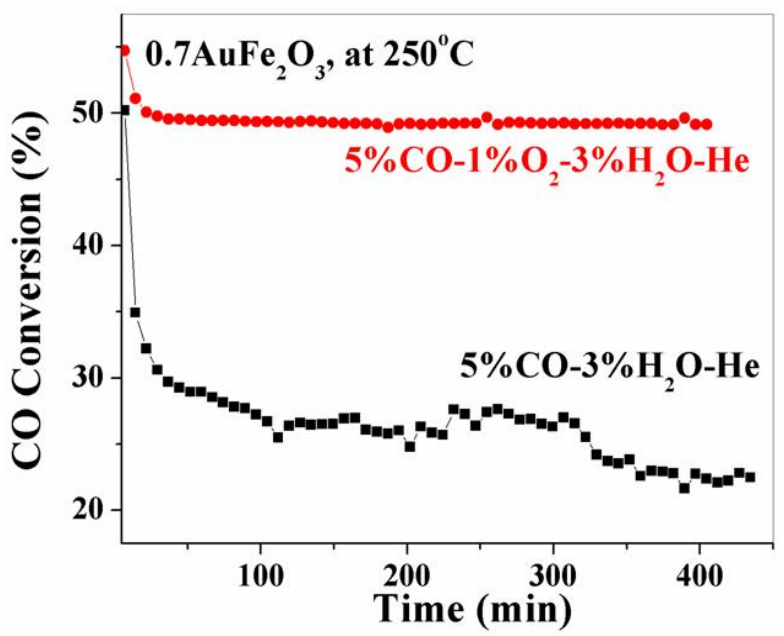


Figure 5.7 $O_2$-free and $O_2$-assisted isothermal WGS reaction stability over the 0.7Au-$Fe_2O_3$ catalyst.

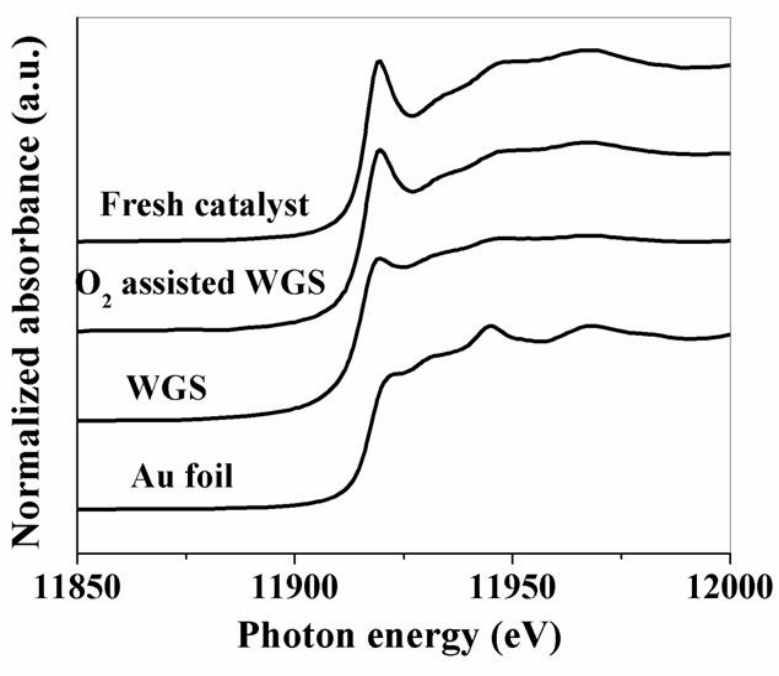


Figure 5.8 Au $L_{III}$-edge XANES spectra of 0.7Au-$Fe_2O_3$ under various conditions. Fresh; WGS: After 1 h WGS reaction at 250 $^oC$ in 5%CO-3%$H_2O$-He; $O_2$ assisted WGS: After 1 H WGS reaction at 250 $^oC$ in 5%CO-1%$O_2$-3%$H_2O$ -He.

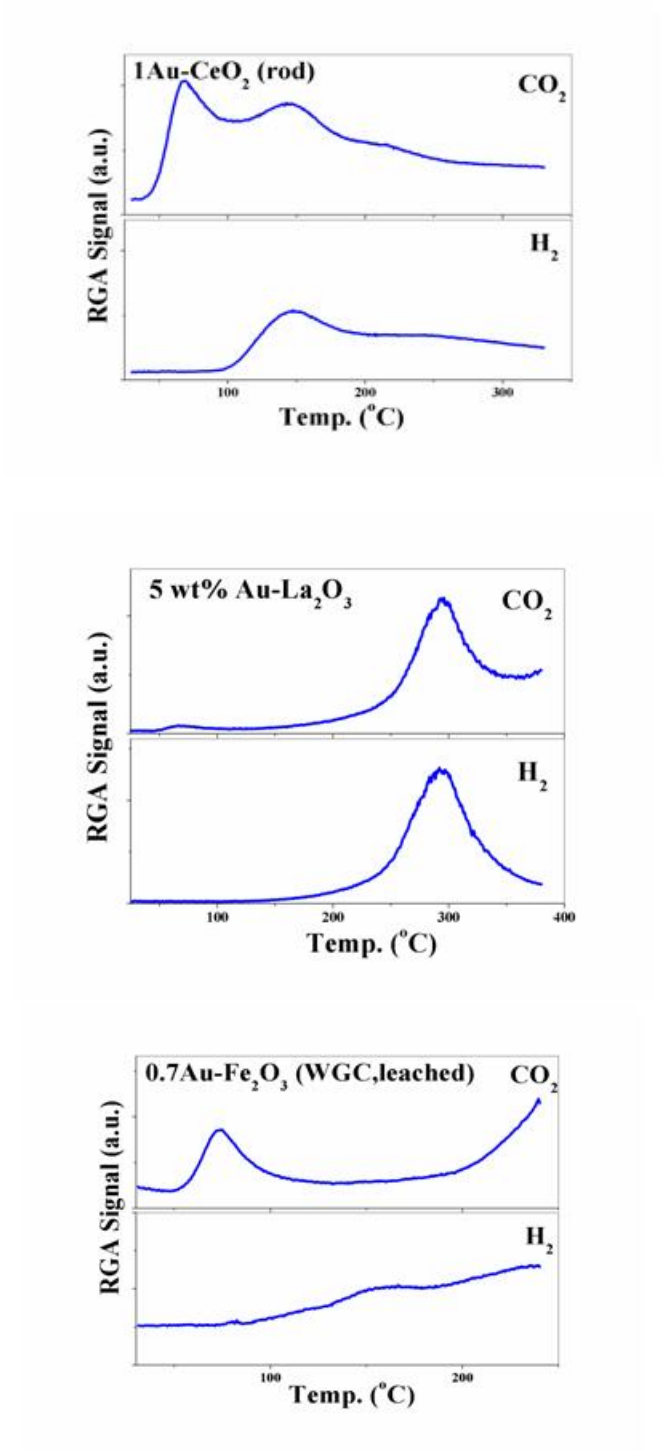


Figure 5.9 CO-TPR over Au-based catalysts, with $CeO_2$, $La_2O_3$, and $Fe_2O_3$ as supports respectively. 5%CO-He, 30 ml/min, at 5 $^oC$/min.

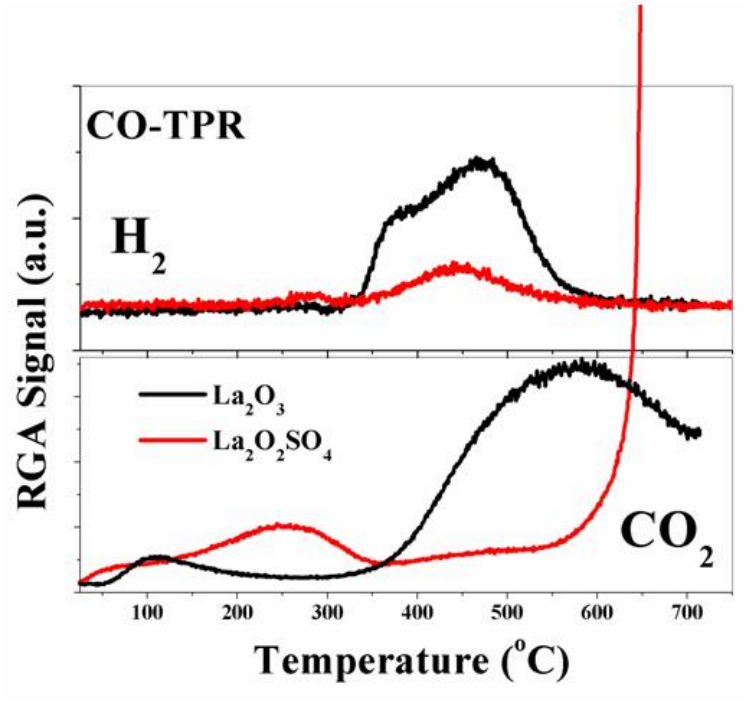


Figure 5.10 CO-TPR over $La_2O_3$ and $La_2O_2SO_4$ supports. 5%CO-He, 30 ml/min, at 10 $^oC$/min.

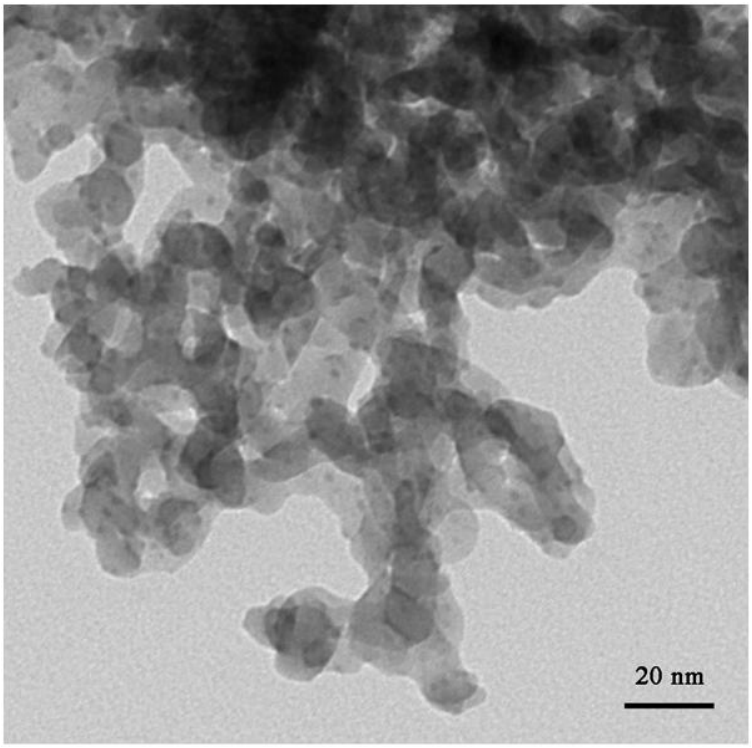


Figure 5.11 TEM image of fresh 5Au-$La_2O_3$ sample (calcination at 400 $^{o}$C for 4 h in static air).

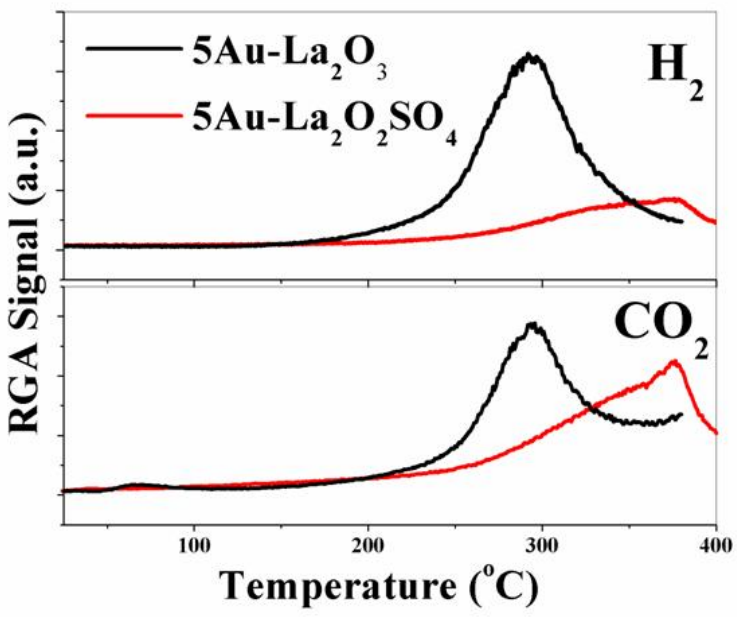


Figure 5.12 CO-TPR profiles over 5Au-$La_2O_3$ and 5Au-$La_2O_2SO_4$ samples. 5%CO-He, 30 ml/min, at 10 $^oC$/min.

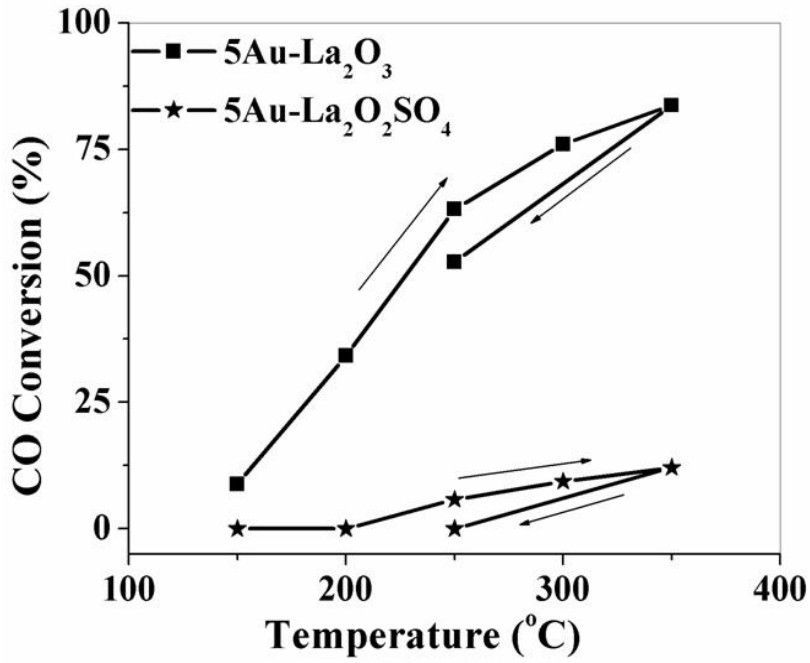


Figure 5.13 Steady-state CO conversion in WGS reaction over 5Au-$La_2O_3$ and 5Au-$La_2O_2SO_4$ catalysts. Gas composition: 2%CO-10%$H_2O$-He, 0.09 g.s/cc.

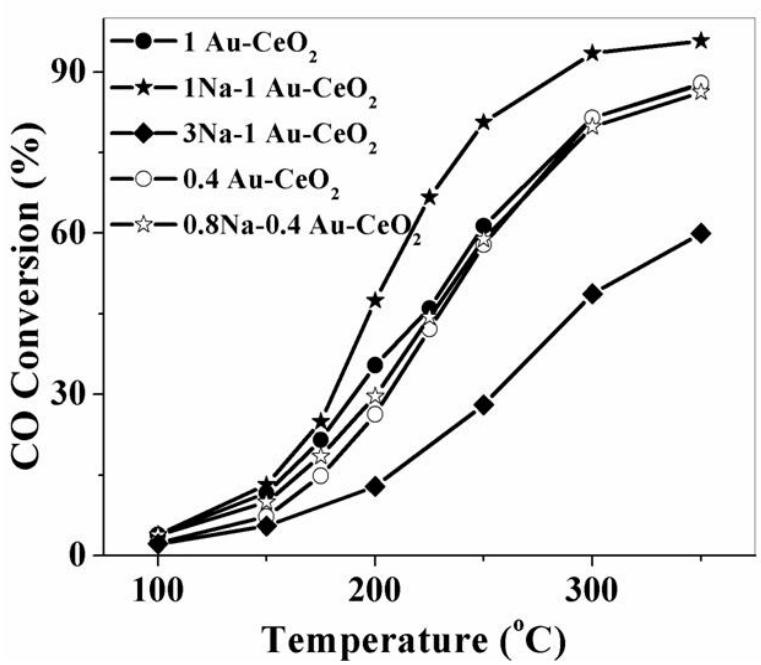


Figure 5.14 Alkali-effect on the steady-state CO conversion in the WGS over $CeO_2$-supported Au catalysts. Gas composition: 2%CO-10%$H_2O$-He, 0.09 g.s/cc.

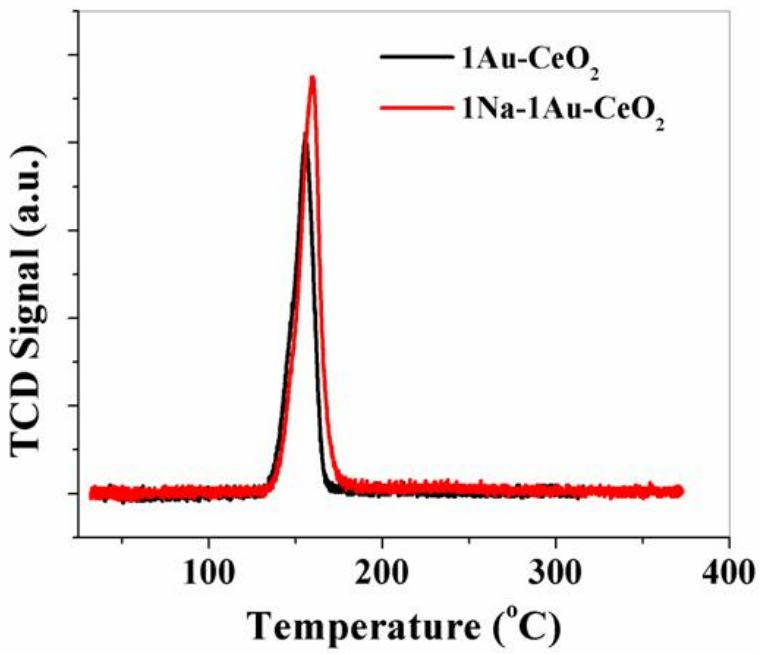


Figure 5.15 $H_2$-TPR: Alkali-effect on the reducibility of Au-$CeO_2$ catalysts.

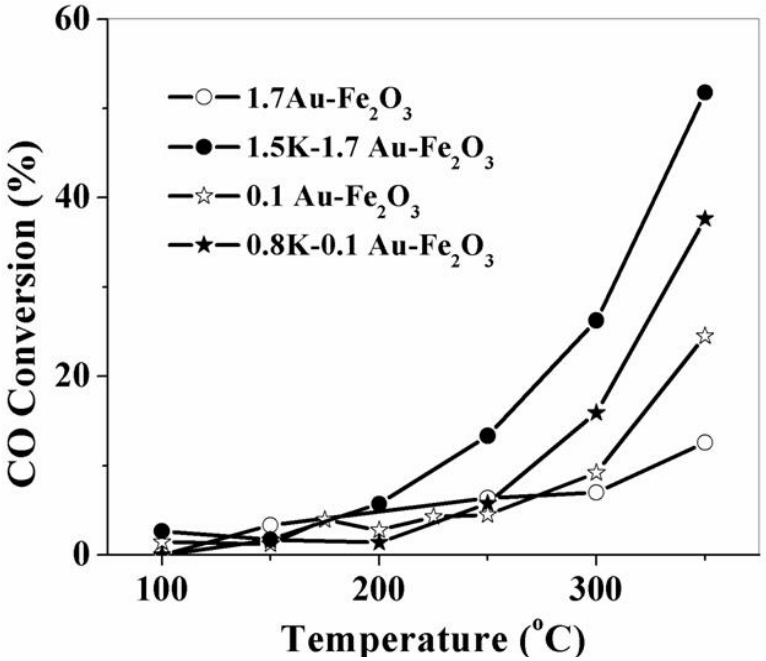


Figure 5.16 Steady-state CO conversion in the WGS reaction over $FeO_x$-supported Au catalysts. Gas composition: 2%CO-10%$H_2O$-He.

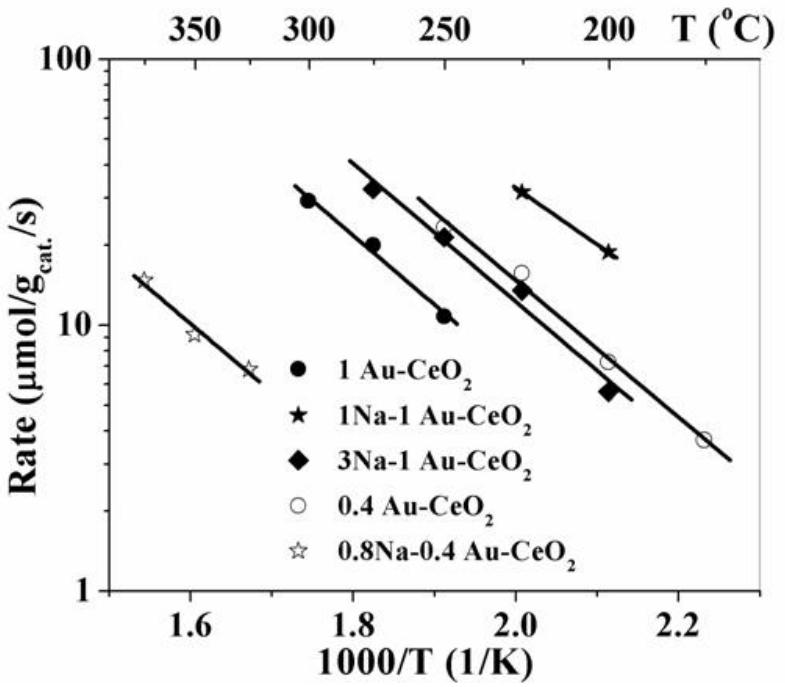


Figure 5.17 Alkali-effect on the steady-state WGS reaction rates over $CeO_2$-supported Au catalysts, measured in 11%CO-26%$H_2O$-26%$H_2$-7%$CO_2$-He.

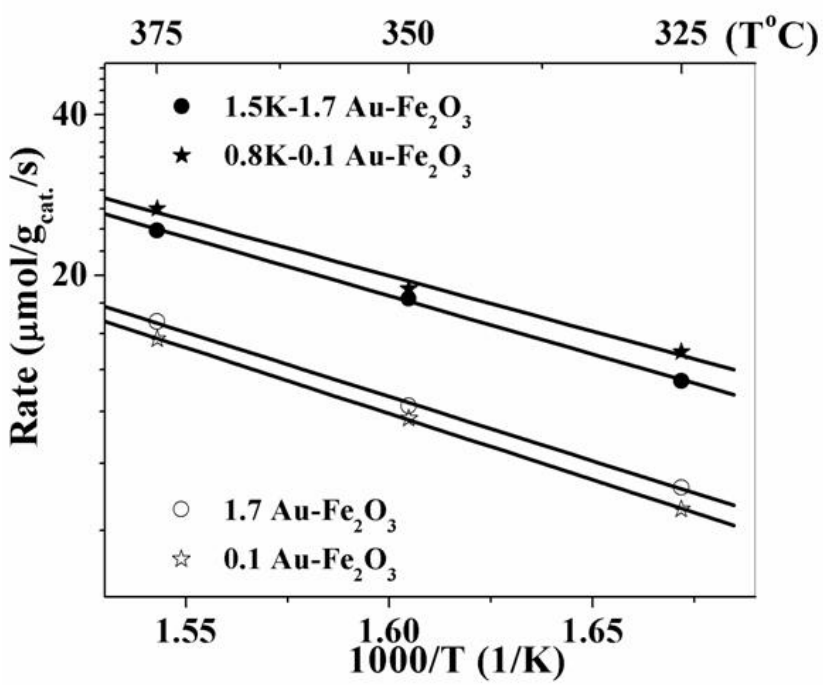


Figure 5.18 Steady-state WGR reaction rates over $Fe_2O_3$-supported Au catalysts, measured in 11%CO-26%$H_2O$-26%$H_2$-7%$CO_2$-He.

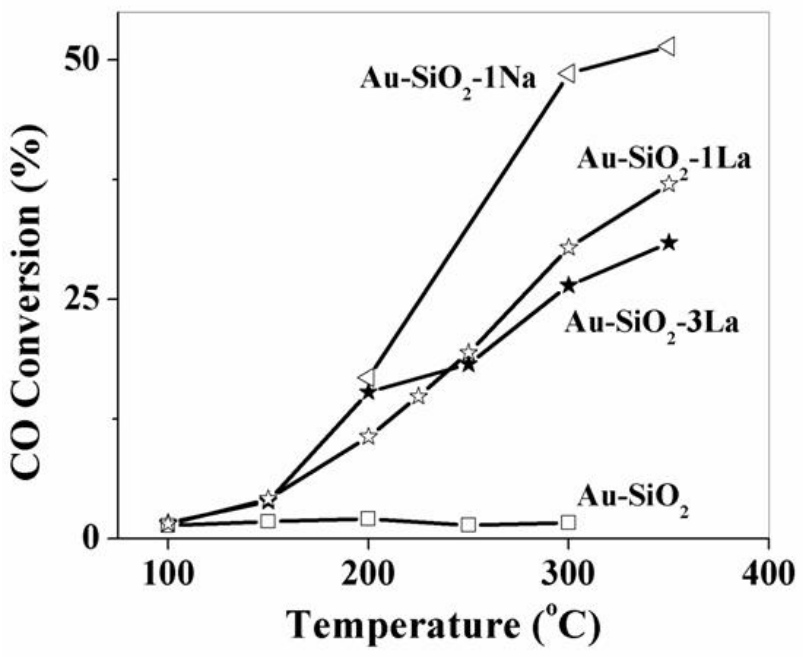


Figure 5.19 Steady-state CO conversion in the WGS reaction over Au-$SiO_2$ based samples. Gas composition: 2%CO-10%$H_2O$-He, 0.09 g.s/cc.

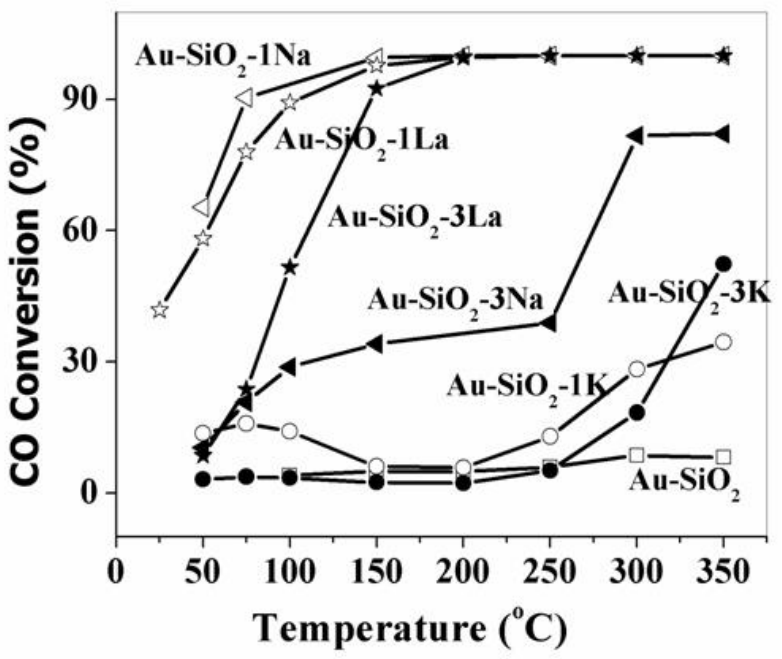


Figure 5.20 Steady-state CO conversion in CO oxidation over Au-$SiO_2$ based catalysts. Gas composition: 1%CO-2%$O_2$-He, 0.1 g.s/cc.

## 5.5 References

[1] W. Deng, A.I. Frenkel, R. Si, M. Flytzani-Stephanopoulos, J. Phys. Chem. C 112 (2008) 12834-12840.

[2] W. Deng, C. Carpenter, N. Yi, M. Flytzani-Stephanopoulos, Top. Catal. 44 (2007) 199-208.

[3] T. Tabakova, V. Idakiev, D. Andreeva, I. Mitov, Appl. Catal., A 202 (2000) 91-97.

[4] D. Andreeva, V. Idakiev, T. Tabakova, A. Andreev, J. Catal. 158 (1996) 354-355.

[5] F. Boccuzzi, A. Chiorino, M. Manzoli, D. Andreeva, T. Tabakova, J. Catal. 188 (1999) 176-185.

[6] K.T. Rim, D. Eom, L. Liu, E. Stolyarova, J.M. Raitano, S.-W. Chan, M. Flytzani-Stephanopoulos, G.W. Flynn, The Journal of Physical Chemistry C 113 (2009) 10198-10205.

[7] L.F. Allard, A. Borisevich, W. Deng, R. Si, M. Flytzani-Stephanopoulos, S.H. Overbury, J Electron Microsc (Tokyo) 58 (2009) 199-212.

[8] L.F. Allard, M. Flytzani-Stephanopoulos, S.H. Overbury, Microsc. Microanal. 16 (2010) 375-385.

[9] W. Deng, PhD, Tufts University, 2007.

[10] A.A. Herzing, C.J. Kiely, A.F. Carley, P. Landon, G.J. Hutchings, Science 321 (2008) 1331-1335.

[11] I.X. Green, W. Tang, M. Neurock, J.T. Yates, Science 333 (2011) 736-739.

[12] W.D. Williams, M. Shekhar, W.-S. Lee, V. Kispersky, W.N. Delgass, F.H. Ribeiro, S.M. Kim, E.A. Stach, J.T. Miller, L.F. Allard, J. Am. Chem. Soc. 132 (2010) 14018-14020.

[13] K.T. Rim, M. Flytzani-Stephanopoulos, G.W. Flynn, ACS Nano submitted (2011).

[14] G.M. Veith, A.R. Lupini, N.J. Dudney, The Journal of Physical Chemistry C 113 (2008) 269-280.

[15] G.M. Veith, A.R. Lupini, S.J. Pennycook, N.J. Dudney, ChemCatChem 2 (2010) 281-286.

[16] T. Takei, I. Okuda, K.K. Bando, T. Akita, M. Haruta, Chem. Phys. Lett. 493 (2010) 207-211.

[17] A.C. Gluhoi, B.E. Nieuwenhuys, Catal. Today 122 (2007) 226-232.

[18] Q. Fu, A. Weber, M. Flytzani-Stephanopoulos, Catal. Lett. 77 (2001) 87-95.

[19] Q. Fu, H. Saltsburg, M. Flytzani-Stephanopoulos, Science 301 (2003) 935-938.

[20] I. Valsamakis, M. Flytzani-Stephanopoulos, Appl. Catal., B 106 (2011) 255-263.

[21] Q. Fu, S. Kudriavtseva, H. Saltsburg, M. Flytzani-Stephanopoulos, Chem. Eng. J. 93 (2003) 41-53.

[22] Q. Fu, W. Deng, H. Saltsburg, M. Flytzani-Stephanopoulos, Appl. Catal., B 56 (2005) 57-68.

[23] W. Deng, M. Flytzani-Stephanopoulos, Angew. Chem. Int. Ed. 45 (2006) 2285-2289.

[24] T. Luo, J.M. Vohs, R.J. Gorte, J. Catal. 210 (2002) 397-404.

[25] Y. Li, Q. Fu, M. Flytzani-Stephanopoulos, Appl. Catal., B 27 (2000) 179-191.

[26] A. Goguet, M. Ace, Y. Saih, J. Sa, J. Kavanagh, C. Hardacre, Chem. Commun. (2009) 4889-4891.

[27] M. Mihaylov, E. Ivanova, Y. Hao, K. Hadjiivanov, H. Knozinger, B.C. Gates, The Journal of Physical Chemistry C 112 (2008) 18973-18983.

[28] X. Zhu, M. Shen, L.L. Lobban, R.G. Mallinson, J. Catal. 278 (2011) 123-132.

[29] M. Machida, K. Kawamura, K. Ito, Chem. Commun. (2004) 662-663.

[30] V.R. Choudhary, S.A.R. Mulla, V.H. Rane, Journal of Chemical Technology & Biotechnology 72 (1998) 125-130.

[31] A.C. Gluhoi, X. Tang, P. Marginean, B.E. Nieuwenhuys, Top. Catal. V39 (2006) 101-110.

# Chapter 6 Conclusions and Recommendations

## 6.1 Conclusions

In the development of the PEM fuel cell applications, highly active and stable catalysts are required for the low temperature WGS reaction to catalytically remove the carbon monoxide. Based on numerous investigations, $CeO_2$-supported precious-metal catalysts, especially Pt and Au have emerged as potential candidates for this CO removal process. Pt-O-Ce or Au-O-Ce species regarded as the active sites for the WGS reaction. From an economic viewpoint, low precious metal loading and alternative oxide supports are of the current research interest regarding the design of the catalysts because of the high cost of the precious and rare-earth oxides. In this thesis work, it was aimed to promote the precious metal-based catalysts for the low temperature WGS reaction with alkali ions. With inert oxides as the supports, *e.g.* $SiO_2$, $Al_2O_3$, the promotion effect of alkali ions on the catalytic activity of Pt-based catalysts was investigated in detail. Considering the cost and deactivation problem of Pt-$CeO_2$, it is believed that the alkali-modified Pt catalysts on earth-abundant oxide supports are more promising for practical fuel cell applications. Such alkali-modification was extended to the Au catalysts as well.

The following are the major conclusions from this thesis work:

1. Alkali and alkaline-earth ions (Li, Na, K, Cs, Mg, Ca, Ba) added in small amounts activate Pt for the low-temperature WGS reaction even when the Pt is supported on inert oxide supports, such as $SiO_2$ or $Al_2O_3$. These promoted catalysts are as active as $CeO_2$-supported Pt which is reported as one of the most active catalysts for the WGS reaction [1, 2]. The effect appears to be structural, *i.e.* the alkali ions stabilize atomically dispersed platinum species, positively charged, on the support. In turn, through Pt-O linkages, the alkali and alkaline-earth ions are stabilized around one or few-atom Pt cluster. Also alkali ions introduce surface OH groups, which are activated by close-by adsorbed CO at low temperatures, as low as ~100 $^{o}$C, hence, the WGS reaction can now occur at low temperature; whereas unpromoted Pt-$Al_2O_3$ is typically a high-temperature WGS catalyst.

2. The apparent activation energy for the low-temperature WGS reaction over all alkali-promoted Pt catalysts supported on alumina or silica is similar 70 ± 5 kJ/mol, which is also the same over $TiO_2$ [3], $CeO_2$ [1, 2, 4], or $ZrO_2$ [5] supported Pt samples, A common site, Pt-$O_x(OH)_y$-M is thus proposed to be the active site for the WGS reaction in all Pt-based catalysts. Normalizing the reaction rate by the active OH groups brings the Arrhenius plots over alkali- and alkaline-earth- promoted Pt-$SiO_2$ samples into a single line. Similar TOF is found over Pt-$CeO_2$ [2], which further demonstrates that the alkali/alkaline-earth additives as well as ceria create similar active sites on Pt catalysts for the WGS reaction, and the structure of the active site, Pt-$O_x(OH)_y$ appears to be both support- and additive-independent.

3. The WGS reaction stability of the alkali-promoted Pt catalysts is very good. The characterization of the used samples reveals that alkali ions can stabilize sub-nm and atomic Pt species (HAADF/STEM), while XANES and XPS show that a part of Pt remains electron deficient even after several hours under the WGS reaction at realistic conditions.

4. The strong Pt-$O_x(OH)_y$-Na association in the Na-promoted Pt-$SiO_2$ samples was determined by a D.I. water treatment. The Pt oxidation states, the amount and onset of the $H_2$ production in the washed and parent samples are the same, and so is the WGS reaction activity, demonstrating that the active sites comprise non-washable Na on Pt-$O_x(OH)_y$-Na sites. The combined information from the body of the experimental work was used to arrive at plausible structures of the active sites by our collaborator, Prof. Manos Mavrikakis and his research group at the University of Wisconsin, Madison. Using ab initio Molecular Dynamics, they modeled the K-promoted Pt structure as $PtK_6O_4(OH)_2$ [27]. This site preserves Pt in an oxidized state, adsorbs CO weakly, and dissociates water with very little energy (almost thermoneutral dissociation).

5. With Quick-XANES and cyclic CO-TPR measurements, it is demonstrated that a reducing atmosphere reduces and sinters the alkali-free dispersed Pt clusters, while those associated with alkali ions are stabilized and responsible for the observed long-term catalyst activity. No formate species were observed over the $SiO_2$-supported catalysts by in situ DRIFTS analysis carried out at Prof. Meunier's lab at the University

of Caen, France. Potentially the formate species found on other supports are bound to the support, but are spectator species for the WGS reaction [6, 7]. The carboxyl reaction pathway is invoked to explain the Na-promotion effect. The addition of Na ions keeps the Pt in an oxidized state, active sites for the WGS reaction, and facilitates the dissociation of $H_2O$ to regenerate active OH groups. CO is oxidized by the OH groups, and this step is proposed as the rate limiting step for the WGS reaction over Pt-$SiO_2$ catalysts.

6. In work with Au-based catalysts, the evolution of reaction-relevant Au structures on Au-$Fe_2O_3$ during different conditions was followed by in situ XANES and EXAFS. Similar to the case of Au-$CeO_2$, atomically dispersed gold as [$Au_n$-O-Fe] species catalyze the WGS reaction. Highly reducing gas mixtures destabilize the [$Au_n$-O-Ce, Fe] sites and cause gold cluster/particle formation and deactivation. Activity recovery is possible by re-oxidation (350-400 $^oC$). Catalyst stability is improved if gas mixtures with higher oxygen potential are used. Therefore oxygen-assisted WGS operation is recommended.

7. OH-rich oxide supports were applied to create and stabilize Au-O active sites for the reaction. By comparing the catalytic performance of $La_2O_3$ or $La_2O_2SO_4$ supported Au catalysts it was further shown that OH-rich surfaces can stabilize the dispersed Au species during the synthesis and thermal treatment steps, and provide reactant for the reaction pathway. An alkali-promotion effect was observed on all Au catalysts, whether supported on reducible oxides, *e.g.* $CeO_2$, $Fe_2O_3$, or inert oxides, *e.g.* $SiO_2$. The alkali-free and alkali-promoted Au-$CeO_2$ or Au-$Fe_2O_3$ have the same apparent activation energy, which indicates that alkali ions, added in certain small amounts, can enhance the activity for WGS reaction, but they do not change the reaction pathway, or the structure of the active sites for the reaction. A common active site, Au-$O_x(OH)_y$, is thus proposed for all Au-based catalysts for the WGS reaction.

8. While demonstrating similar promotion of Pt- and Au-based catalysts by alkali, the stability of the Au catalysts is not good either in OH-rich or alkali-modified surfaces. The electronegativity of the oxide or promoter metal seems to play an essential role on the stability of the Au active sites. A large amount of alkali doping leads to high

concentration of surface OH groups, enhancing the surface basicity of the support, but also favoring the reduction of Au species to metallic gold and then the sintering of gold particles.

## 6.2 Recommendations

1. A lot of effort has been devoted on finding the optimal Na:Pt ratio to obtain the best catalytic performance with a low Pt loading. As presented in this thesis work, alkali ions decorate the dispersed Pt species only so it is important to start with atomically dispersed Pt species without the interference from particles. Also to demonstrate the effect in the absence of possible metal-support interaction, $SiO_2$-supported catalyst was a good study case for this thesis work. However, the commercial $SiO_2$ we used is a fumed powder, which has a pore volume as high as 3 ml/g. With the thermal treatment after IMP the pore collapsed dramatically and caused a big change in the support morphology which in turn affected the Pt dispersion. This also presented difficulties to the XAFS, XPS, and HAADF/STEM measurements. Thus, a more stable silica support in regard to its physical properties is recommended to use in a similar future study. Mesoporous $SiO_2$, such as SBA-15, should be tried. SBA-15 could allow for a more uniform distribution of Pt. All stabilized SBA-15 has also been reported as a good support for Pt earlier this year [8]. This should be studied when a new investigation of the optimal Na:Pt ratio in this type of material in undertaken.

2. The promotion effect is regarded as a structural one, but as reported in the literature CO adsorption is affected by the alkali doping. For example, in the case of Pt-$Al_2O_3$ modified with potassium, and the interaction between CO and Pt became weaker with the addition of potassium [9, 10]. The CO chemisorption results shown in this thesis work also indicate an altered CO adsorption site by the alkali-doping. Other than probing such effects by suitable spectroscopy techniques, such as IR, it is also important to carry out systematic kinetics measurement to investigate where alkali-ions influence the reaction orders of the reactants and products of the WGS reaction rate.

3. Low-temperature activated OH groups are considered as crucial for the WGS. Titrating the OH by CO-TPR after washing the samples to remove the unassociated alkali

species, and after a reduction step (followed by room temperature rehydration) to consider only the active and regenerable OH groups for the WGS reaction, is proposed as a good, complementary method to IR and other spectroscopies that could be used for the same purpose. Detailed analysis of XPS at $O_{1s}$ is also recommended to complement the OH counting.

4. As discussed in Chapter 4, the properties of additives (M), such as their electronegativity, and basicity, may affect the stability of the Pt-$O_x$(OH)-M associations. Theoretical calculations and experimental approaches are both important. For the experimental approach, Quick-XAFS could be applied to follow the reaction-relevant Pt structure changes with different promoters under thermal treatments or reaction conditions. This should rank order the various promoters in regarde to their imparted stability of the active sites. Moreover, additional information about the dynamic changes of Pt oxidation states with these promoters will be collected. DFT calculations, making use of this information are recommended to guide further design of new catalysts.

5. Similar to Pt, detailed examined of alkali-promoted Au catalysts is recommended. Potentially, the promotion effect will apply to other metals as well when an active site for the WGS reaction is created.

## 6.3 References

[1] Q. Fu, H. Saltsburg, M. Flytzani-Stephanopoulos, Science 301 (2003) 935-938.

[2] D. Pierre, W. Deng, M. Flytzani-Stephanopoulos, Top. Catal. 46 (2007) 363-373.

[3] P. Panagiotopoulou, J. Papavasiliou, G. Avgouropoulos, T. Ioannides, D.I. Kondarides, Chem. Eng. J. 134 (2007) 16-22.

[4] A.A. Phatak, N. Koryabkina, S. Rai, J.L. Ratts, W. Ruettinger, R.J. Farrauto, G.E. Blau, W.N. Delgass, F.H. Ribeiro, Catal. Today 123 (2007) 224-234.

[5] K.G. Azzam, I.V. Babich, K. Seshan, L. Lefferts, J. Catal. 251 (2007) 163-171.

[6] H. Evin, G. Jacobs, J. Ruiz-Martinez, G. Thomas, B. Davis, Catal. Lett. 120 (2008) 166-178.

[7] J.M. Pigos, C.J. Brooks, G. Jacobs, B.H. Davis, Appl. Catal., A 328 (2007) 14-26.

[8] A.K. Medina-Mendoza, M.A. Cortés-Jácome, J.A. Toledo-Antonio, C. Angeles-Chávez, E. López-Salinas, I. Cuauhtémoc-López, M.C. Barrera, J. Escobar, J. Navarrete, I. Hernández, Appl. Catal., B 106 (2011) 14-25.

[9] S. Derrouiche, P. Gravejat, B. Bassou, D. Bianchi, Appl. Surf. Sci. 253 (2007) 5894-5898.

[10] H. Tanaka, M. Kuriyama, Y. Ishida, S.-i. Ito, T. Kubota, T. Miyao, S. Naito, K. Tomishige, K. Kunimori, Appl. Catal., A 343 (2008) 125-133.

.